REPORT DOCUMENTATION PAGE

Form Approved
OMB No. 0704-0188

1. AGENCY USE ONLY (Leave blank)	2. REPORT DATE	3. REPORT TYPE AND DATES COVERED
	July 1994	Final 1 Jun 92-31 May 94

4. TITLE AND SUBTITLE

The Small-scale Structure of Dispersing Clouds in the Atmosphere

5. FUNDING NUMBERS

DAAL03-92-C-0020

6. AUTHOR(S)

R. Ian Sykes, Robert S. Gabruk, and Douglas S. Henn

7. PERFORMING ORGANIZATION NAME(S) AND ADDRESS(ES)

The Titan Corporation
Titan Research & Technology Div.
P.O. Box 2229;
Princeton, NJ 08543-2229

8. PERFORMING ORGANIZATION REPORT NUMBER

A.R.A.P. Report No. 710

9. SPONSORING/MONITORING AGENCY NAME(S) AND ADDRESS(ES)

U.S. Army Research Office
P.O. Box 12211
Research Triangle Park
NC 27709-2211

10. SPONSORING/MONITORING AGENCY REPORT NUMBER

ARO 29369.5-GS

11. SUPPLEMENTARY NOTES

The views, opinions and/or findings contained in this report are those of the author(s) and should not be construed as an official Department of the Army position, policy, or decision, unless so designated by other documentation.

12a. DISTRIBUTION/AVAILABILITY STATEMENT

Approved for public release; distribution is unlimited.

12b. DISTRIBUTION CODE

13. ABSTRACT (Maximum 200 words)

The fractal properties of a plume dispersing in a turbulent velocity field have been examined using Large-Eddy Simulation results for neutral and convective boundary layers. A fractal generation technique has been developed that correctly matches a specified mean and variance distribution for the plume. The spatial correlation scale of the fractal realizations can also be specified, and the one-point probability density function can be chosen as clipped normal or lognormal. Realizations generated with the fractal technique show reasonably close resemblance to the LES results.

The small-scale structure of the plume is further analyzed using multifractal techniques, and a the generation methodology is extended to incorporate unequal partitioning of the random variance during the refinement process. This procedure corresponds to the localization of small-scale energy in the turbulent cascade process which leads to an intermittent dissipation field. The multifractal spectrum of the dissipation field can be adjusted to match observations and the LES calculation results. The visual appearance of the dissipation field from the fractal/multifractal model is much more intermittent than the fractal realization, and the concentration field shows more localized small-scale fluctuations. These features give better correspondence to the LES realizations.

14. SUBJECT TERMS

Atmospheric dispersion
Turbulence
Fractals

15. NUMBER OF PAGES

16. PRICE CODE

17. SECURITY CLASSIFICATION OF REPORT	18. SECURITY CLASSIFICATION OF THIS PAGE	19. SECURITY CLASSIFICATION OF ABSTRACT	20. LIMITATION OF ABSTRACT
UNCLASSIFIED	UNCLASSIFIED	UNCLASSIFIED	UL

A.R.A.P Report No. 710

The Small-scale Structure of Dispersing Clouds in the Atmosphere

R. I. Sykes
R. S. Gabruk
D. S. Henn

The Titan Corporation
Titan Research & Technology Div.
P.O. Box 2229
Princeton, NJ 08543-2229

Army Research Office

CONTRACT No. DAAL03-92-C-0020

July 1994

SUMMARY

The fractal properties of a plume dispersing in a turbulent velocity field have been examined using Large-Eddy Simulation results for neutral and convective boundary layers. Scalar concentration isosurfaces were found to have a fractal dimension of about 1.3 from a two-dimensional plume cross-section, consistent with atmospheric and laboratory results. A fractal generation technique has been developed that correctly matches a specified mean and variance distribution for the plume. The spatial correlation scale of the fractal realizations can also be specified, and the one-point probability density function can be chosen as clipped-normal or lognormal. Realizations generated with the fractal technique show reasonably close resemblance to the LES results.

The small-scale structure of the plume is further analyzed using multifractal techniques, and a the generation methodology is extended to incorporate unequal partitioning of the random variance during the refinement process. This procedure corresponds to the localization of small-scale energy in the turbulent cascade process which leads to an intermittent dissipation field. The extended fractal/multifractal model maintains the fractal isosurface properties, but also yields a multifractal dissipation field consistent with laboratory observations. The multifractal spectrum of the dissipation field can be adjusted to match observations and the LES calculation results. The visual appearance of the dissipation field from the fractal/multifractal model is much more intermittent than the fractal realization, and the concentration field shows more localized small-scale fluctuations. These features give better correspondence to the LES realizations.

1. INTRODUCTION

The dispersion of material in the atmosphere is a chaotic process, due to the turbulent nature of the wind field. Molecular diffusivity is very small, and contaminants are transported by the local wind, which induces distortions into the evolving concentration field. The stretching and shearing motions of the turbulent wind field produce an increasingly complex concentration field, and eventually cascade the scale of the variations down to the smallest sizes where molecular diffusivity is effective. The detailed structure of a dispersing plume of material is therefore highly convoluted, and the smooth Gaussian shapes predicted by most dispersion models are only relevant to long term or ensemble averages.

Many applications of atmospheric dispersion modeling are concerned with short-term or near-instantaneous concentration measurements. An example is the obscuration problem, where the ability to see through an obscurant cloud depends on the instantaneous distribution of material. Long-term averages are not an appropriate measure for this problem, since the 'average' cloud does not exist at any instance in time. Instead, we need to characterize the random fluctuations in the cloud to determine the probability of obscuration. We may also need to characterize the temporal and spatial variations of the obscuration, if the duration and extent of periods of visibility are important factors. Other examples where the small-scale statistical structure is important include the dispersion of highly toxic materials, where short-term exposure can cause serious health effects, and chemically reactive dispersion, where interaction between species can occur on very fast timescales and is determined by very localized conditions.

The preceding discussion has introduced the notion of an instantaneous cloud as a random field with complicated structure on all scales down to the molecular mixing scale. This random nature of a dispersing cloud or plume has long been recognized by atmospheric dispersion modelers, and attempts to represent the phenomenon were initiated by Gifford (1959) using the meandering plume concept. Model validation was one of the principal reasons for the study of the statistical fluctuations, since the inherently unpredictable variation in an observed concentration can mask any model errors or differences between models (Fox, 1981). However, direct interest in short-term concentration values for assessing either toxic effects, flammability limits, or visibility estimates has also prompted recent research in this area (e.g., Durbin, 1980; Fackrell and

Robins, 1982a,b; Sawford and Hunt, 1986; Dinar et al., 1988; Chatwin and Sullivan, 1990; Mylne and Mason, 1991).

Gifford's (1959) model only accounts for the large-scale, meandering motions which move the entire plume in a coherent fashion. These motions are a major contributor to the variance in the concentration close to the plume source, but the meandering plume model neglects the small-scale fluctuations entirely. A practical methodology for predicting the total concentration fluctuation variance was developed by Sykes et al. (1986) under the sponsorship of the Electric Power Research Institute (EPRI). The basis of the modeling is second-order turbulence closure, and the variance prediction has been incorporated into a Gaussian plume and a Gaussian puff model. The model development is described in a series of reports by Lewellen et al. (1988).

For some applications, a prediction of the variance or one-point probability distribution function is insufficient. In order to represent the visual appearance of a plume, for example, a complete realization of the instantaneous concentration field as a function of time and space is necessary. The one-point information is an important part of the fluctuation description, but a more complete representation of the spatial and temporal structure is needed. Some useful information is obtainable from photographic data or other experimental measurements (Sreenivasan, 1991), but complete quantitative descriptions are very difficult to obtain. A complementary data source is numerical simulation, and the Large-Eddy Simulation (LES) studies of dispersing plumes by Sykes and Henn (1992) and Henn and Sykes (1992) provide detailed results on the three-dimensional, time-dependent behavior of a plume dispersing in a neutral and a convective boundary layer, respectively.

While LES provides a complete description of the instantaneous plume over the range of resolved calculation scales, the technique demands large computational resources since the flow dynamics must be computed in addition to the plume dispersal. A more practical scheme is required that can utilize the statistical information from an ensemble average prediction to generate realistic spatial and temporal variability without explicit dynamics. The most appropriate description of the turbulent field geometry is in terms of fractal structures, which embody the self-similar characteristics of the Kolmogorov inertial range and have been extensively applied to turbulent flows, e.g. Sreenivasan and Meneveau (1986), Prasad and Sreenivasan (1990a,b), Lovejoy and Mandelbrot (1985).

The objective of the study reported here is the development of techniques for generating representations of dispersing plumes that properly describe the random small-scale structure of the fluctuating concentration field. Fractal geometry provides the framework for analyzing and constructing the complex random fields; we analyze the LES plume data of Sykes and Henn (1992) and Henn and Sykes (1992), and incorporate the information into new fractal generation methods. We should emphasize that our objective in generating a fractal plume realization is not simply to adjust parameters of a fractal model to obtain a field similar to an atmospheric plume, but rather to develop a methodology that can utilize the quantitative predictions of models such as that described by Sykes et al. (1986). We therefore require a fractal field that is consistent with a predicted mean concentration, the fluctuation variance, and a spatial/temporal correlation scale. In addition, the generated realization should match the statistical structure of the small-scale variations as closely as possible, and the fractal analysis of the LES fields will be employed to determine the important characteristics of the small scales. Section 2 describes the results of the analysis and the development of a fractal generation technique based on a recursive or iterative refinement.

Recently, much research on random fields has focused on the multifractal nature of singular quantities such as energy dissipation (e.g., Meneveau and Sreenivasan, 1987). The concept of a fractal is actually only applicable to a set of points, as distinct from a continuous field, and is generally applied to isosurfaces or contour levels. This does not provide a complete description of the entire concentration field, and there is evidence that the fractal properties may depend somewhat on the choice of level (Lane-Serff, 1993). The multifractal definition is based on a functional description and therefore gives a more complete description of a field, but the definition is couched in terms of the singularities of the field and describes the measure of the sets of spatial points where the function displays a particular rate of divergence as the sampling scale is reduced. This is clearly appropriate for dissipation fields, which are concentrated in very small regions when the Reynolds number is high and the molecular diffusivity is very small. In Section 3, we discuss the multifractal properties of the dispersing plume and incorporate some of these properties into the fractal generation model. The extended fractal/multifractal model gives an improved representation of the small-scale plume structure and in particular provides a proper dissipation field.

Section 4 describes the application of our fractal generation methodology to the animation of a plume. The time-dependence can be considered as an independent

dimension, similar to the spatial dimensions, but the localized nature of the generation technique allows the realization to be constructed locally in time. This avoids the requirement that the entire time series be pre-computed and stored before display. Instead, storage is only needed for the spatial field, which is modified as time is advanced. The small scales are modified more rapidly than the large scales and the proper fractal/multifractal is preserved. This technique could form the basis of a real-time display with relatively small storage requirements. Concluding remarks are presented in Section 5.

2. FRACTAL ANALYSIS AND REPRESENTATION

As a preliminary step towards a realistic description of a turbulent plume in the atmosphere, we have examined some simple fractal field generation methods to determine their consistency with known plume characteristics. The detailed description of this work is included as Appendix A to this report and is briefly summarized here. Fractal geometry has been used to analyze turbulent fields in several contexts (Sreenivasan and Meneveau, 1986; Prasad and Sreenivasan, 1990a,b; Lovejoy and Mandelbrot, 1985), and provides a natural method for describing the self-similar nature of the turbulent cascade process. The characterization of scalar isosurfaces in terms of monofractal properties is imperfect, but is a reasonable step toward a more general approach. Fractal fields can be generated with the appropriate degree of complexity and spatial structure and can be used to produce 'cloud-like' fields (Lovejoy and Mandelbrot, 1985). Our objective here is not simply to produce a visual image reminiscent of a dispersing plume, but rather to generate a 'realization' that is statistically consistent with a given plume and can therefore be used for quantitative analysis.

We have also analyzed the LES (Large-Eddy Simulation) plume calculation data of Sykes and Henn (1992) and Henn and Sykes (1992), which provide a number of time-dependent, three-dimensional 'realizations' of the instantaneous plume. The numerical results have previously been analyzed to obtain statistical measures such as concentration moments, spatial and temporal correlations, and one-point probability distribution functions, and these parameters will be required for a fractal generation scheme. We performed fractal dimension analyses of the concentration fields in these 'realizations' in order to quantify a fractal description of the LES plumes. Perimeter-area relations and box counting methods were utilized, and the dimension of a concentration contour in a two-dimensional cross-section was found to be roughly 1.30 - 1.35 using the two different estimation methods. This is slightly smaller than observational estimates from natural clouds.

We next examined techniques for generating a fractal field with the correct ensemble mean and variance values. A simple method for producing a random fractal realization was demonstrated, giving either a 'clipped-normal' probability distribution (Lewellen and Sykes, 1986) or a lognormal probability distribution. The recursive refinement technique was adapted to provide a consistent representation of the mean and

variance of an inhomogeneous concentration field. The interpolation methodology of the standard method was replaced by a randomized pulse approach to obtain a good match with the ensemble statistics. It was found that the concentration statistics were modified by the interpolation step, which gives the concentration value on the successively refined grid before the addition of the new random component. The interpolation effectively reduces the local variance, since it averages two random numbers, so the ensemble statistics of the realizations becomes increasingly inaccurate as each new level of grid points is added. The randomization of the pulse position in the new method avoids the implicit averaging problem and gives correct ensemble statistics for inhomogeneous fields, such as a dispersing plume. The fractal generation scheme can be used to generate a concentration field with the desired fractal dimension and accurate ensemble mean moments of first and second order; the scheme also requires the specification of a spatial correlation scale as the outer scale for the fractal field.

Finally, we compared the characteristics of the fractal-generated plume cross-sections with the LES realizations. The application of the resulting technique using ensemble statistics produced reasonably good 'realizations' of the LES plume.

3. MULTIFRACTAL ANALYSIS AND REPRESENTATION

The representation of a concentration field, which is a function of space and/or time, as a fractal is known to be incomplete since fractal concepts strictly only apply to sets of points. The generation technique described in Section 2 (and Appendix A) produces a concentration field with the appropriate mean and variance and also with isosurfaces that exhibit the correct fractal dimension. Recently, the multifractal concept has been introduced to characterize the behavior of intermittent fields such as the energy dissipation. The definition of a multifractal involves the functional behavior of the field, and therefore gives a more complete description than conventional fractal analysis. The fractal fields generated by the methods of Section 2 were therefore analyzed to determine their multifractal properties and compared with those of the LES realizations and laboratory data. The detailed description of this work is given in Appendix B, and is summarized here.

We analyzed the pseudo-dissipation field from the fractal realizations, defined as the square of the concentration gradient, for comparison with the observational data on true scalar dissipation fields. The scalar pseudo-dissipation field derived from the fractal generation scheme of Section 2 fails to exhibit the intermittent, multifractal behavior observed in experimental measurements of scalar dissipation fields (Prasad and Sreenivasan, 1990b). The homogeneous nature of the random pulse addition gives small scale energy everywhere with the same likelihood. Since the gradient operator emphasizes the smallest scales, we find a dense distribution of dissipation peaks rather than intermittent spikes. The multifractal analysis shows that the dissipation field is essentially monofractal, that is the multifractal spectrum consists of a single point.

We therefore generalized the fractal model to produce a multifractal dissipation field while maintaining the simple fractal nature of the scalar field. Noting that a simple binomial multiplicative cascade process produces intermittent distributions and has been shown to agree well with measurements of turbulent kinetic energy dissipation (Meneveau and Sreenivasan, 1987), a model was constructed which randomly allocates *variance* unequally in a fixed ratio to successive levels of refinement. The unequal partition of the variance as the cascade proceeds concentrates variance in localized regions and actually produces a multifractal distribution of the variance. Since the scalar

field is made up of a summation of random pulses from many refinement levels with decreasing variance, it is dominated by the larger scale structures that contain most of the variance. The fractal behavior of the concentration field is maintained since the average variance at each iteration level is still controlled by co-dimension, H, and, hence, the power spectra is unchanged. The fractal behavoir of the scalar field remains unchanged since the total variance at each level is still controlled by the given codimension. However, the gradient operator involved in calculating the pseudo-dissipation field emphasizes small scales. In fact, the summation of pulse *gradients* diverges, so that the pseudo-dissipation field becomes highly intermittent and exhibits multifractal behavior. The partition parameter can be chosen to match observational dissipation data, while the concentration field still exhibits the appropriate fractal isosurface behavior. An important feature of the model is that it is still completely local and may be applied to inhomogeneous fields.

Idealized time series were generated with the new fractal/multifractal model using clipped-normal and lognormal distributions to define the pulses. An analysis of these show that the resulting multifractal spectra agree very well with the (assumed) universal spectrum derived from measurements of turbulent jets and wakes, even though the pseudo-dissipation fields from the two distributions are somewhat different in character. Analysis of LES neutral boundary layer plumes shows that the pseudo-dissipation fields reveal multifractal behavior, although the scaling range is limited. Application of the fractal/multifractal model using the LES statistics yields plumes realizations which are similar in appearance to the LES realizations. The fractal dimensions of plume isosurfaces from the LES and model are close (1.36 and 1.30 respectively); the model dimension is unchanged from the simple fractal model results given in Section 2 (Appendix A). The LES multifractal spectrum is close to the model and experimental spectra, although it may indicate less intermittency in the LES pseudo-dissipation fields. However, given the uncertainty resulting from the small scaling range, the match with the presumed universal spectrum is reasonably good.

4. SCALAR FIELD CONSTRUCTION FOR ANIMATION

A fractal animation model has been developed which simulates the time evolution of scalar fields in one, two, or three dimensions. This animation model is simply an extension of our successive refinement technique by considering time as an independent dimension. In this fractal animation scheme, 'time pulses' are generated in addition to the 'spatial pulses' of the static fractal models.

Consider a one-dimensional fractal generation. In the static model we add random pulses on successively smaller spatial scales with appropriately scaled variance. The location of the pulses is randomized in order to give an accurate representation of the scalar field variance. The method has also been adapted for inhomogeneous fields and provides either clipped-normal or lognormal one-point probability density functions. The concentration field, $c(x)$, can thus be written schematically in the form

$$c(x) = \bar{c} + \sum_n \sum_i a_{ni} P_n(x - x_{ni}) \tag{4.1}$$

where the overbar denotes the ensemble average, n is the refinement level, and i is the range of overlapping spatial pulse functions that contribute to the concentration fluctuation at the location x. The spatial pulse function, $P_n(x - x_{ni})$, with width Δ and centered at x_{ni}, is defined in one dimension as

$$P(x - x_0) = \begin{cases} 1 - \dfrac{|x - x_0|}{\Delta}, & |x - x_0| < \Delta \\ 0, & |x - x_0| \geq \Delta \end{cases} \tag{4.2}$$

The pulse amplitude a_{ni} is chosen randomly from a Gaussian distribution with zero mean and standard deviation σ_n, where, $\sigma_n = 2^{-nH}\sigma_0$. The constant H controls the fractal dimension of the generated field. Now, consider time as an added dimension. The local concentration can now be written

$$c(x,t) = \bar{c} + \sum_n \sum_i \sum_m a_{nim} P(x - x_{ni}) T(t - t_{nm}) \tag{4.3}$$

where m is the range of overlapping time pulse functions at a given iteration level n. The time pulse function, $T(t - t_{nm})$, with width Δ_t at time t_0 is defined as

$$T(t-t_0)=\begin{cases}1-\dfrac{|t-t_0|}{\Delta_t}, & |t-t_0|<\Delta_t \\ 0, & |t-t_0|\geq\Delta_t\end{cases} \tag{4.4}$$

This process can be envisioned as a one-dimensional field sweeping through static time pulses. At each new instant in time, time pulses are interpolated as they lose or gain influence on the field. Consider iteration level n_t with time pulses of half-width $\Delta_{n_t}=2^{-n_t}\Delta_0$. Once the field has moved through a time Δ_{n_t}, an older time pulse loses its influence on the concentration field and a new time pulse gains influence. At any given time, only three pulses affect the field since the pulse centroids fall within Δ_{n_t} while the width of the pulses is twice Δ_{n_t}. Therefore, it is only necessary to store three time pulses at each level of iteration, and the summation of overlapping time pulses is carried out over only three pulses.

The animation technique is easily extended to higher dimensions by using the product of spatial triangular functions for each dimension as well as the time pulse function. Therefore, for two dimensions we have

$$c(x,y,t)=\bar{c}+\sum_n\sum_i\sum_j\sum_m a_{nijm}P(x-x_{ni})P(y-y_{nj})T(t-t_{nm}) \tag{4.5}$$

where y is the second space coordinate and j is the corresponding range of overlapping pulses.

Real plumes generally have some mean flow translation and large scale meandering along with time evolution. Translation is created by adding a further extension to our simple animation procedure, namely using a mean flow velocity to move the streamwise spatial pulse locations downstream. Accordingly, at each time step, new streamwise pulses are created at the domain origin to replace the pulses that move downstream. Unfortunately, accounting for large scale meandering is not a simple task and a complete procedure has yet to be established.

5. CONCLUDING REMARKS

The instantaneous structure of a plume of material dispersing in the atmosphere is a random field with detailed structure on a wide range of scales. The self-similar nature of the turbulence spectrum suggests a fractal description of the scalar concentration field, and Large-Eddy Simulation results for a plume in both a neutral and a convective boundary layer have been analyzed to determine appropriate fractal properties. It is found that the LES concentration isosurfaces exhibit a fractal dimension in general agreement with atmospheric observations of water and smoke clouds.

Using a combination of the successive refinement and random pulse techniques, we have developed a method for generating a fractal field with given statistics. The method adds successively smaller scale triangular pulses with random amplitude and random location. The scale of the pulse is halved at each refinement, and the amplitude variance is reduced appropriately. Ensemble mean and variance as well as the spatial correlation scale can be specified arbitrarily and the one-point probability distributions can be specified as clipped-normal or lognormal. The realizations generated using this technique will be consistent with the given statistics.

The fractal generation technique was generalized to incorporate a multifractal aspect in the small-scale fluctuations. It was shown that an unequal partition of the variance during the refinement process yields a multifractal dissipation field but maintains the fractal isosurface properties. The resulting realizations are much improved as representations of a turbulent plume, and the small-scale variations are correctly localized in regions of intermittent dissipation.

We have developed a technique for representing the instantaneous structure of a dispersing plume. The technique requires the specification of the mean and variance of the concentration field, as well as the spatial correlation scale, and the realizations will be consistent with the given statistics. The statistics can be inhomogeneous, so that the plume can be localized in space, and the technique can be efficiently implemented for animation purposes since the pulses are defined in real space and time and only need to be considered locally. The generation method can therefore be used with a dispersion model such as that of Sykes et al. (1986) to produce a representation of a complete plume.

While much progress has been made in developing techniques for representing the instantaneous structure, there are several areas for further investigation. First, we are currently restricted to a choice of clipped-normal or lognormal statistics for the concentration fluctuations, while observations and numerical simulations show intermediate distributions between these two. Early time meandering plumes and plume edges tend to be intermittent and close to a clipped-normal distribution, while the plume interior far downstream from the source is closer to a lognormal distribution. The transition between the two probability distributions needs to be characterized and a generalized representation technique needs to be found to improve the fractal realizations.

The second area for future research is in the representation of large scale coherence and spatial anisotropy of the fluctuations. The early plume often contains a meandering component, where the entire plume is moved coherently by the large eddies. The plume also exhibits different characteristics in the streamwise and transverse directions. The techniques described in this report are essentially isotropic, and give the same characteristics on all scales. One can imagine a technique that modifies the simple triangular pulse shape to describe different spatial structures, but it is far from clear how to specify the appropriate shapes for a given plume. Further research is needed to characterize this behavior and develop appropriate representation techniques.

6. REFERENCES

Chatwin, P. C. and P. J. Sullivan (1990), "A simple and unifying physical interpretation of scalar fluctuation measurements from many turbulent shear flows", *J. Fluid Mech.*, **212**, 533-557.

Dinar, N., H. Kaplan and M. Kleinman (1988), "Characterization of concentration fluctuations of a surface plume in a neutral boundary layer", *Boundary-Layer Met.*, **45**, 157-175.

Durbin, P. A. (1980), "A stochastic model of two-particle dispersion and concentration fluctuations in homogeneous turbulence", *J. Fluid Mech.*, **100**, 279-302 .

Fackrell, J. E. and A. G. Robins (1982a), "Concentration fluctuations and fluxes in plumes from a point source in a turbulent boundary layer", *J. Fluid Mech.*, **117**, 1-26 .

Fackrell, J. E. and A. G. Robins (1982b), "The effects of source size on concentration fluctuations in plumes", *Boundary-Layer Met.*, **22**, 335-350.

Fox, D. G. (1981), "Judging air quality model performance", *Bull. Amer. Met. Soc.*, **62**, 599-609.

Gifford, F. A. (1959), "Statistical properties of a fluctuating plume dispersal model", *Adv. Geophys.*, **6**, 117-137.

Henn, D. S. and R. I. Sykes (1992), "Large-eddy simulation of dispersion in the convective boundary layer", *Atmos. Env.*, **26A**, 3145-3159.

Lane-Serff, G. F. (1993), "Investigation of the fractal structure of jets and plumes", *J. Fluid Mech.*, **249**, 521-534.

Lewellen, W. S. and R. I. Sykes (1986), "Analysis of concentration fluctuations from lidar observations of atmospheric plumes", *J. Clim. & Appl. Met.*, **25**, 1145-1154.

Lewellen, W. S., R. I. Sykes, S. F. Parker, D. S. Henn, N. L. Seaman, D. R. Stauffer and T. T. Warner (1988), "A hierarchy of dynamic plume models incorporating uncertainty, Volume 1: Overview", EPRI EA-6095 Volume 1, Project 1616-28.

Lovejoy, S. and B.B. Mandelbrot (1985), "Fractal properties of rain, and a fractal model", *Tellus*, **37A**, 209-232.

Meneveau, C. and K. R. Sreenivasan (1987), "Simple multifractal cascade model for fully developed turbulence", *Phys. Rev. Lett.*, **59**, 1424-1427.

Meneveau, C. and K. R. Sreenivasan (1991), "The multifractal nature of turbulent energy dissipation", *J. Fluid Mech.*, **224**, 429-484.

Mylne, K. R. and P. J. Mason (1991), "Concentration fluctuation measurements in a dispersing plume at a range up to 1000m", *Quart. J. Roy. Met. Soc.*, **117**, 177-208.

Prasad, R.R. and K.R. Sreenivasan (1990a), "Quantitative three-dimensional imaging and the structure of passive scalar fields in fully turbulent flows", *J. Fluid Mech.*, **216**, 1-34.

Prasad, R.R. and K.R. Sreenivasan (1990b), "The measurement and interpretation of fractal dimensions of surfaces in turbulent flows", *Phys. Fluids A*, **2**, 792-807.

Sawford, B. L. and J. C. R. Hunt (1986), "Effects of turbulence structure, molecular diffusion and source size on scalar fluctuations in homogeneous turbulence", *J. Fluid Mech.*, **165**, 373-400.

Sreenivasan, K. R. (1991), "Fractals and multifractals in fluid turbulence", *Ann. Rev. Fluid Mech.*, **23**, 539-600.

Sreenivasan, K.R. and C. Meneveau (1986), "The fractal facets of turbulence", *J. Fluid Mech.*, **173**, 357-386.

Sykes, R. I. and D. S. Henn (1992), "Large-eddy simulation of concentration fluctuations in a dispersing plume", *Atmos. Env.*, **26A**, 3127-3144 .

Sykes, R. I., W. S. Lewellen and S. F. Parker (1986), "A Gaussian plume model of atmospheric dispersion based on second-order closure", *J. Clim. & Appl. Met.*, **25**, 322-331.

A.R.A.P REPORT NO. 710

APPENDIX A

Fractal Representation of Turbulent Dispersing Plumes

R.I. Sykes and R.S. Gabruk

ARAP Group, California Research and Technology Division

Titan Corporation

Princeton, NJ

Published in Journal of Applied Meteorology,

June 1994, vol. 33, pp. 721-732.

Abstract

Fractal analysis techniques have been applied to the concentration fields from Large-Eddy Simulations of plume dispersion in a turbulent boundary layer. Fractal dimensions between 1.3 and 1.35 are obtained from perimeter-area and box-counting analyses for neutral and convective conditions. These values are close to previous estimates from atmospheric data. Methods for generating fractal fields with given statistical moments are examined and the simplest of these, the recursive refinement technique, is shown to be inadequate. The problem is shown to be the interpolation step of the procedure, which intrinsically reduces the variance with each refinement. Accurate statistical representation is obtained by replacing the interpolation step of the refinement technique with a sum of random pulses of appropriate width and random location. The pulse technique can easily be adapted to generate either clipped-normal or log-normal one-point probability distributions. Results from the fractal generation technique using simulated mean statistics are compared with realizations of instantaneous plume cross-sections from the Large-Eddy Simulations. The simulated probability distributions lie between the clipped-normal and the log-normal, so the fractal fields cannot match the realizations precisely. However, larger scale features of the plumes are generally well represented by the fractal method.

1. Introduction

Turbulent dispersion of a contaminant in the planetary boundary layer is a chaotic process. The instantaneous concentration field exhibits variations on a range of length scales and time scales, corresponding to the spectrum of motions in the turbulent velocity field. This random character of tracer dispersion has been recognized by atmospheric modelers and has lead to explicit statistical descriptions of the concentration variable. There has been extensive research on characterizing the small-scale fluctuations in the concentration field, both experimentally in the laboratory (Fackrell and Robins, 1982) and observationally in the atmosphere (Lewellen and Sykes, 1986; Sawford, 1987; Mylne and Mason, 1991). These studies have been supported by modeling efforts (Durbin, 1980; Kaplan and Dinar, 1988; Sykes et al, 1984) and considerable progress has been made in our understanding of the fluctuation statistics.

For model evaluation applications, where it is important to characterize the variability in a sampler observation, one-point statistics are usually sufficient. Most tracer measurements involve a time-average at a fixed location. However, there are other situations where more detailed information about the spatial and temporal structure of the plume is required. For example, any system with a nonlinear response to the concentration level needs more statistical information to predict the integrated response from passage through the plume. Such response systems might include human health effects and toxicity, or visibility and optical propagation phenomena. A realistic representation of the complete concentration distribution is useful for the assessment of parameterized effects models.

As a preliminary step towards a general description, we examine some simple fractal field generation methods to determine their consistency with known plume characteristics. Fractal geometry has been used to analyze turbulent fields in several

contexts (Sreenivasan and Meneveau, 1986; Prasad and Sreenivasan, 1990a,b; Lovejoy and Mandelbrot, 1985), and provides a natural method for describing the self-similar nature of the turbulent cascade process. Multifractal cascade models have also been successfully applied to the study of turbulent flow fields (e.g., Prasad et al., 1988; Sreenivasan, 1991), but the mathematical definition of multifractal properties in terms of the structure of the field singularities (Lovejoy and Schertzer, 1991) is most appropriate for highly intermittent fields such as energy dissipation or scalar fluctuation dissipation. Scalar concentration fields do not exhibit singularities and are generally described in terms of a simple fractal isosurface dimension (Sreenivasan, 1991; Lane-Serff, 1993). The characterization of scalar isosurfaces in terms of monofractal properties is imperfect, but is a reasonable step toward a more general approach.

Fractal fields can be generated with the appropriate degree of complexity and spatial structure and can be used to produce 'cloud-like' fields (Lovejoy and Mandelbrot, 1985). Our objective here is not simply to produce a visual image reminiscent of a dispersing plume, but rather to generate a 'realization' that is statistically consistent with a given plume and can therefore be used for quantitative analysis. We note, however, that simple fractal representations cannot necessarily reproduce the large-scale 'coherent structures' in a flow field (Sreenivasan and Meneveau, 1986), since the large-scale structures are generally determined by the mean flow geometry and do not exhibit self-similar structure

The principal data source for the fractal parameters is the LES (Large-Eddy Simulation) plume calculations of Sykes and Henn (1992) and Henn and Sykes (1992). These explicit numerical calculations of the time-dependent, three-dimensional plume dispersion have provided a number of 'realizations' of the instantaneous plume. The numerical results have previously been analyzed to obtain statistical measures such as concentration moments, spatial and temporal correlations, and one-point probability

distribution functions, and these parameters will be required for a fractal generation scheme. In this paper, we shall present fractal dimension analyses of the concentration fields in order to quantify a fractal description of the LES plumes.

Given the statistical plume parameters, we examine techniques for generating a fractal field with the correct ensemble mean and variance values. We present a simple method for producing a random realization with either a 'clipped-normal' probability distribution (Lewellen and Sykes, 1986) or a log-normal distribution. Finally, we compare the characteristics of the fractal-generated plume cross-sections with the LES realizations.

2. Fractal Analysis of the LES Plumes

A detailed description of the numerical methodology employed in the LES calculations is given by Sykes and Henn (1992). Simulations were performed for a neutral, wind-tunnel boundary layer and for a free-convection layer driven by a surface buoyancy flux. Dispersion from elevated releases of a passive scalar was calculated for each flow, and the evolving plume was computed for several boundary layer heights downstream. A uniform translation velocity was imposed on the free-convection layer to produce a statistically-steady plume.

The fractal analysis of the neutral and free-convection boundary layers was performed with both area-perimeter and box-counting analyses. Area-perimeter analysis, a method for estimating the fractal dimension of planar shapes, was first proposed by Mandelbrot (1977) and is the method used by Lovejoy (1982) in his investigation of satellite and radar pictures of rain and cloud areas. The area-perimeter relationship determines the complexity of the boundary of a shape since a very convoluted perimeter will be longer than a smooth one for the same enclosed area. The fractal dimension, D,

characterizes the degree of contortion of the boundary and is obtained from the relation $P \propto A^{D/2}$, where P is the perimeter and A is the area. A reasonable estimate of D requires a data set of area-perimeter pairs covering sufficient range for the exponent to be reliably determined. Lovejoy and Schertzer (1991) showed that the area-perimeter relation in its original form (given above) can only be used when non-fractal areas are enclosed by fractal perimeters.

In Lovejoy's analysis (1982) of rain and cloud areas, a large database of satellite and radar pictures supplied the necessary information over a wide range of scales. However, for the LES plumes used in the current research, the range of cloud (plume) sizes was somewhat limited. In order to extend the range of sizes, cross-sections of the plume where taken at locations ranging from 0.83 to 6.67 boundary layer heights downstream of the source for the neutral case and 1 to 8 boundary layer heights for the convective case. Lovejoy showed that when the threshold on the satellite data of his study was varied, the sizes of the clouds changed, but the perimeters changed in the same self-similar manner. Therefore, in order to further extend the range of sizes, the threshold value defining the plume boundary was varied. Multiple independent realizations of each plume (eight for the neutral and six for the convective) were analyzed to improve statistical confidence in the power law relationship.

Box-counting, a recursive technique for estimating the fractal dimension of a set, is described by both Mandelbrot (1982) and Feder (1988), and is employed by Malinowski and Zawadzki (1993) in their recent analysis of cloud surfaces. Similar approaches were used by Sreenivasan and Meneveau (1986) and Sreenivasan (1991) in their research on turbulent flows. The box-counting method utilizes a grid of rectangular boxes to cover the space occupied by a set, and counts the number of boxes needed to completely cover the set itself. This number will depend on the size of the covering boxes. If the number varies in proportion to a power of the box size, the exponent is

called the box dimension of the set (Feder, 1988). The estimate of the box dimension can vary slightly due to the uncertainty in the placement of a given grid since a slight shift in grid location may change the number of boxes counted. Therefore, in order to obtain a better approximation of the fractal dimension of the set, the grid location was shifted on each level and the number of boxes counted was averaged. Edge effects due to data set truncation were avoided by only counting boxes centered within the range of data.

The data sets chosen for box-counting analysis were iso-concentration contours obtained from vertical transverse slices of the LES plumes. LES calculations were performed on grids of 240 x 90 for the neutral boundary layer and 80 x 50 for the convective layer. Figure 1 shows typical contours for the neutral and convective boundary layers. In Fig. 1, $\bar{c}_m$ is the maximum mean concentration obtained from multiple realizations of the concentration field. Although the contour level is somewhat arbitrary, the chosen values fell within a range of concentrations ($0.003 < c/\bar{c}_m < 0.3$) that produced approximately the same fractal dimension (± 0.05). The concentration value must be small enough to give an extensive contour but not so small that numerical errors are significant. The locations of the plume slices were 5 and 8 boundary layer heights downstream of the source for the neutral and convective layers, respectively. For the convective layer, z_i denotes the mixed layer depth, while H is the depth of the neutral layer (Sykes and Henn, 1992). Results of the area-perimeter and box-counting analyses for the neutral and free-convection boundary layers are shown in Figs. 2 and 3, respectively.

Both Figs. 2(a) and (b) display approximately linear sections over most of the plot range. Since these two plots are on log-log scales, the linear sections indicate power law relations between the abscissa and ordinate variables. For the area-perimeter analysis, the relation $P \propto A^{D/2}$ is used to determine the fractal dimension (D) of the plume boundary by a least squares regression of the data set. The areas of the plume cross-sections were

determined to be non-fractal, thus legitimizing the use of the area-perimeter relation for determination of the fractal dimension of the perimeter. The box dimension is also determined from a regression line fit through the box-counting results. For the neutral boundary layer (Fig. 2), the box dimension is 1.34 in the area-perimeter analysis and 1.36 in the box-counting analysis. Results from the free-convection boundary layer (Fig. 3) indicate a fractal dimension of 1.32 using both methods. These fractal dimensions all had uncertainties of about ±0.05.

A direct comparison between the results of the LES fractal analyses and those of other atmospheric fractal studies is not a simple task. Most previous fractal analyses have utilized cloud radiances (obtained by radar or satellite) and not cloud densities (as in this study). There is no simple one-to-one correspondence between radiance and density, according to Cahalan and Joseph (1989). However, the lack of results pertaining to cloud densities necessitates comparisons between density and radiance results with the understanding that there is not necessarily a simple relationship between the two.

Although the data sets studied here are neither rain nor cloud areas, it is reasonable to compare the results with those of cloud areas since both are being shaped by the ambient turbulence of the atmosphere. The results of the present study are consistent with those of Lovejoy (1982), who found (using the perimeter-area relation on cloud radiances) the cloud perimeter fractal dimension to be 1.35±0.05. Rys and Waldvogel (1986) also used area-perimeter analysis, however, their data set was radar-echo data of severe convective storms. They determined that large clouds had a fractal dimension of 1.36±0.1 large clouds and 1.0±0.04 for smaller clouds ($P^{1/D} < 3$ km). The low dimension for the smaller clouds was believed to be due to strong vertical winds found in thunderstorms. Furthermore, Prasad and Sreenivasan (1990b) estimated a dimension of 1.36 for typical cumulus clouds from box-counting analysis of cloud boundaries in ground-based photographs. Malinowski and Zawadzki (1993), however,

report a much higher value of 1.55 from one-dimensional horizontal sections through small cumulus clouds, but this is a different fractal measure and is not necessarily comparable with the planar section perimeter dimension reported here.

In addition to fractal studies on cloud data, other laboratory and analytical results have been published. Prasad and Sreenivasan (1990b) used the box-counting method to analyze images of jet sections (produced from laser-induced fluorescence techniques) and determined that the fractal dimension of jet boundaries was 1.36. Over a wide range, this value was independent of the threshold defining the boundary. In addition, based on the relative turbulent diffusion theory, Hentschel and Procaccia (1984) predicted a slightly higher cloud perimeter fractal dimension in the range between 1.37 and 1.41.

3. Fractal Generation Technique

The most basic fractal field generation method uses recursive grid refinement with a random addition at each level of iteration (Peitgen and Sauper, 1988). In one dimension, random values are generated on an initial coarse grid of size Δ_0. The random numbers are selected from a Gaussian distribution with zero mean and standard deviation σ_0. The refinement process interpolates the initial values onto a finer grid with size $\Delta_1=\Delta_0/2$, and then adds a random number to every point in the new grid from a distribution with standard deviation σ_1. The fractal dimension of the resulting field is controlled by the specification of $\sigma_1 = \sigma_0 2^{-\alpha}$. The process can be repeated to give a field on a grid of size $\Delta_n = 2^{-n}\Delta_0$, using a standard deviation of $\sigma_n = 2^{-n\alpha}\sigma_0$ to generate the random numbers at that level. The process is illustrated schematically in Fig. 4, and yields a fractal dimension of $D = 2-\alpha$ for an isosurface in two dimensions.

In considering the recursive refinement technique for the representation of a scalar plume, we must remember that the concentration distribution is non-negative. This can

be achieved in two very simple ways. We can either truncate the field after generation, i.e., reset all negative values to zero, or we can generate the logarithm of the concentration. If we use a Gaussian probability distribution for the random numbers at each iteration level in the recursive generation, then the final sum will also have a Gaussian distribution. Thus, truncation of the negative values will produce a clipped-normal distribution, while generation of $\ln c$ (where c is the concentration value) will give a log-normal distribution. The recursive refinement technique can thus be used to produce fields with two of the most commonly used probability distributions. It should be noted that atmospheric observations (Sawford, 1987) as well as the LES calculations show that the concentration pdf (probability distribution function) is more complex than either the above distributions, but both are valuable representations in appropriate regimes.

The transformation of the Gaussian pdf into the clipped normal or lognormal pdf by this simple technique does not affect the fractal properties of an iso-surface. Our analysis of the fractal nature of the scalar field has only considered scalar iso-surfaces, so we must consider the effect of the transformation on these level surfaces.. The method can be described as a two-step process; first an untransformed scalar field, g, is generated, then the desired concentration field is defined as $c=F(g)$. The nonlinear function F represents either truncation or exponentiation for the two distributions described above. A level surface of c is defined as the set of points, $\boldsymbol{x}$, where $c(\boldsymbol{x})=c_0$, say. If F is monotonic, then a unique value g_0 exists such that $F(g_0)=c_0$, provided c_0 is a realizable value, i.e., it lies within the range of F. Then the iso-surface $c=c_0$, is identical to the level surface $g=g_0$, i.e., it is the same set of spatial points. The fractal properties are then obviously identical. The two transform functions utilized in our generation scheme are both monotonic, so we preserve the iso-surface fractal properties of the Gaussian field.

In order to test the generation scheme, we consider a one-dimensional, homogeneous field, $c(x)$, with unit mean and variance σ_c^2. We generate a periodic field on a domain of length L using an initial grid size Δ_0. The clipped normal Gaussian parameters (μ_G, σ_G) are defined so that the pdf

$$p(c) = \gamma\delta(c) + \frac{1}{\sigma_G\sqrt{2\pi}}\exp\left(\frac{-(c-\mu_G)^2}{2\sigma_G^2}\right), \; c \geq 0 \tag{1}$$

has unit mean and variance σ_c^2. The intermittency, γ, is defined as

$$\gamma = \frac{1}{2}\left[1 - erf\left(\frac{\mu_G}{\sigma_G\sqrt{2}}\right)\right] \tag{2}$$

(Lewellen and Sykes, 1986). Similarly, the log-normal parameters (μ_l, σ_l) defined as

$$\mu_l = -\frac{1}{2}\ln\left(1+\sigma_c^2\right) \tag{3}$$

$$\sigma_l^2 = \ln\left(1+\sigma_c^2\right) \tag{4}$$

so that

$$p(x) = \frac{1}{\sigma_l\sqrt{2\pi}}\exp\left(-\frac{(x-\mu_l)}{2\sigma_l^2}\right) \tag{5}$$

where x=ln$c$ (Csanady, 1973). In the rest of this discussion, we use the clipped-normal parameters to be specific, but all results apply similarly for the log-normal distribution.

The initial variance for the recursive iteration, σ_0^2, must be chosen to produce the required variance, σ_G^2. Since the random additions are independent, the final variance after N iterations is the sum of the geometric series, so that

$$\begin{aligned}\sigma_G^2 &= \sigma_0^2\sum_{r=0}^{N} 2^{-2r\alpha} \\ &= \sigma_0^2\,\frac{1-2^{-2(N+1)\alpha}}{1-2^{-2\alpha}}\end{aligned} \tag{6}$$

for N refinements of the original grid.

The mean concentration value is obtained by specifying μ_G as an initial value for the iteration on the coarse grid. This will be preserved through the random additions since they all have zero mean. The final result for $c(x)$ is obtained by truncating the random field at c=0.

Results from this scheme are illustrated in Fig. 5 for 10 refinements on a unit domain, i.e., L=1 and Δ_0=0.25. The results are shown for σ_c=0.25, with mean statistics from 1000 realizations of the fractal field and α=0.7. The realization shown in the figure is typical of the set. The ensemble mean is close to unity, as required, but the variance shows distinct non-uniformity across the domain.

The problem with the variance is easily traceable to the interpolation step in the iteration. The geometric sum (6) is only valid on the initial grid. Intermediate points all involve an interpolation between random values which necessarily reduces the variance. The reduction is evident in the complex pattern of the variance, which shows increasing errors on finer grid locations. The initial coarse grid points are isolated points with the correct variance.

It might be argued that the variance error is not important since the location of the initial grid can be randomly selected to produce a homogeneous ensemble variance. However, this ensemble average will be smaller than σ_c^2. Furthermore, the mean value also shows errors, as illustrated in Fig. 6, when σ_c is larger. Here, σ_c=2 and the realization shows the highly intermittent nature of the concentration field. The reduction in the variance prior to the truncation affects the ensemble mean value here, as can be seen from (1). If σ_G is reduced while μ_G remains fixed at some negative value, then the probabilities of zero concentration will increase and the mean and variance will decrease. In this case, randomizing the location of the initial grid will produce an erroneous ensemble mean value.

The origin of the homogeneity problem is the choice of the initial grid and subsequent interpolation onto the finer grid. We can incorporate the 'sum of pulses' concepts of Lovejoy and Mandelbrot (1985) to randomize the fractal generation and maintain homogeneity. Lovejoy and Mandelbrot use square pulses with an exponential smoothing factor, but we prefer to use triangular functions to simplify the computation. We adapt the method to the recursive iteration framework by replacing the addition of a random number on the grid of size Δ_n by the addition of an appropriate pulse.

Define the unit triangle function of width Δ at location x_0 as

$$T(x\,;x_0,\Delta)=\begin{cases}1-\dfrac{|x-x_0|}{\Delta}\;, & |x-x_0|<\Delta\\[2ex] 0\qquad\quad\;, & |x-x_0|\geq\Delta\end{cases} \tag{7}$$

Consider iteration level n at grid size Δ_n with the set of locations

$$\left\{x_i^{(n)}=(i-1)\Delta_n\,,i=1,M\right\}.$$

The concentration field is augmented at this level by the addition of the function,

$$c^{(n)}(x)=\sum_{i=1}^{M}\varepsilon_i^{(n)}T\left(x;y_i^{(n)},\Delta_n\right) \tag{8}$$

where $\varepsilon_i^{(n)}\in N(0,\sigma_n)$, i.e., a random selection from a normal distribution with zero mean and standard deviation σ_n. Also, the pulse locations, $y_i^{(n)}$, are randomly selected from a uniform distribution over the interval $\left[x_i^{(n)}-\Delta_n/2\,,x_i^{(n)}+\Delta_n/2\right]$. The triangular pulse is thus randomized over the appropriate scale and avoids defining any special initial grid. Note that the concentration increment $c^{(n)}(x)$ is a continuous function of x and must

therefore be added onto the finest grid. It should be noted that the recursive refinement method is recovered by setting $y_i^{(n)} = x_i^{(n)}$, i.e., non-random pulse locations.

The variance scaling to obtain σ_0 is more complicated for the triangular pulses since we have to account for the random position of the pulse, but a straightforward integration of the shape function yields

$$\sigma_G^2 = \frac{2}{3}\sigma_0^2 \frac{\left(1-2^{-2(N+1)\alpha}\right)}{1-2^{-2\alpha}}. \tag{9}$$

The results from the pulse method with σ_c=2 are shown in Fig. 7. The ensemble statistics show very good homogeneity and agreement with the analytic prescription. The randomized pulse locations remove the special nature of the initial grid and retain a properly scaled fractal.

The application of the generation technique to represent real plumes must deal with inhomogeneous fields, however, so we next consider a Gaussian concentration distribution. Suppose

$$\bar{c} = e^{-x^2}$$

$$\overline{c'^2} = \sigma_c^2 e^{-x^2}$$

where the overbar denotes ensemble mean, and the prime denotes fluctuation from the mean. We generate the representation for $x \in [-5,5]$ and we use Δ_0=1.25. This implies a relative large spatial correlation relative to the spread of the distribution, but is typical of the LES results.

The first test, shown in Fig. 8, uses the value of $\sigma_n^2(x)$ at $x_i^{(n)}$ as the variance for the selection of $\varepsilon_i^{(n)}$, i.e., the random number is selected on the basis of the variance at the mean centroid of the pulse. As in the homogeneous case, the mean value $\mu_G(x)$ is

used as the initial concentration field to maintain the correct ensemble mean. The use of the local value causes difficulties, however, as seen in the figure. The relative large correlation scale distorts the tails of the distribution. The problem stems from the inaccurate representation of the local statistics by the triangular pulse. With the pulse amplitude determined by the centroid location variance, there is an effective spatial smoothing of the concentration statistics. The nonlinear character of the clipped-normal transformation induces severe distortions in the final results, as seen in the figure.

The predictions for the inhomogeneous case were greatly improved by using a local variance to scale the triangular pulse. Thus, equation (8) is replaced by

$$c^{(n)}(x) = \sum_{i=1}^{M} \hat{\varepsilon}_i^{(n)} \sigma_n(x) T\left(x\,;\, y_i^{(n)}, \Delta_n\right) \tag{10}$$

where $\hat{\varepsilon}_i^{(n)} \in N(0,1)$. Results using (10) are shown in Fig. 9 for the Gaussian concentration distribution. The agreement with the ensemble statistics is greatly improved.

Spatial correlations are an important characterization of the larger scale plume fluctuations, and will be controlled by our selection of Δ_0, since this represents the maximum range of the correlation. Spatial correlation functions for both a homogeneous fractal and the inhomogeneous Gaussian field are shown in Fig. 10 for several values of α. The correlation is defined at x=0, i.e.,

$$\rho(x) = \frac{\overline{c'(0)c'(x)}}{\left(\overline{c'^2(0)}\;\overline{c'^2(x)}\right)^{1/2}}$$

and shows a similar monotonic decrease for both cases. We actually show $1-\rho$ on a log-log scale to confirm the power law behavior for small separations; the correct slope for a fractal field is 2α. As might be expected, the integral scale is smaller for smaller values

of α , that is, for higher fractal dimensions, since there is relatively more fluctuation variance in the smaller scales. The point where ρ falls to 0.5 ranges from $0.2\Delta_0$ to $0.4\Delta_0$ as α increases from 0.4 to 0.8. For α =0.65, as used in our fractal field generation in section 4, the corresponding value was roughly $0.33\Delta_0$. This relationship allows us to specify Δ_0 if we are given the correlation scale of the plume fluctuations.

The pulse generation technique is easily extended to higher dimensions by using the product of triangle functions for each separate dimension. The definition of the variance in (9) will contain a 2/3 factor for each dimension, but the rest of the methodology is unchanged.

4. Comparison With LES Realizations

The fractal generation scheme described in the previous section can be applied to the fields from the LES plume calculations. We first consider the free-convection case at x/z_i =8. This corresponds to a non-dimensional distance X=2 downstream, as defined by Henn and Sykes (1992). Here,

$$X = \frac{x}{z_i}\frac{w_*}{U}$$

and z_i is the mixed layer depth, U is the horizontal translation speed, and w_* is the convective scaling velocity (Deardorff, 1970). The mean concentration and the r.m.s. fluctuation for the cross-section at x/z_i =8 are shown in Fig. 11. The plume is almost completely mixed throughout the depth of the turbulent layer, and the fluctuation intensity, $\sigma_c / \overline{c}$, is roughly 1 in the main part of the plume. The fractal generation also requires a correlation scale to determine the initial grid size, Δ_0. The lateral correlation scale, defined as the range at which the correlation coefficient is 0.5, was shown to be

roughly $0.25z_i$ at the plume centerline (Henn and Sykes, 1992). Thus, using the results from the previous section with α=0.65, we specify Δ_0=$0.75z_i$.

The LES realizations are shown in Fig. 12 while the fractal representations using a clipped-normal distribution are presented in Fig. 13; the log-normal fractal is shown in Fig. 14. The general character of the plume is well represented by the fractal model. The LES resolution is insufficient to check very small scale fluctuations, but the scale and magnitude of the dominant features match well. The principal difference between the three sets of realizations is evident in the low concentration regions. The clipped-normal representation produces too many zero values compared with the LES, while the log-normal has too few. This is completely consistent with the one-point pdf results from the LES, which showed that the distribution was intermediate between the two idealized shapes.

Box-counting results for the fractally generated convective boundary layer plume are shown in Fig. 15 for both clipped-normal and log-normal distributions. Both plots demonstrate self-similarity over most of the range of scales and are consistent with the fractal analysis of the LES convective plume. The fractal dimension is 1.32±0.05 for the clipped-normal distribution and 1.27±0.05 for the log-normal, compared with the specified dimension of 1.32, as found in the fractal analysis of the LES convective boundary layer plume. The log-normally generated realizations tended to produce a fractal dimension slightly lower than the specified value, and this is attributable to finite resolution and statistical sampling. The dimension is obtained from a relatively low isosurface value, so that a reasonably extensive contour is available, but the probability distribution becomes increasingly intermittent in the edges of the plume and increasingly large samples are required to represent the fluctuations properly. The fractal measure was obtained for contour values in the same range as used for the LES data analysis, and showed a tendency to reduce as the threshold was reduced. The clipped normal

distribution does not show the same effect, since all small threshold values define the clipped region which is not strongly dependent on the outer regions of the plume.

Examples of the neutral boundary layer LES plume statistics and realizations are given in Figs. 16 and 17 and can be compared with the fractal plumes in Fig. 18. The log-normal distributions are shown here, since the LES pdf's were closer to log-normal. The spatial correlation scale was shown to be about $0.09H$ (Sykes and Henn, 1992), and we therefore use $\Delta_0=0.25H$ in the fractal generation scheme. The fractal technique is not able to reproduce the coherent distortion of the plume that can be seen in the LES realizations, such as the rolled-up feature on the left of Fig. 17(b). There is an appropriate spatial length scale for the structures in the fractal field, however, and we have accurately matched the one-point statistics. The one-point pdf is strictly log-normal, due to the addition of independent normally distributed contributions, and we know that this is only a good approximation for the central region of the neutral layer plume. The distribution in the LES plume edges is more intermittent, as can be seen in the larger region of low-level concentration in the fractal fields. The LES realization shows regions of "clean" air mixed well into the plume, implying an intermittent pdf. The fractal dimension of the generated 'plumes' was 1.30 ± 0.05, somewhat lower than that specified from the LES neutral boundary layer results (D=1.36). The clipped normal distribution is too intermittent, however, and further work is needed to develop a proper representation of the general probability distribution.

5. Concluding Remarks

The LES results of Sykes and Henn (1992) and Henn and Sykes (1992) for turbulent plume dispersion have been used to determine a fractal dimension for the concentration field. Perimeter-area relations and box counting methods were utilized in the analysis of scalar concentration fields. The dimension of a concentration contour in a

two-dimensional cross-section was found to be roughly 1.30 - 1.35 using the two different estimation methods. This is slightly smaller than observational estimates from natural clouds.

The recursive refinement technique has been adapted to provide a consistent representation of the mean and variance of an inhomogeneous concentration field with a clipped-normal or log-normal one-point pdf. The interpolation methodology of the standard method was replaced by a randomized pulse approach to obtain a good match with the ensemble statistics. The fractal generation scheme can be used to generate a concentration field with the desired fractal dimension and accurate ensemble mean moments of first and second order; the scheme also requires the specification of a spatial correlation scale as the outer scale for the fractal field.

The application of the resulting technique using ensemble statistics produced reasonably good 'realizations' of the LES plume. The general structure of the plume is reproduced well, although there are differences between the LES pdf's and the idealized shapes. Further work will be needed to generalize the pdf's.

In summary, we have presented a relatively simple fractal generation technique capable of reproducing the mean and variance of an inhomogeneous field in multiple dimensions. The technique can be used in conjunction with parameterized dispersion models such as Sykes et al. (1986), which predict mean and variance of the concentration, to generate quantitatively accurate realizations of an instantaneous field.

Acknowledgment

This work was supported by the U.S. Army Research Office under contract number DAAL03-92-C-0020

References

Cahalan, R.F. and J.H. Joseph, 1989: Fractal statistics of cloud fields. *Mon. Wea. Rev.*, 117, 261-272.

Csanady, G.T., 1973: *Turbulent diffusion in the environment.* Reidel.

Deardorff, J.W., 1970: Convective velocity and temperature scales for the unstable planetary boundary layer and for Rayleigh convection. *J. Atmos. Sci.*, **27**, 1211-1213.

Durbin, P.A., 1980: A stochastic model of two-particle dispersion and concentration fluctuations in homogeneous turbulence. *J. Fluid Mech.*, **100**, 279-302.

Fackrell, J.E. and A.G. Robins, 1982: Concentration fluctuations and fluxes in plumes from a point source in a turbulent boundary layer. *J. Fluid Mech.*, **117**, 1-26.

Feder, J., 1988: *Fractals*. Plenum Press, 283 pp.

Henn, D.S. and R.I. Sykes, 1992: Large-eddy simulation of dispersion in the convective boundary layer. *Atmos. Env.*, **26A**, 3145-3159.

Hentschel, H.G.E. and I. Procaccia, 1983: Fractal nature of turbulence as manifested in turbulent diffusion. *Phys. Rev. A*, **27**, 1266-1269.

Hentschel, H.G.E. and I. Procaccia, 1984: Relative diffusion in turbulent media: The fractal dimension of clouds. *Phys. Rev. A*, **29**, 1461-1470.

Kaplan, H. and N. Dinar, 1988: A stochastic model for dispersion and concentration distribution in homogeneous turbulence. *J. Fluid Mech.*, **190**, 121-140.

Lane-Serff, G.F., 1993: Investigation of the fractal structure of jets and plumes. *J. Fluid Mech.*, **249**, 521-534.

Lewellen, W.S. and R.I. Sykes, 1986: Analysis of concentration fluctuations from lidar observations of atmospheric plumes. *J. Clim. & Appl. Met.*, **25**, 1145-1154.

Lovejoy, S., 1982: Area-perimeter relation for rain and cloud areas. *Science*, **216**, 185-187.

Lovejoy, S. and B.B. Mandelbrot, 1985: Fractal properties of rain, and a fractal model. *Tellus*, **37A**, 209-232.

Lovejoy, S. and D. Schertzer, 1991: Multifractal analysis techniques and the rain and cloud fields from 10^{-1} to 10^{6} m. *Scaling, fractals and non-linear variability in geophysics.* D. Schertzer and S. Lovejoy, Eds. Kluwer, 111-144.

Malinowski, S.P. and I. Zawadzki, 1993: On the surface of clouds. *J. Atmos. Sci.*, **50**, 5-13.

Mandelbrot, B.B., 1977: *Fractals: form, chance and dimension.* W. H. Freeman, 365 pp.

Mandelbrot, B.B,. 1982: *The fractal geometry of nature*. W. H. Freeman, 468 pp.

Mylne, K.R. and P.J. Mason, 1991: Concentration fluctuation measurements in a dispersing plume at a range up to 1000m. *Quart. J. Roy. Met. Soc.*, **117**, 177-208.

Peitgen, H.-O. and D. Sauper, 1988: *The science of fractal images*. Springer-Verlag, 312 pp.

Prasad, R. R., C. Menevau and K.R. Sreenivasan, 1988: Multifractal nature of the dissipation field of passive scalars in fully developed turbulent flows. *Phys. Rev. Lett.*, **61**, 74-77.

Prasad, R.R. and K.R. Sreenivasan, 1990a: Quantitative three-dimensional imaging and the structure of passive scalar fields in fully turbulent flows. *J. Fluid Mech.*, **216**, 1-34.

Prasad, R.R. and K.R. Sreenivasan, 1990b: The measurement and interpretation of fractal dimensions of surfaces in turbulent flows. *Phys. Fluids A*, **2**, 792-807.

Rys, F.S. and A. Waldvogel, 1986: Fractal shape of hail clouds. *Phys. Rev. Lett.*, **56**, 784-787.

Sawford, B.L., 1987: Conditional concentration statistics for surface plumes in the atmosphere. *Boundary-Layer Met.*, **38**, 209-223.

Sreenivasan, K.R. and C. Meneveau, 1986: The fractal facets of turbulence. *J. Fluid Mech.*, **173**, 357-386.

Sreenivasan, K.R., 1991: Fractals and multifractals in fluid turbulence. *Annu. Rev. Fluid Mech.*, **23**, 539-600.

Sykes, R.I. and D.S. Henn, 1992: Large-eddy simulation of concentration fluctuations in a dispersing plume. *Atmos. Env.*, **26A**, 3127-3144 .

Sykes, R.I., W.S. Lewellen and S.F. Parker, 1984: A turbulent-transport model for concentration fluctuations and fluxes. *J. Fluid Mech.*, **139**, 193-218.

Sykes, R.I., W.S. Lewellen and S.F. Parker, 1986: A Gaussian plume model of atmospheric dispersion based on second-order closure. *J. Clim. & Appl. Met.*, **25**, 322-331.

Figure captions

Figure 1. Transverse cross-section of instantaneous iso-concentration contours from high-resolution LES fields with $c/\bar{c}_m = 0.01$, where $\bar{c}_m$ is the maximum mean concentration over multiple realizations. (a) Neutral boundary layer at x/H=5. (b) Convective boundary layer at x/z_i=8.

Figure 2. Fractal analyses of neutral boundary layer. (a) Perimeter-area analysis. P is perimeter in meters and A is area in square meters. (b) Box-counting analysis. R is normalized box size and N is the number of boxes counted.

Figure 3. Fractal analyses of convective boundary layer. (a) Perimeter-area analysis. P is perimeter in meters and A is area in square meters. (b) Box-counting analysis. R is normalized box size and N is the number of boxes counted.

Figure 4. Schematic illustration of recursive refinement. Points on initial grid shown as solid circles with linear interpolation as solid line. First refinement shown as open circles with random displacement from first level function.

Figure 5. One-dimensional recursive refinement fractal generation for a homogeneous concentration field with $\sigma_c/\bar{c} = 0.25$. Solid lines are from fractal generation and dashed lines are the target statistics. (a) Individual realization. (b) Mean ($\bar{c}$) and r.m.s. fluctuation concentration (σ) from 1000 realizations.

Figure 6. One-dimensional recursive refinement fractal generation for a homogeneous concentration field with $\sigma_c/\bar{c} = 2$. Solid lines are from fractal generation and dashed lines are the target statistics. (a) Individual realization. (b) Mean ($\bar{c}$) and r.m.s. fluctuation concentration (σ) from 1000 realizations.

Figure 7. One-dimensional random pulse fractal generation for a homogeneous concentration field with $\sigma_c/\overline{c} = 2$. Solid lines are from fractal generation and dashed lines are the target statistics. (a) Individual realization. (b) Mean ($\overline{c}$) and r.m.s. fluctuation concentration (σ) from 1000 realizations.

Figure 8. One-dimensional random pulse fractal generation for an inhomogeneous concentration field with $\sigma_c/\overline{c} = 2$ and no local scaling. Solid lines are from fractal generation and dashed lines are the target statistics. (a) Individual realization. (b) Mean ($\overline{c}$) and r.m.s. fluctuation concentration (σ) from 1000 realizations.

Figure 9. One-dimensional random pulse fractal generation for a inhomogeneous concentration field with $\sigma_c/\overline{c} = 2$ and local scaling. Solid lines are from fractal generation and dashed lines are the target statistics. (a) Individual realization. (b) Mean ($\overline{c}$) and r.m.s. fluctuation concentration (σ) from 1000 realizations.

Figure 10. Correlation coefficient for one-dimensional fractal generation. Solid lines are from fractal model and dashed lines are theoretical values (slope=2α). (a) homogenous concentration field. (b) inhomogeneous concentration field.

Figure 11. Transverse cross-section of the mean concentration and the r.m.s. fluctuation contours for convective boundary layer. Contours normalized by the maximum mean concentration ($\overline{c}_m$). Downstream location is at x/z_i=8. (a) Mean concentration. (b) R.m.s. fluctuation.

Figure 12. Two LES convective boundary layer realizations of $c/\overline{c}_m$ at x/z_i=8. Contours at 0.1, 0.2, 0.5, 1, and 2. Stippled areas are equal to or greater than 1.

Figure 13. Two fractal realizations of $c/\bar{c}_m$ at x/z_i=8 using LES convective boundary layer statistics with clipped-normal distribution. Contours at 0.1, 0.2, 0.5, 1, and 2. Stippled areas are equal to or greater than 1.

Figure 14. Two fractal realizations of $c/\bar{c}_m$ at x/z_i=8 using LES convective boundary layer statistics with log-normal distribution. Contours at 0.1, 0.2, 0.5, 1, and 2. Stippled areas are equal to or greater than 1.

Figure 15. Box-counting analyses of fractally generated convective boundary layer plume. (a) Clipped-normal distribution. (b) Log-normal distribution. R is normalized box size and N is the number of boxes.

Figure 16. Transverse cross-section of the mean concentration and the r.m.s. fluctuation contours for neutral boundary layer. Contours normalized by the maximum mean concentration $(\bar{c}_m)$. Downstream location is at x/H=5. (a) Mean concentration. (b) R.m.s. fluctuation.

Figure 17. Two LES neutral boundary layer realizations of $c/\bar{c}_m$ at x/H=5. Contours at 0.1, 0.2, 0.5, 1, 2, and 5. Stippled areas are equal to or greater than 1.

Figure 18. Two fractal realizations of $c/\bar{c}_m$ at x/H=5 using LES neutral boundary layer statistics with log-normal distribution. Contours at 0.1, 0.2, 0.5, 1, 2, and 5. Stippled areas are equal to or greater than 1.

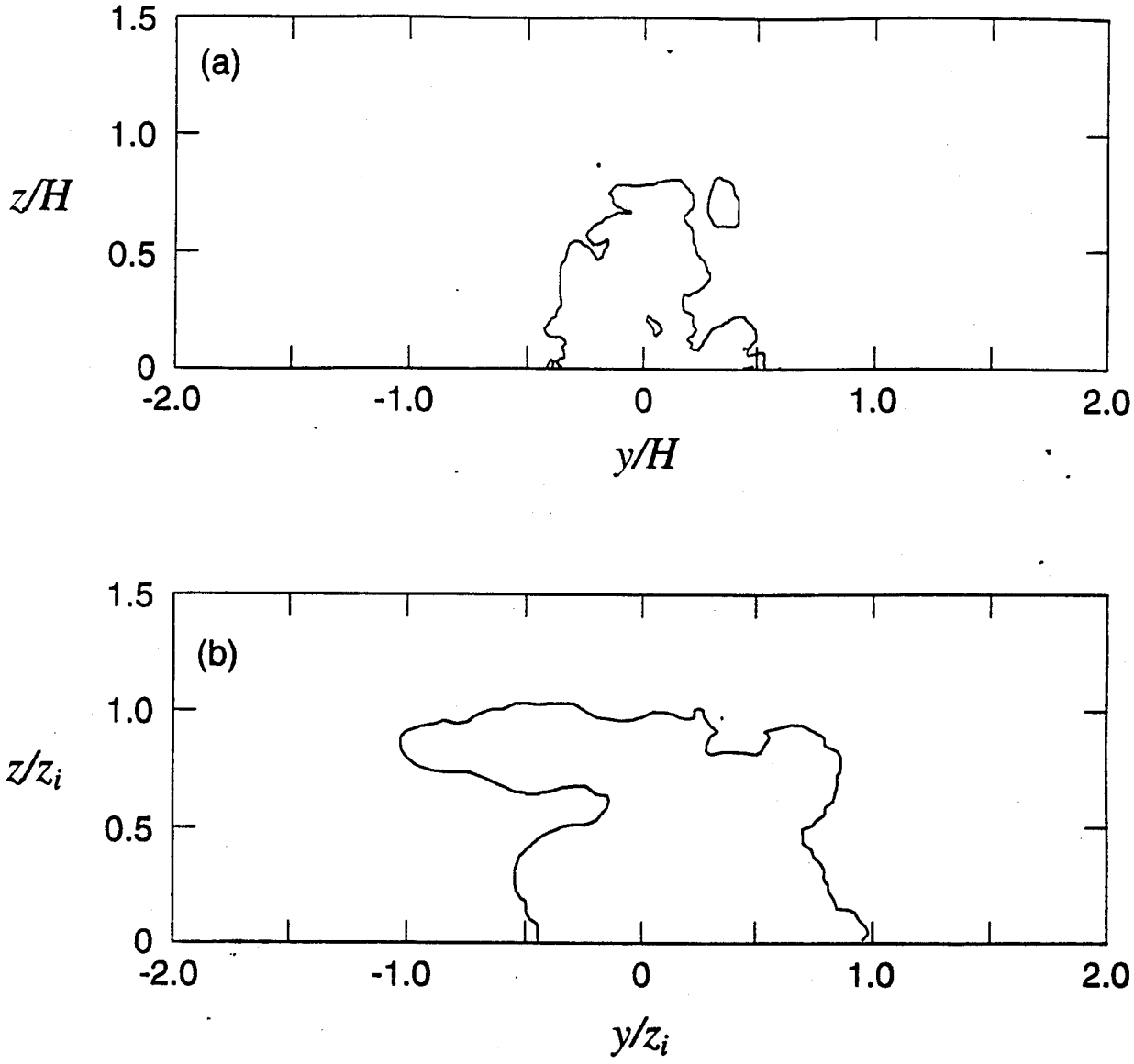

Figure 1. Transverse cross-section of instantaneous iso-concentration contours from high-resolution LES fields with $c / \overline{c}_m = 0.01$, where $\overline{c}_m$ is the maximum mean concentration over multiple realizations. (a) Neutral boundary layer at x/H =5. (b) Convective boundary layer at x/z_i=8.

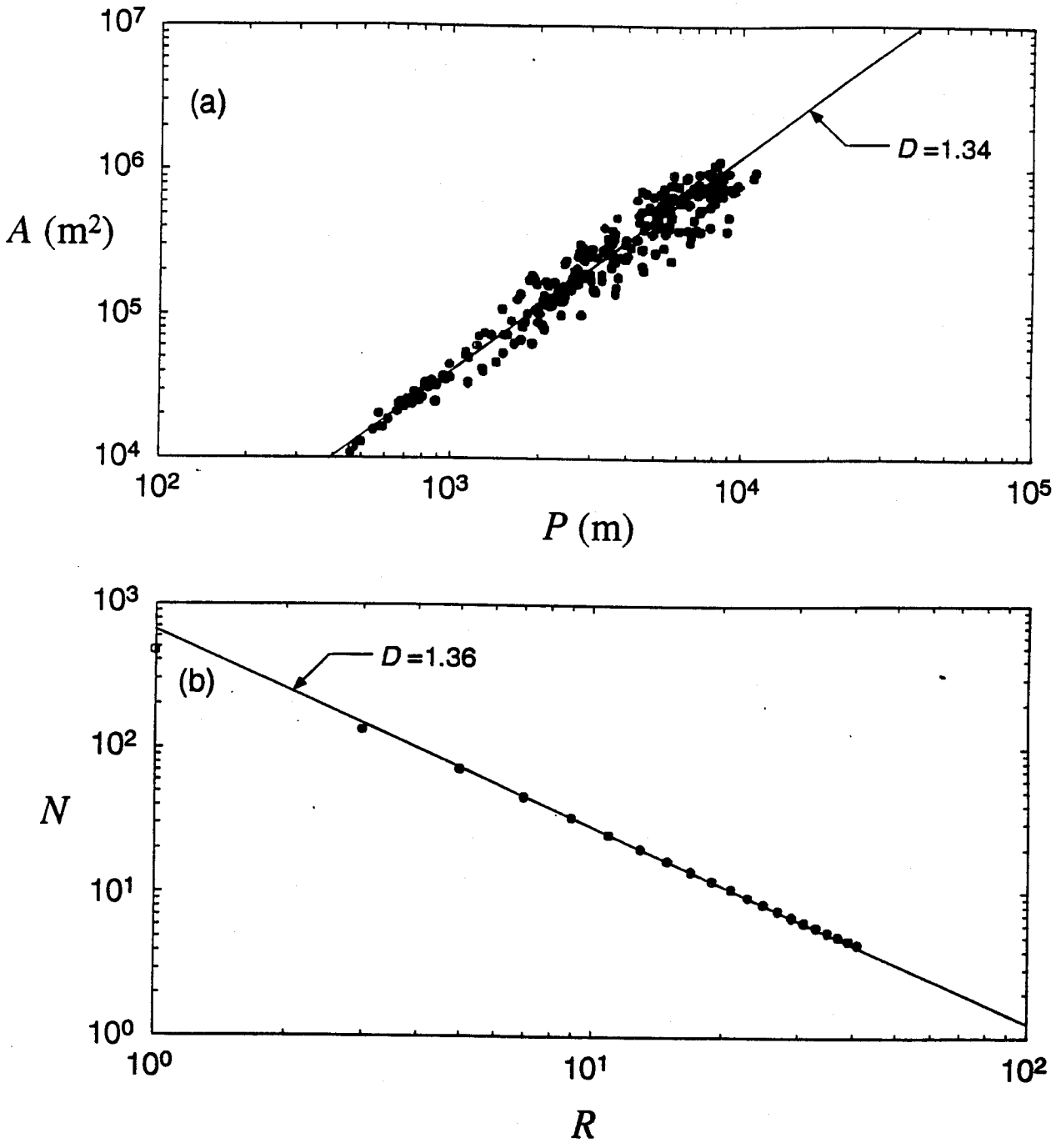

Figure 2. Fractal analyses of neutral boundary layer. (a) Perimeter-area analysis. P is perimeter in meters and A is area in square meters. (b) Box-counting analysis. R is normalized box size and N is the number of boxes counted.

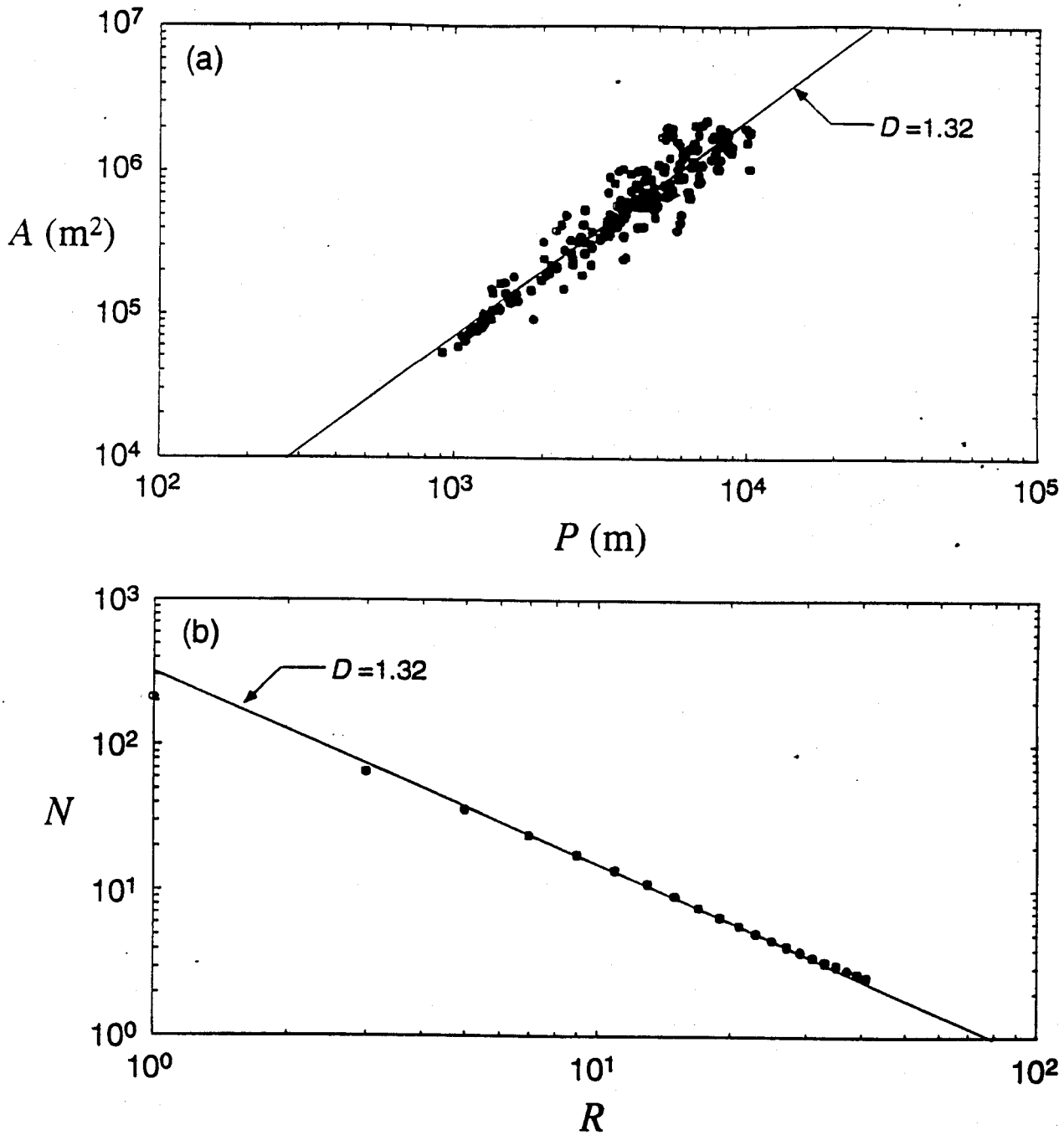

Figure 3. Fractal analyses of convective boundary layer. (a) Perimeter-area analysis. P is perimeter in meters and A is area in square meters. (b) Box-counting analysis. R is normalized box size and N is the number of boxes counted.

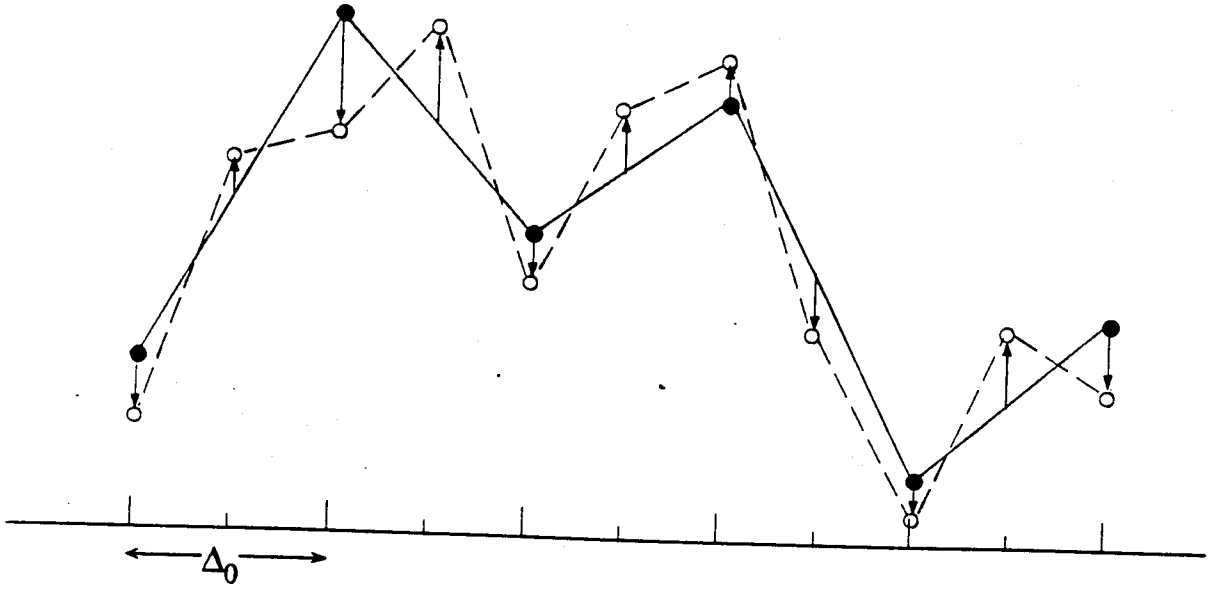

Figure 4. Schematic illustration of recursive refinement. Points on initial grid shown as solid circles with linear interpolation as solid line. First refinement shown as open circles with random displacement from first level function.

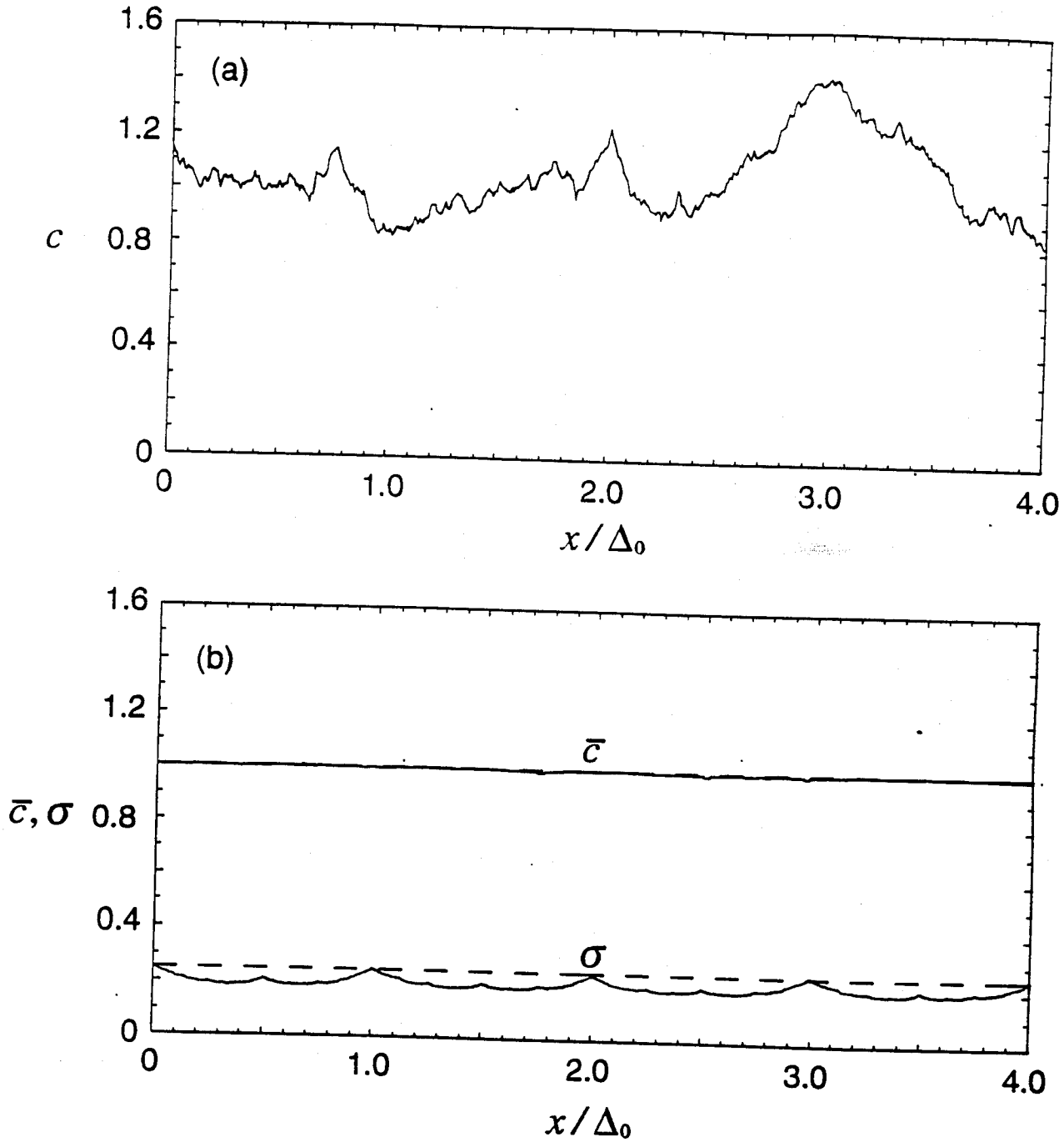

Figure 5. One-dimensional recursive refinement fractal generation for a homogeneous concentration field with $\sigma_c / \bar{c} = 0.25$. Solid lines are from fractal generation and dashed lines are the target statistics. (a) Individual realization. (b) Mean ($\bar{c}$) and r.m.s. fluctuation concentration (σ) from 1000 realizations.

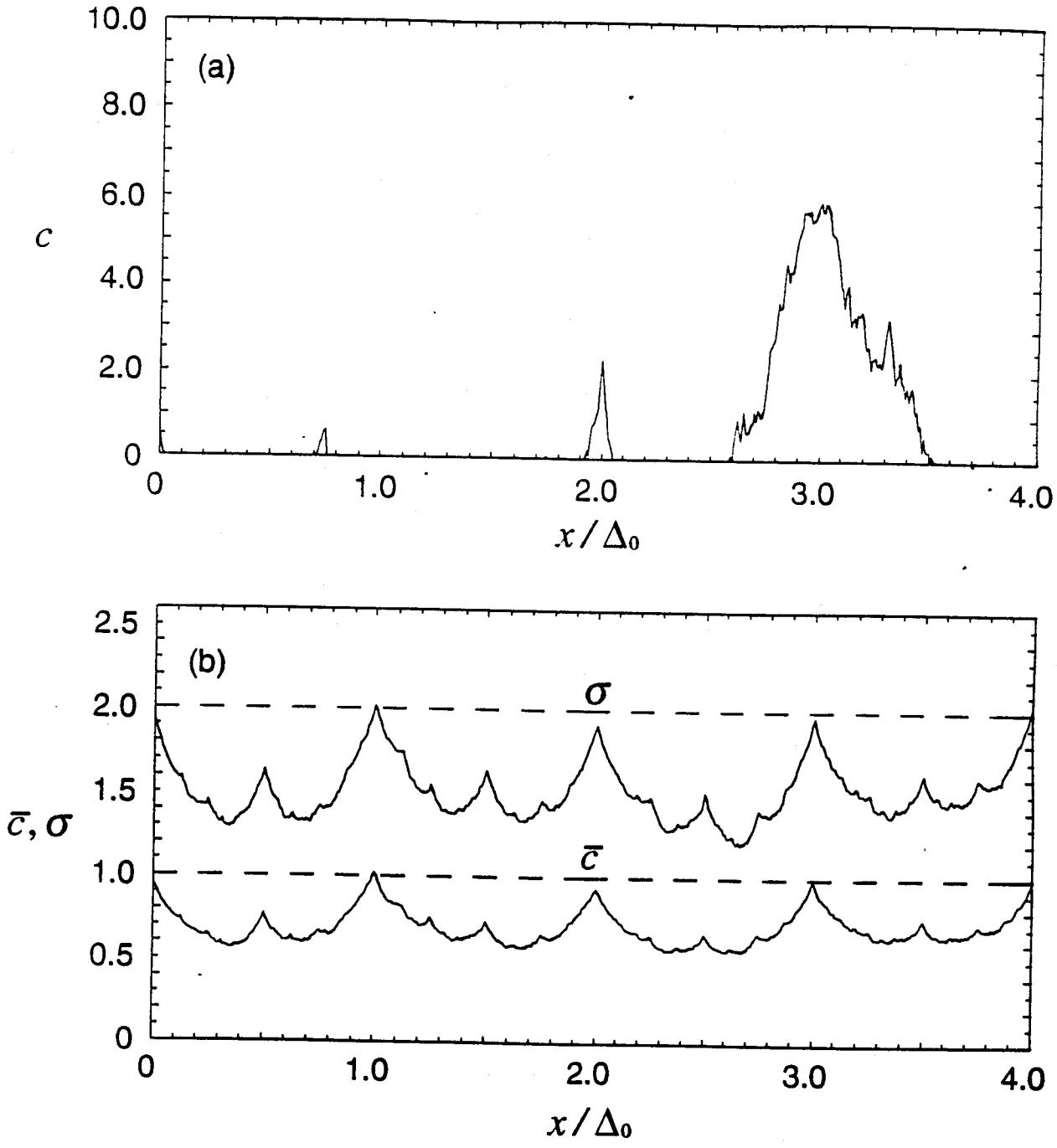

Figure 6. One-dimensional recursive refinement fractal generation for a homogeneous concentration field with $\sigma_c / \bar{c} = 2$. Solid lines are from fractal generation and dashed lines are the target statistics. (a) Individual realization. (b) Mean ($\bar{c}$) and r.m.s. fluctuation concentration (σ) from 1000 realizations.

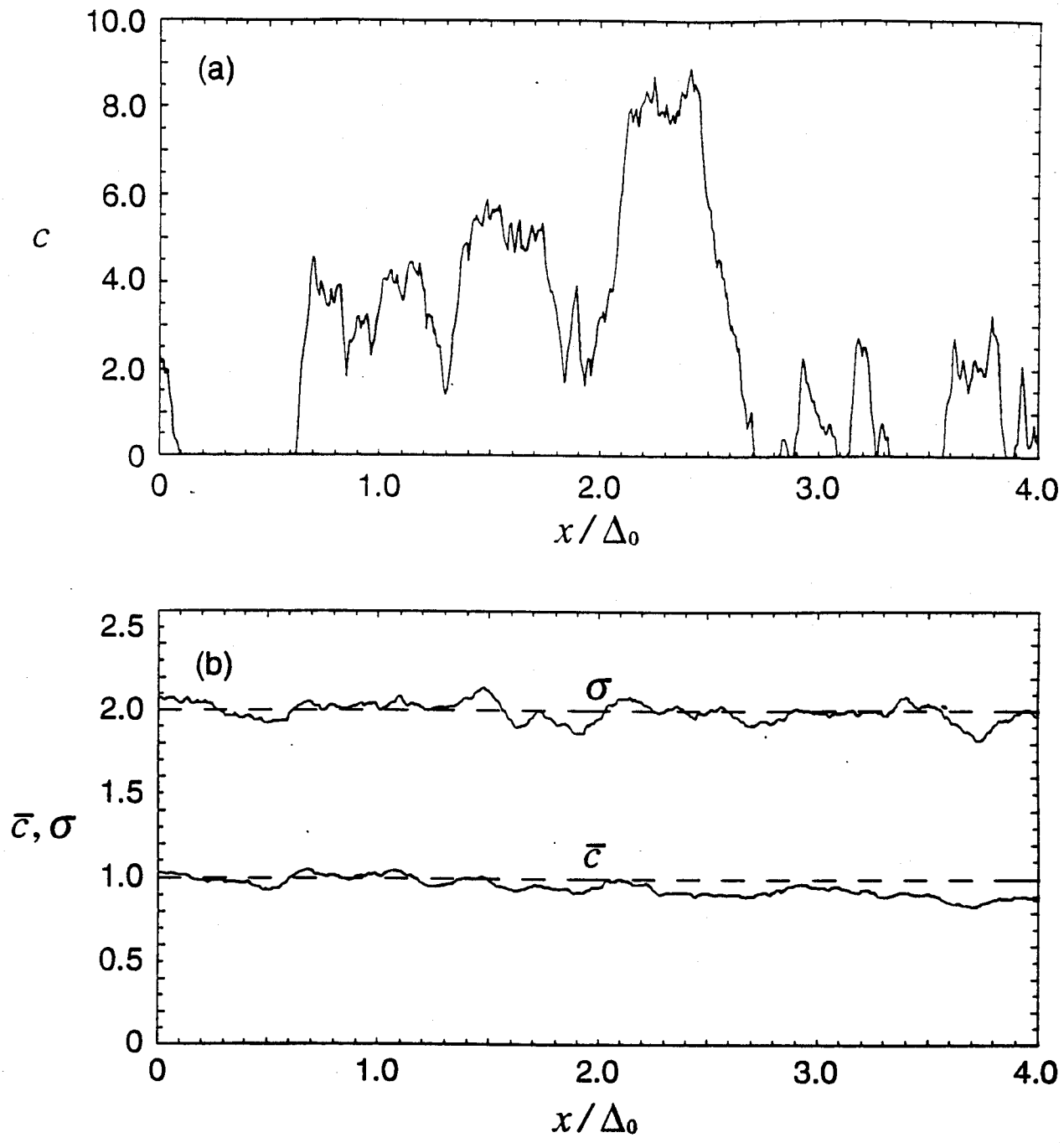

Figure 7. One-dimensional random pulse fractal generation for a homogeneous concentration field with $\sigma_c / \bar{c} = 2$. Solid lines are from fractal generation and dashed lines are the target statistics. (a) Individual realization. (b) Mean ($\bar{c}$) and r.m.s. fluctuation concentration (σ) from 1000 realizations.

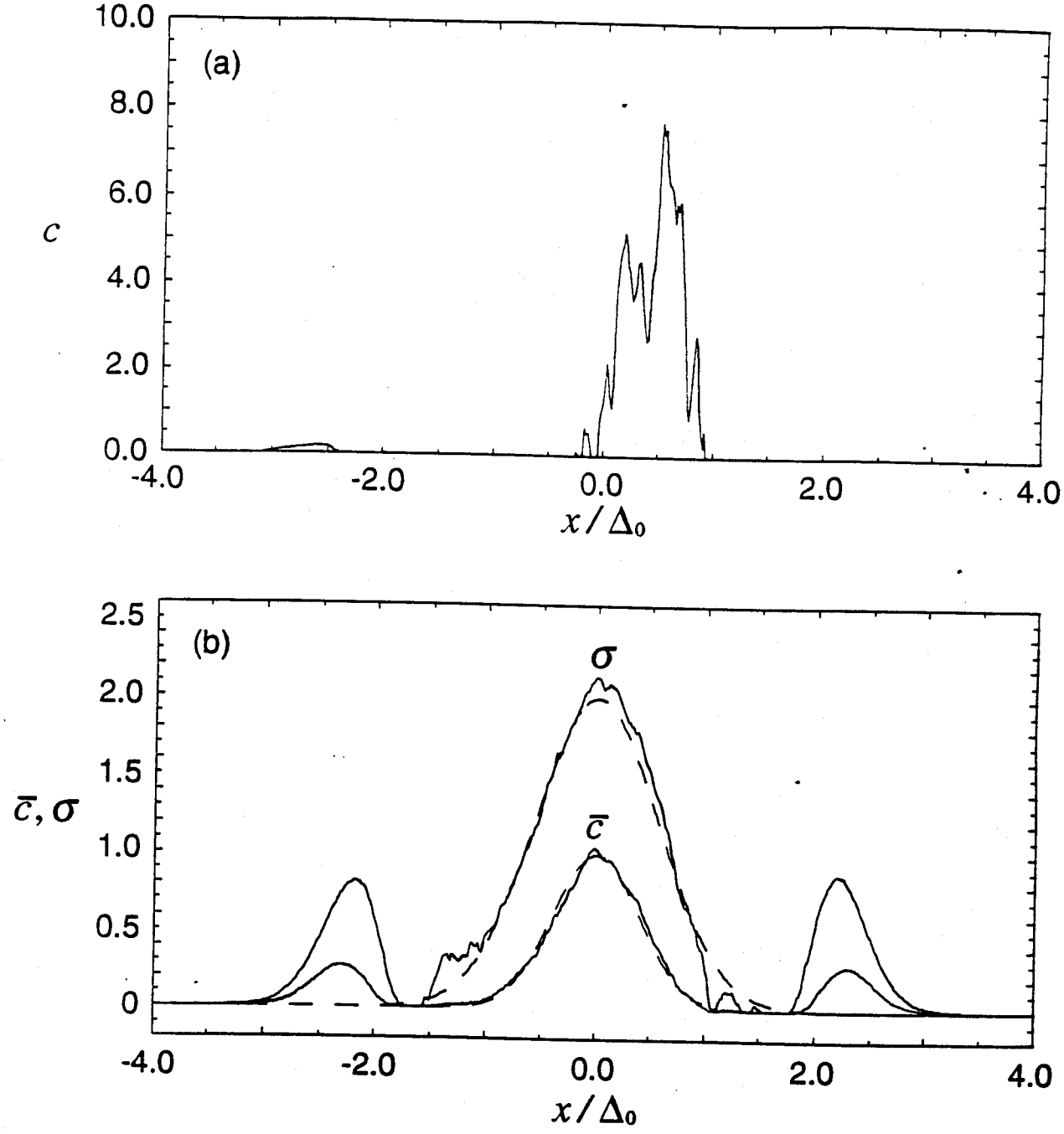

Figure 8. One-dimensional random pulse fractal generation for an inhomogeneous concentration field with $\sigma_c / \bar{c} = 2$ and no local scaling. Solid lines are from fractal generation and dashed lines are the target statistics. (a) Individual realization. (b) Mean ($\bar{c}$) and r.m.s. fluctuation concentration (σ) from 1000 realizations.

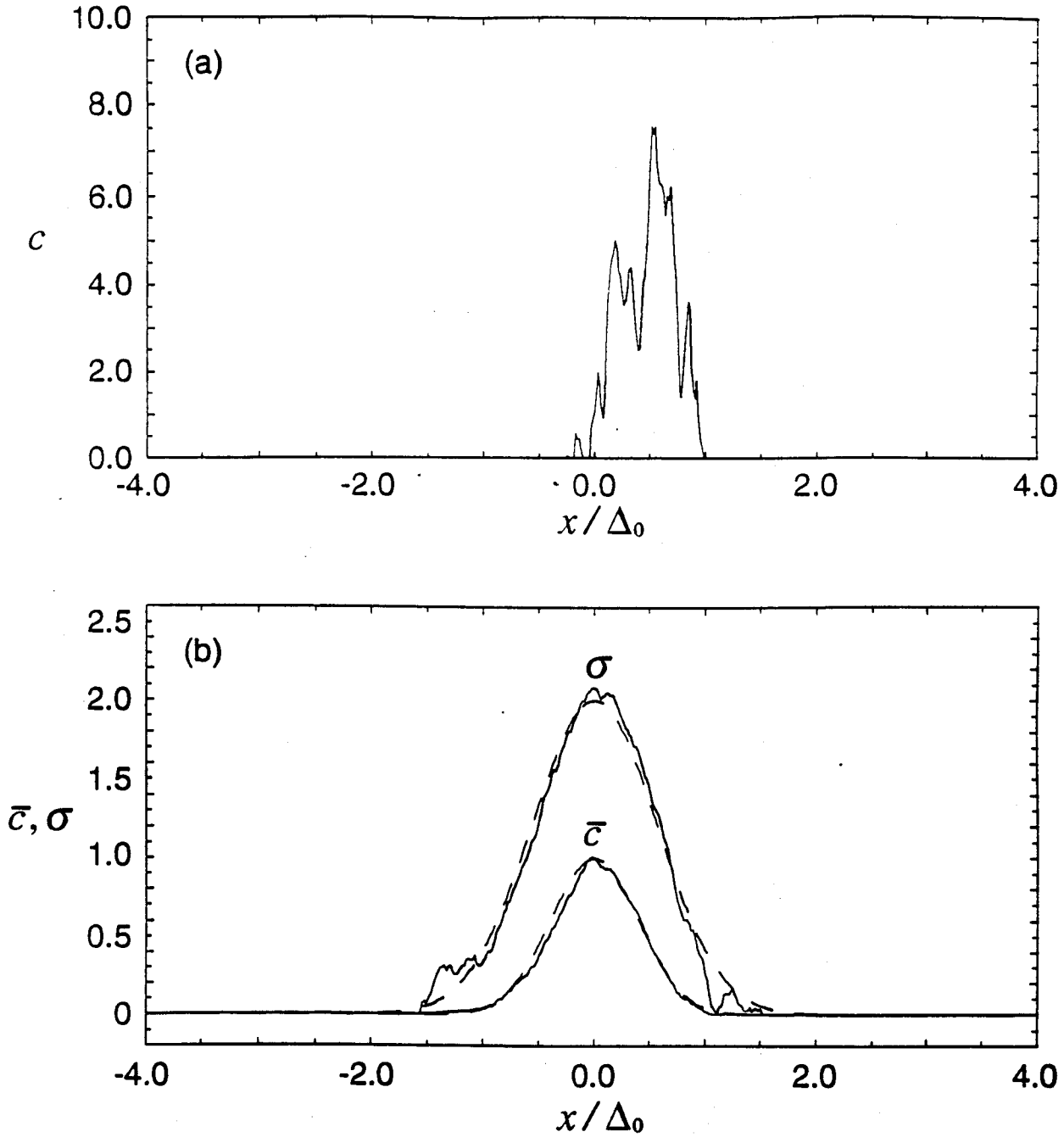

Figure 9. One-dimensional random pulse fractal generation for an inhomogeneous concentration field with $\sigma_c / \bar{c} = 2$ and local scaling. Solid lines are from fractal generation and dashed lines are the target statistics. (a) Individual realization. (b) Mean ($\bar{c}$) and r.m.s. fluctuation concentration (σ) from 1000 realizations.

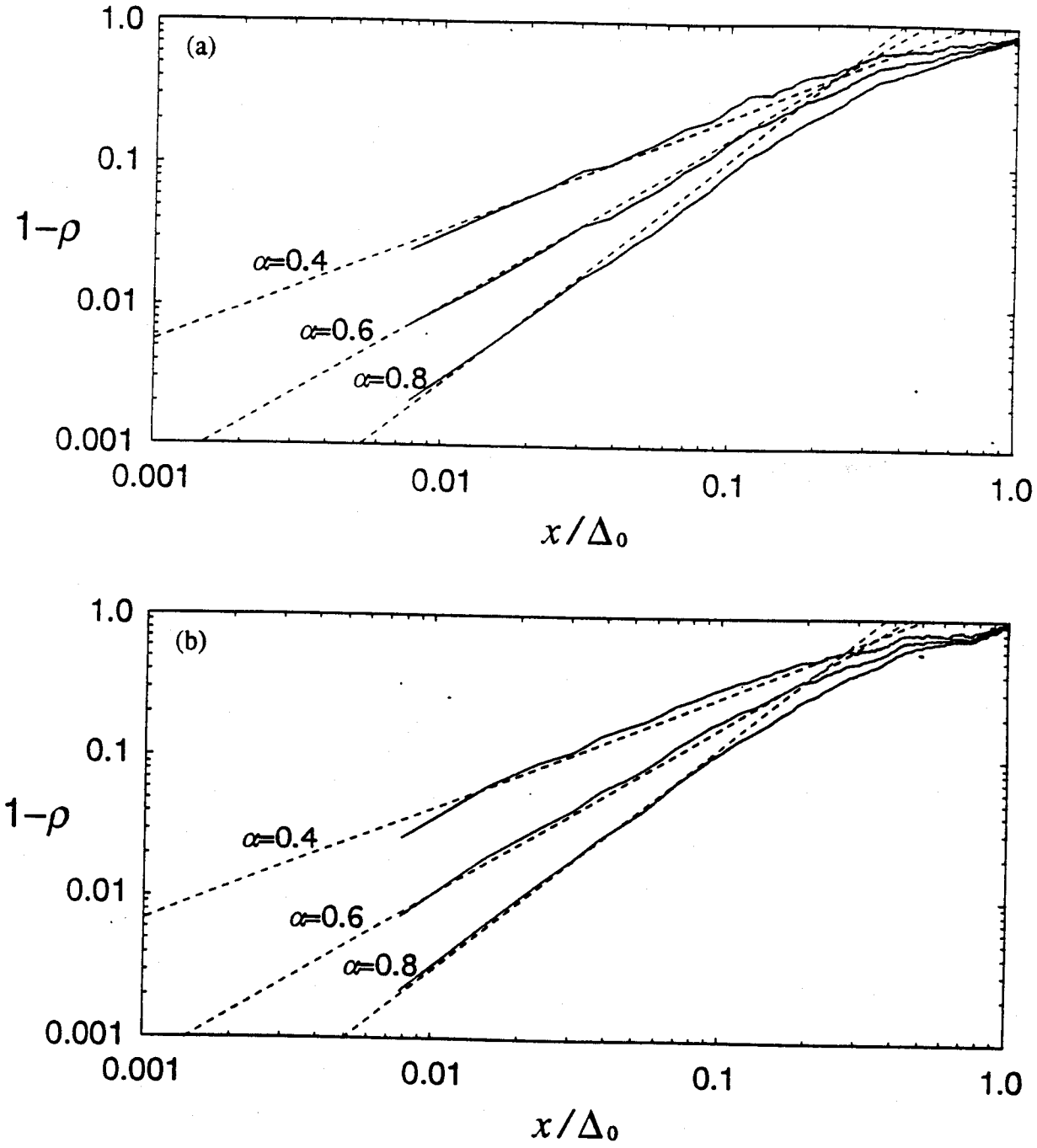

Figure 10. Correlation coefficient for one-dimensional fractal generation. Solid lines are from fractal model and dashed lines are theoretical values (slope=2α). (a) homogeneous concentration field. (b) inhomogeneous concentration field.

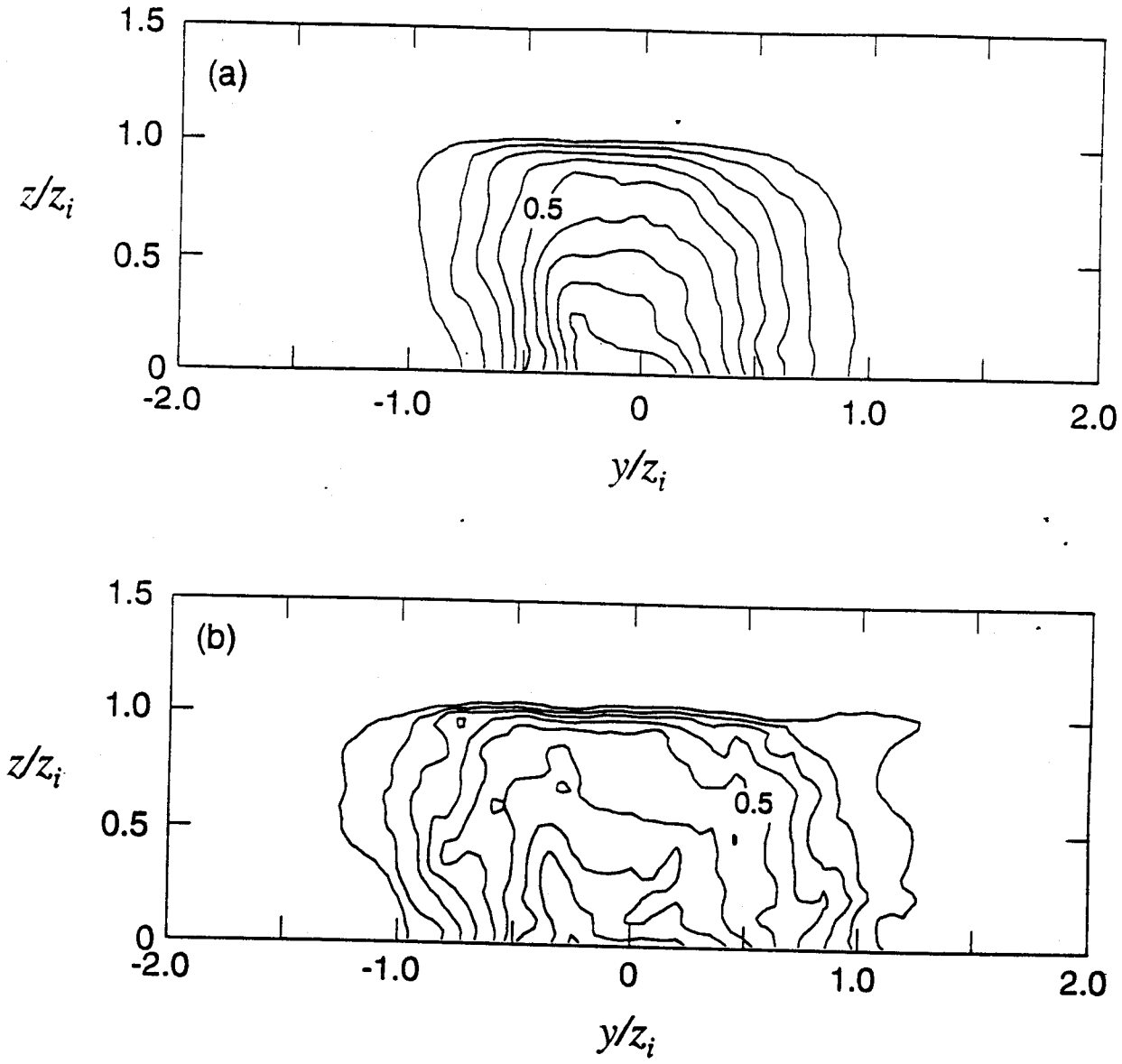

Figure 11. Transverse cross-section of the mean concentration and the r.m.s. fluctuation contours for convective boundary layer. Contours normalized by the maximum mean concentration ($\bar{c}_m$). Contour interval of 0.1. Downstream location is at x/z_i=8. (a) Mean concentration. (b) R.m.s. fluctuation.

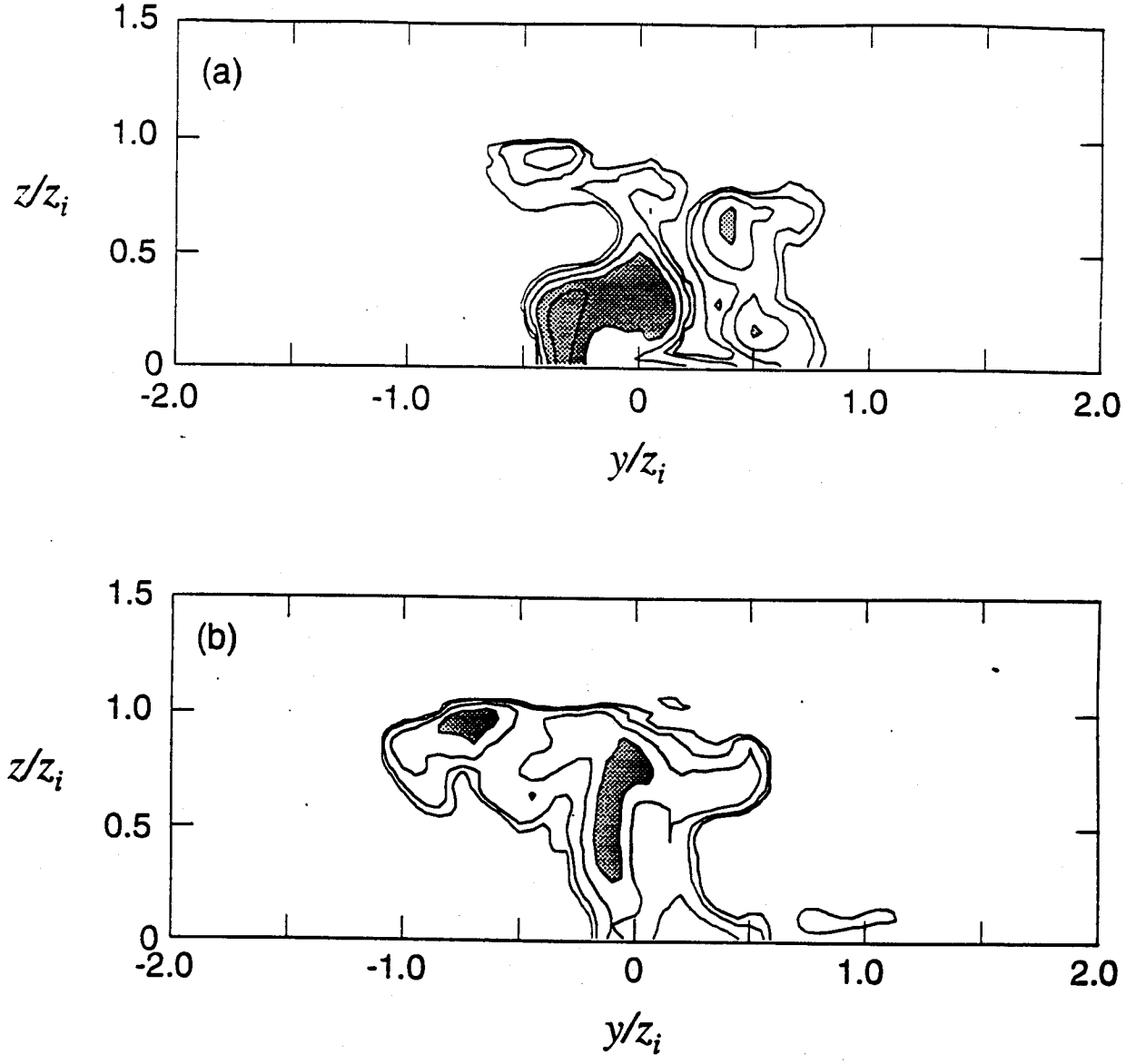

Figure 12. Two LES convective boundary layer realizations of $c / \bar{c}_m$ at x/z_i=8. Contours at 0.1, 0.2, 0.5, 1, and 2. Stippled areas are equal to or greater than 1.

A.R.A.P REPORT NO. 710

APPENDIX B

A Fractal/Multifractal Representation of the Small-Scale Structure in a Turbulent Plume

R. I. Sykes

R. S. Gabruk

D. S. Henn

ARAP Group, Titan Research and Technology Division

Titan Corporation

Princeton, New Jersey

Submitted to Journal of Applied Meteorology

July 1994

Abstract

An improved method for representing the small-scale structure of a turbulent scalar field using fractal recursion techniques is described. The model generalizes the fractal successive refinement method described by Sykes and Gabruk (1994) to include a more realistic description of the pseudo-dissipation field, i.e., the square of the scalar gradient. Turbulent dissipation fields are known to be multifractal, so a multifractal generation technique has been incorporated into the fractal refinement model to yield a scalar field with fractal iso-surfaces but with a multifractal pseudo-dissipation field.

The model fields are compared with LES realizations of turbulent scalar dispersion and shown to provide improved agreement with the small-scale structure. The simple combination of fractal and multifractal properties employed in the model also provides insight into the structural nature of the random scalar field. Finally, the generation technique is completely localized in physical space and is therefore applicable to inhomogeneous fields.

1. Introduction

The complex structure of the scalar concentration field as it is dispersed in a turbulent flow has been extensively studied using the techniques of fractal geometry. Initial attempts to characterize the concentration field were based on analyzing the 'cloud boundary' from photographic data (e.g., Lovejoy 1982; Rys and Waldvogel 1986; Prasad and Sreenivasan 1990a) and used the classical 'perimeter-area' relations or 'box-counting' methods of fractal geometry (Mandelbrot, 1982). For a fractal boundary, there is a power-law increase in the length of the boundary as it is increasingly resolved in finer detail. This type of analysis can only be applied to sets of points, in this case the boundary of a cloud, and cannot give a complete description of the function, $c(\boldsymbol{x})$, i.e., the concentration value as a function of spatial location, $\boldsymbol{x}$. More recently, the multifractal has been introduced (Benzi et al. 1984; Frisch and Parisi 1985; Halsey et al. 1986; Meneveau and Sreenivasan 1987a) to characterize the behavior of intermittent fields such as the turbulent kinetic energy dissipation. The definition of a multifractal involves the functional behavior of the field, and therefore gives a more complete description than conventional fractal analysis.

While the fractal boundary analysis can be criticized as incomplete since it attempts to characterize a field through examination of level sets or isosurfaces, this is still the predominant description of the concentration field. Sreenivasan (1991) reviews many of the fractal turbulence results, and makes a clear distinction between isosurface analysis of the concentration field and multifractal analysis of the dissipation field. The reason for the distinction lies in the nature of the multifractal spectrum, which is a way of describing the distribution of singularities in a field.

We now present a brief discussion of the multifractal spectrum. See Sreenivasan (1991) and Feder (1988) and references therein for greater detail. If we consider a

measure of the field χ, e.g. the scalar dissipation, the total measure inside a subregion Ω_r of characteristic size r (a sphere of radius r for example) is given by

$$X_r = \int_{\Omega_r} \chi(\mathbf{x}) d^d x \tag{1}$$

where there superscript d denotes the space dimensionality. The multifractal formalism asserts that

$$X_r / X_L \sim (r/L)^{\alpha} \tag{2}$$

where X_L represents the dissipation within the total domain Ω_L. The exponent α depends on the position of the subregion since the multifractal scaling is strictly local and is associated with the strength of singularities. This can be seen by noting that $X_r \sim r^{\alpha}$ implies $\chi \sim r^{\alpha - d}$ which diverges for $\alpha < d$, with smaller values of α associated with narrower spikes. Assuming that the entire measure is made up of an infinite number of iso-α sets, one attempts to relate the number of r-sized subregions (or "boxes") with α -strength singularities in a bandwidth $d\alpha$:

$$N(\alpha) d\alpha \sim \rho(\alpha) (r/L)^{-f(\alpha)} d\alpha \tag{3}$$

where $\rho(\alpha)$ is some α-dependent prefactor. Here, $f(\alpha)$ is the singularity or multifractal spectrum; it is analogous to the fractal dimension for simple self-similar measures (where $N(r) \sim r^{-D}$), but is a function of the singularity strength. (Thus, the measure is made up of a multiplicity of fractal sets or multifractals.)

This definition is appropriate for singular fields, such as the energy dissipation, where the classical power spectrum diverges at high wavenumber and the localization of the dissipation in the smallest scales is properly described by the multifractal spectrum. While this is precisely the measure required for description of the dissipation field, it is not appropriate for a scalar concentration field, which is usually finite at every point in space and exhibits a convergent power spectrum. In fact, the multifractal spectrum of the

scalar field, which has been shown to have a simple fractal measure, is simply a single point.

Another way of examining a multifractal measure, which turns out to be convenient for analysis, is through moment exponents or generalized dimensions. Multifractal measure obey a power law relationship given by (e.g. Prasad and Sreenivasan 1990)

$$\sum (X_r/X_L)^q \sim (r/L)^{(q-1)D_q} \tag{4}$$

where D_q can be identified as the generalized dimension of Hentschel and Procaccia (1983). For $q > 0$, the sum on the left is increasingly dominated by larger peaks as q increases, whereas for $q < 0$, the sum is increasingly dominated by regions which tend towards zero as q decreases. Halsey et al. (1986) show that the (q,D_q) analysis can be related to the multifractal spectrum by the following Legendre-transform relations:

$$\alpha(q) = \frac{d}{dq}\left[(q-1)D_q\right] + 1 - d \tag{5a}$$

$$f[\alpha(q)] = q[\alpha(q) - 1 + d] - (q-1)D_q \tag{5b}$$

The functional description of the dissipation field as a multifractal is more complete than the iso-surface fractal description, and has lead several researchers to the view that a scalar field should be constructed from a properly defined dissipation field. Thus, Wilson, et al. (1991) and Tessier, et al. (1993) invoke 'fractional integration' to derive a scalar concentration field from a dissipation field that has been generated using multifractal techniques. Unfortunately, the definition of the dissipation as the square of the concentration gradient necessarily involves loss of information, and the concentration field cannot be determined without arbitrary assumptions. In fact, the fractional

integration is carried out in Fourier space and does not maintain the correct local relation between the dissipation field and the concentration gradient.

The correct relation between the concentration and dissipation fields can only be maintained by generating a scalar concentration field with the proper gradient behavior. We therefore begin with a technique for producing the concentration field and investigate ways of improving the dissipation field representation. The next section briefly reviews the fractal generation method of Sykes and Gabruk (1994) and examines the dissipation results from this simple model. Section 3 describes an extension of the model with an improved description of the dissipation field and compares the results with laboratory measurements of turbulent jets. In Section 4 large-eddy simulations (LES) of a plume dispersing in a neutral boundary layer are analyzed and compared with the new model.

2. The Recursive Refinement Model

Sykes and Gabruk (1994) present a fractal generation scheme for representing the scalar concentration field in a dispersing plume of material using the technique of successive refinement. The basic methodology consists of adding random pulses on successively smaller spatial scales with appropriately scaled variance, and is given in Peitgen and Saupe (1988) and Feder (1988) as one of the methods for generating fractional Brownian motion. Sykes and Gabruk (1994) modify the original scheme to randomize the location of the pulses in order to give accurate representation of the scalar field variance. They show how the method can be adapted to represent an inhomogeneous field and can provide either lognormal or clipped-normal one-point probability density functions. The scheme is compared with LES results for turbulent plume dispersion from Sykes and Henn (1992) and Henn and Sykes (1992), and shown to

give good agreement with the fractal iso-surface results and also qualitative agreement with the instantaneous plume structure.

The fractal generation scheme for a homogeneous scalar field, $c(x)$, can be written schematically in the form

$$c(x) = \bar{c} + \sum_n \sum_i a_{ni} P_n(x - x_{ni}) \tag{6}$$

where the overbar denotes the ensemble average, n represents the refinement level, and i represents the range of overlapping pulse functions that contribute to the concentration fluctuation at the location x. The pulse function, $P_n(x - x_{ni})$, is triangular in this scheme and centered at x_{ni} with a half-width of Δ_n, where $\Delta_n = 2^{-n}\,\Delta_0$. The pulse amplitude a_{ni} is chosen randomly from a Gaussian distribution with zero mean and standard deviation σ_n, where $\sigma_n = 2^{-nH}\sigma_0$. The relationship of the initial variance σ_0^2 to the ensemble variance is given in Sykes and Gabruk (1994). The fractal dimension of the field is controlled by the parameter, H, which is the co-dimension and is set to 0.65 based on the LES results. The fractal dimension of a level surface in a two-dimensional cross-section is then 2–H; it is 1-H for a time series . A non-negative concentration field is generated by truncated negative values of c at zero (giving a clipped-normal distribution), or by exponentiating c (giving a lognormal distribution). The clipped-normal and lognormal parameters are defined in Sykes and Gabruk (1994).

Since it has been shown experimentally by Prasad et al. (1988) and Prasad and Sreenivasan (1990b) that the scalar dissipation field is multifractal, we now investigate the multifractal properties of the generated fields by examining the pseudo-dissipation field, $\chi = \left(\delta c/\delta t\right)^2$. The recursive refinement model (6) can be implemented in arbitrary spatial dimension by defining the appropriate pulse functions, P_n. Examples of one-dimensional concentrations fields and the corresponding dissipation fields from clipped-normal and lognormal distributions with unit mean and variance are shown in Figs. 1 and

2, respectively. In these idealized cases, a periodic field is generated on a unit domain with an initial grid size of Δ_0=0.25. The fields shown are typical fractal generation realizations. Other than the clipped regions, the scalar fields are quite similar. Furthermore, χ appears almost uniformly noisy except in areas of very low (or zero) concentration. This result is contrary to the intermittent character observed in various flow fields as noted in Prasad et al. (1988) and Prasad and Sreenivasan (1990b) and implies that the fractal model does not produce a multifractal dissipation field.

The absence of multifractal behavior is confirmed by a moment analysis of the dissipation field generated by the fractal model. Intermittent fields can be quantified by the behavior of various moments of the spatially-averaged dissipation field as described in Section 1. By way of using (4), we define

$$M_q(r) = \sum (X_r/X_L)^q \qquad (7)$$

where X_r denotes the sum of χ over r time increments, δt. In order to demonstrate the use of (4) and (7) in multifractal analysis, one-dimensional realizations 8 times longer than those shown in Figures 1 and 2 were created. We could perform a multifractal analysis on the actual dissipation fields shown in the figures, however, a longer time series is more illuminating since it covers a wider scaling range. Figures 3 shows log-log plots of $M_q^{1/(q-1)}$ versus r for typical clipped-normal and lognormal realizations. The moment curves of a multifractal measure appear linear when plotted in this way so the slope of the log-log curve then gives the generalized dimension D_q. Only the positive moments are shown because M_q is undefined for $q < 0$ when $c = 0$ for the clipped-normal distribution. For the larger scales the moment curves indicate monofractal behavior since they show the same slope of D_q for all q. However, at the smaller scales, the curves diverge and appear to be nonlinear. (This may be due to numerical resolution problems rather than indicating

any particular behavior.) These results are in contrast to the experimental observations of Prasad et al. (1988) and Prasad and Sreenivasan (1990b). Therefore, a different generation scheme is required to produce a dissipation field that is consistent with those observations.

3. Generation of a Multifractal Dissipation Field

Multifractal fields can be generated using a very simple multiplicative cascade process. This method has been applied in the so-called 'p-model' of the turbulent kinetic energy dissipation field structure by Meneveau and Sreenivasan (1987b). The p-model simply involves unequal division of an initially uniform field among the subdivided cells in a recursive refinement process. Thus, in a one-dimensional model, when a cell is divided into 2 equal length sub-cells, one cell receives a fraction p of the value in the original cell, while the other receives a fraction $1-p$. The process is randomized by assigning the fraction p to either cell with probability 0.5; it is assumed that $p \geq 0.5$. The process is repeated with fixed p until the smallest scale is reached. It obviously conserves the total integral of the field. This model concentrates the dissipation field into localized regions, and has been shown to give a multifractal (Benzi et al. 1984).

The p-model is useful for generating a representation of the dissipation field, but our objective is the generation of a scalar concentration field which possesses the proper dissipation field structure. As mentioned in Section 1, Wilson et al. (1991) and Tessier et al. (1993) have used the multifractal representation of the dissipation field to obtain a scalar concentration field by means of 'fractional integration'. Although it does preserve the definition of the dissipation as the square of the concentration gradient, the procedure is apparently an arbitrary filtering technique. Furthermore, it is also performed in Fourier space, which makes its application to inhomogeneous fields difficult. The p-model, on the other hand, is completely localized in space and we therefore seek to

incorporate some of the features of the p-model into the recursive refinement technique, (6), as a means of improving the dissipation field representation.

The basis of the refinement technique is the addition of random pulses at each of a succession of smaller scales. The amplitude of the pulses is chosen randomly from a distribution with a specified variance. The fractal dimension of the field is determined by the rate at which the variance decreases with the scale of the pulses. This procedure clearly allocates fluctuation variance uniformly among the pulses at each scale, and produces the non-intermittent dissipation result illustrated in Figs. 1b and 2b. Since the dissipation field is dominated by the smallest scales, we can incorporate intermittency by using the p-model to allocate variance at each level of refinement. Thus, instead of simply defining

$$\sigma_{n+1}^2 = 2^{-2H}\sigma_n^2 \tag{8}$$

where n refers to the refinement level, we define a local value for each pulse as

$$\sigma_{n+1}^2 = 2^{1-2H}\sigma_n^2 p' \tag{9}$$

where p' is randomly chosen from the pair $\{p, 1-p\}$, and σ_n^2 refers to the variance in the 'parent' cell of the refinement. Each parent cell is divided into 2^d 'offspring' cells with half allocated the variance defined by (9) and the other half allocated the same variance with p' replaced by $1-p'$. The p'-factor is multiplicative since it is applied at each level of refinement, but the ensemble average variance is conserved by (9). The variance definition contains a factor $2p'$, which clearly has an average value of unity.

The scheme defined by (6) and (9) consists of a sum of pulses with random amplitudes drawn from a local distribution determined by a multiplicative process . That is, the p-model is used to determine the local variance for the random pulse amplitude, and therefore the smaller scales can be expected to become increasingly intermittent. On

the other hand, the concentration field is obtained from the sum of all the pulses and so will not be dominated by small scale intermittency. The sum is convergent everywhere provided $p < 2^{2H-1}$, which is trivially satisfied if $H > 0.5$. Examples of time series generated by the new model with $p = 0.80$ are presented in Figs. 4 and 5. The value of 0.80 was chosen to give a good fit to the multifractal spectrum (shown below) measured by Prasad et al. (1988). It is to close the value of 0.70 used by Meneveau and Sreenivasan (1987b) in modelling the turbulent kinetic energy dissipation and 0.75 mentioned by Sreenivasan (1991) for scalar dissipation, although in these cases the actual dissipation rates are being split instead of variance. The concentration time series look similar to the fractal model results in Figs. 1a and 2a, but the χ realizations are clearly more intermittent. The intermittency is confirmed by the moment analysis, shown in Figure 6, which now shows evidence of multifractal structure. Typical log-log plots of the moment curves show distinct linear regions over 2 orders of magnitude as well as a variation of slope with q, all in contrast the original fractal model results. As with the original fractal model analysis, time series 8 times longer than those shown in the figures are used to compute the moment curves. The linear range appears to hold down to $r \cong 16$, i.e., 8 times the smallest pulse width. Below this size, the number of grid refinements is inadequate to make reliable estimates of M_q.

The model-generated multifractal spectra, $f(a)$, for both the clipped-normal and lognormal distributions are shown in Figure 7. These are determined using (5a,b) with averaged estimates of D_q from 100 realizations. The fractal/multifractal generation scheme gives a very good representation of the spectrum of Prasad et al. (1988). This is important since Prasad and Sreenivasan (1990b) suggest that the scalar dissipation multifractal spectrum is universal for high Reynolds numbers based on turbulent jet and wake experiments. Similarly, Meneveau and Sreenivasan (1987a, 1991) show the universality of the kinetic energy dissipation multifractal spectrum based on

measurements from wind tunnel boundary layers, wakes, grid turbulence and the atmospheric surface layer.

The analysis of the complete fractal/multifractal model is complicated by the summation of the random pulses from a multiplicative cascade process. However, the multifractal behavior of the pseudo-dissipation field can be understood as a result of the emphasis of the small scales by the gradient operator. Although the series for the concentration field is convergent, provided $p < 2^{2H-1}$, the series for the concentration gradient is divergent for $H < 1$. The dissipation field is therefore dominated by the smallest scales under consideration, and therefore exhibits the properties of the standard p-model without summation. The concentration field itself is non-singular and is more strongly influenced by the larger scale features which contain more variance.

As given above, (6) and (9) are applicable to higher dimensions so we now examine two-dimensional plume cross-sections generated by the fractal/multifractal model. Realizations of c and χ from the clipped-normal and lognormal distributions are shown in Figs. 8 and 9. The clipped-normal scalar field is characterized by broad areas of either fairly high or zero concentration. The lognormal distribution results in relatively few, isolated regions of high concentration surrounded by broad areas of small (but non-zero) concentration. The pseudo-dissipation fields from both distributions show many narrow spikes, but the lognormal distribution tends to produce them in the isolated regions associated with higher concentration levels. The distribution of spikes in χ from the clipped-normal distribution tends to mirror that of c in that are they fairly uniformly distributed over the regions where $c > 0$.

The multifractal moment curves from the two-dimension simulations are given in Fig. 10 and the resulting multifractal spectra in Fig. 11. The moment curves are determined from realizations in a domain 4 times that shown in the Figs. 8 and 9. The

multifractal spectra are essentially averages from 25 such realizations. The moment curves show well-defined linear regions over approximately 2 decades, allowing reliable estimates of D_q. The multifractal spectra for the two distributions are quite similar and also show good agreement with the spectrum presented in Prasad et al. (1988). So although both clipped-normal and lognormal distributions as used in this model produce fields consistent with the universal spectrum, the pseudo-dissipation fields do have somwhat different characteristics. Thus it is important that the correct distribution be known.

3. Comparison with LES data

Sykes and Gabruk (1994) present a fractal analysis of the LES neutral boundary layer plume calculations of Sykes and Henn (1992). That analysis is augmented here by examining the LES-generated pseudo-dissipation field and comparing it with realizations generated with the new fractal/multifractal model. However, it should be noted that the LES results only cover a limited scaling range of just over one decade and so estimates of the generalized dimensions may not be as reliable as in the idealized cases presented in the previous section.

Figures 12 and 13 show one-dimensional time series of c and χ from the LES calculations and a realization generated with the new technique, respectively. The LES time series is taken from a location on the plume centerline at $x/H = 6.67$ (x is the downstream distance from the source) and at the release height of $0.19H$, where H is the boundary layer height . The fluctuation intensity ratio, $\sigma_c/\bar{c}$, is 1 where σ_c is the standard deviation of the concentration fluctuations. The lognormal distribution is used in the fractal generation since that is consistent with the LES-generated distribution at this location. Time is normalized by the autocorrelation time scale τ_c. For the LES,

$\tau_c \cong 0.2H/U_\infty$, where $U_\infty$is the wind speed above the boundary layer. For the fractal model realization, $\tau_c = 0.33\,\Delta_0$ is assumed (Sykes and Gabruk 1994). Since $\Delta_0 = 2^n \Delta t_{LES}$, where n is some positive integer and the LES timestep $\Delta t_{LES} \cong 0.14\tau_c$, τ_c for the model is about three-quarters that of the LES.

The fractal realization is similar qualitatively in character to the LES time series for both c and χ. It can be seen that the spikes of χ in both series are very similar in frequency, duration and amplitude. The similarities are confirmed by the multifractal spectra given in Fig. 14. The LES spectrum is determined from average D_q calculated from 30 segments lasting 16 timesteps . The segments are limited to this duration since fractal/multifractal behavior is not expected for scales much greater than τ_c.

Analyzing two-dimensional LES plume cross-sections and generating corresponding model realizations is somewhat problematic since the cross-sections are inhomogeneous and the multifractal analysis is strictly valid only for homogeneous fields. And it is shown in Sykes and Gabruk (1994) that it is important to use the local variance in simulating inhomogeneous plume cross-sections. Therefore, only relatively small boxes (16x16 LES grid cells) fully contained within the plume are used for analysis so that the regions are "nearly" homogeneous. An LES-generated plume cross-section at $x/H = 5$ and a corresponding model realization are shown in Fig. 15. It should be noted that the model realization utilizes the local mean and variance determined from the LES. The realizations appear similar to one another as well as to the simple fractal model results in Sykes and Gabruk (1994). This is confirmed by the fact that the fractal dimensions of the LES and model-generated plumes are the same as that reported by Sykes and Gabruk (1994), namely 1.36 for the LES and 1.30 for the fractal model. (These represent averages from 6 and 100 realizations, respectively.)

Multifractal analysis of χ also confirms the similarity between LES and fractally generated realizations. This can be seen in the multifractal spectra given in Fig. 16. The fractal/multifractal model results compare very well with the data of Prasad et al. (1988). The LES spectrum goes to zero at slightly larger α than the model or experimental spectra, indicating a less intermittent dissipation field. However, given the limited scaling range and the concomitant uncertainty in D_q, the LES spectrum is reasonably close to the experimental results.

5. Concluding Remarks

It has been shown that the scalar pseudo-dissipation field derived from the fractal generation scheme of Sykes and Gabruk (1994) fails to exhibit the intermittent, multifractal behavior observed in experimental measurements of scalar dissipation fields (Prasad and Sreenivasan 1990b). Therefore, an extension to the fractal model is sought which will produce a multifractal dissipation field while maintaining the simple fractal nature of the scalar field. Noting that a simple binomial multiplicative cascade process produces intermittent distributions and has been shown to agree well with measurements of turbulent kinetic energy dissipation (Meneveau and Sreenivasan 1987b), a model is constructed which randomly allocates *variance* unequally in a fixed ratio to successive levels of refinement. Since the scalar field is made up of a summation of random pulses from many refinement levels of decreasing variance, it is dominated by the larger scale structures that contain most of the variance. The fractal behavior of the scalar field is maintained since the average variance at each level of iteration is still controlled by the co-dimension and, thus, the power spectra remains unchanged. However, the gradient operator involved in calculating the pseudo-dissipation field emphasizes small scales. In fact, the summation of pulse *gradients* diverges, so that the pseudo-dissipation field

becomes highly intermittent and exhibits multifractal behavior. An important feature of the model is that it is completely local so that it may be applied to inhomogeneous fields.

Idealized time series are generated with the new fractal/multifractal model using clipped-normal and lognormal distributions to define the pulses. An analysis of these show that the resulting multifractal spectra agree very well with the (assumed) universal spectrum derived from measurements of turbulent jets and wakes (Prasad and Sreenivasan 1990b), even though the pseudo-dissipations fields from the two distributions are somwhat different in character.

An analysis of LES neutral boundary layer plumes shows that the pseudo-dissipation fields reveal multifractal behavior, although the scaling range is limited. Application of the fractal/multifractal model using the LES statistics yields plumes realizations which are similar in appearance to the LES realizations. The fractal dimensions of plume isosurfaces from the LES and model are close (1.36 and 1.30 respectively); the model dimension is unchanged from the simple fractal model results given in Sykes and Gabruk (1994). The LES multifractal spectrum is close to the model and experimental spectra, although it may indicate less intermittency in the LES pseudo-dissipation fields. However, given the uncertainty resulting from the small scaling range, the match with the presumed universal spectrum is reasonably good.

Acknowledgment

This work was supported by the Army Research Office under contract number DAAL03-92-C-0020.

References

Benzi, R., G. Paladin, G. Parisi and A. Vulpiani (1984), "On the multifractal nature of fully developed turbulence and chaotic systems", *J. Phys. A*, **17**, 3521-3531 .

Feder, J. (1988), *Fractals*, Plenum, New York

Frisch, U. and G. Parisi (1985), "On the singularity of fully developed turbulence", *Turbulence and Predictability in Geophysical Fluid Dynamics and Climate Dynamics*, ed. M. Ghil, R. Benzi and G. Parisi, North-Holland, Amsterdam

Halsey, T. C., M. H. Jensen, L. P. Kadanoff, I. Procaccia and B. I. Shraiman (1986), "Fractal measures and their singularities: the characterization of strange sets", *Phys. Rev. A*, **33**, 1141-1151 .

Henn, D. S. and R. I. Sykes (1992), "Large-eddy simulation of dispersion in the convective boundary layer", *Atmos. Env.*, **26A**, 3145-3159 .

Hentschel, H. G. E. and I. Procaccia (1983), "Fractal nature of turbulence as manifested in turbulent diffusion", *Phys. Rev. A*, **27**, 1266-1269 .

Lovejoy, S. (1982), "Area-perimeter relation for rain and cloud areas", *Science*, **216**, 185-187 .

Mandelbrot, B. B. (1982), *The fractal geometry of nature*, W. H. Freeman and Co., New York

Meneveau, C. and K. R. Sreenivasan (1987a), "The multifractal spectrum of the dissipation field in turbulent flows", *Nucl. Phys. B (Proc. Suppl.)*, **2**, 49-76 .

Meneveau, C. and K. R. Sreenivasan (1987b), "Simple multifractal cascade model for fully developed turbulence", *Phys. Rev. Lett.*, **59**, 1424-1427 .

Meneveau, C. and K. R. Sreenivasan (1991), "The multifractal nature of turbulent energy dissipation", *J. Fluid Mech.*, **224**, 429-484 .

Prasad, R. R., Meneveau C., and K. R. Sreenivasan (1988), "Multifractal nature of the dissipation field of passive scalars in fully turbulent flows", *Phys. Rev. Lett.*, **61**, 74-77.

Prasad, R. R. and K. R. Sreenivasan (1990a), "The measurement and interpretation of fractal dimensions of surfaces in turbulent flows", *Phys. Fluids A*, **2**, 792-807 .

Prasad, R. R. and K. R. Sreenivasan (1990b), "Quantitative three-dimensional imaging and the structure of passive scalar fields in fully turbulent flows", *J. Fluid Mech.*, **216**, 1-34 .

Rys, F. S. and A. Waldvogel (1986), "Fractal shape of hail clouds", *Phys. Rev. Lett.*, **56**, 784-787 .

Sreenivasan, K. R. (1991), "Fractals and multifractals in fluid turbulence", *Annu. Rev. Fluid Mech.*, **23**, 539-600 .

Sykes, R. I. and D. S. Henn (1992), "Large-eddy simulation of concentration fluctuations in a dispersing plume", *Atmos. Env.*, **26A**, 3127-3144 .

Sykes, R. I. and R. S. Gabruk (1994), "Fractal representation of turbulent dispersing plumes", *J. Appl. Met.*, **33**, 721-732 .

Tessier, Y., S. Lovejoy and D. Schertzer (1993), "Universal multifractals: Theory and observations for rain and clouds", *J. Appl. Met.*, **32**, 223-250 .

Voss, R. F. (1988), "Fractals in nature: From characterization to simulation", *The science of fractal images*, ed. H.-O. Peitgen and D. Saupe, Springer-Verglag, New York.

Wilson, J., D. Schertzer and S. Lovejoy (1991), "Continuous multiplicative cascade models of rain and clouds", *Non-Linear Variability in Geophysics*, ed. D. Schertzer and S. Lovejoy, Kluwer, Amsterdam.

Figure captions

Fig. 1. One-dimensional recursive refinement fractal generation for a homogeneous concentration field with clipped-normal distribution and $\sigma_c/\bar{c} = 1$. (a) Concentration field. (b) Dissipation field.

Fig. 2. One-dimensional recursive refinement fractal generation for a homogeneous concentration field with lognormal distribution and $\sigma_c/\bar{c} = 1$. (a) Concentration field. (b) Dissipation field.

Fig. 3. Typical plot of $\left[\sum (X_r/X_L)^q\right]^{1/(q-1)}$ vs. r for the dissipation field of a one-dimensional recursive refinement fractal generation for a homogeneous concentration field with $\sigma_c/\bar{c} = 1$. (a) Clipped-normal distribution. (b) Lognormal distribution. $q = 0$, 1.02, 2, 3, and 4.

Fig. 4. One-dimensional recursive refinement fractal/multifractal generation for a homogeneous concentration field with clipped-normal distribution and $\sigma_c/\bar{c} = 1$. (a) Concentration field. (b) Dissipation field.

Fig. 5. One-dimensional recursive refinement fractal/multifractal generation for a homogeneous concentration field with lognormal distribution and $\sigma_c/\bar{c} = 1$. (a) Concentration field. (b) Dissipation field.

Fig. 6. Typical plot of $\left[\sum (X_r/X_L)^q\right]^{1/(q-1)}$ Vs r for the dissipation field of a one-dimensional recursive refinement fractal/multifractal generation for a homogeneous concentration field with $\sigma_c/\bar{c} = 1$. (a) Clipped-normal distribution. (b) Lognormal distribution. $q = 0$, 1.02, 2, 3, and 4.

Fig. 7. Multifractal spectra from the averaged D_q curves of the dissipation fields of one hundred one-dimensional recursive refinement fractal/multifractal realizations for a homogeneous concentration field with $\sigma_c/\overline{c} = 1$.

Fig. 8. Two-dimensional recursive refinement fractal/multifractal generation for a homogeneous concentration field with clipped-normal distribution and $\sigma_c/\overline{c} = 1$. The vertical axes are scaled arbitrarily. (a) Concentration field. (b) Dissipation field.

Fig. 9. Two-dimensional recursive refinement fractal/multifractal generation for a homogeneous concentration field with lognormal distribution and $\sigma_c/\overline{c} = 1$. The vertical axes are scaled arbitrarily as in Fig. 8. (a) Concentration field. (b) Dissipation field.

Fig. 10. Typical plot of $\left[\sum (X_r/X_L)^q\right]^{1/(q-1)}$ vs. r for the dissipation field of a two-dimensional recursive refinement fractal/multifractal generation for a homogeneous concentration field with $\sigma_c/\overline{c} = 1$. (a) Clipped-normal distribution. (b) Lognormal distribution. $q = 0$, 1.02, 2, 3, and 4.

Fig. 11. Multifractal spectra from the averaged D_q curves of the dissipation fields of twenty-five two-dimensional recursive refinement fractal/multifractal realizations for a homogeneous concentration field with $\sigma_c/\overline{c} = 1$.

Fig. 12. LES neutral boundary layer time series for a sampler at $x/H = 5$ on the plume centerline. Both the concentration and dissipation have been scaled by their maximum values for this LES realization. (a) Concentration field. (b) Dissipation field.

Fig. 13. One-dimensional recursive refinement fractal/multifractal simulation of the LES neutral boundary layer time series shown in Fig. 12. Both the concentration and dissipation have been scaled by the maximum values from the corresponding LES realization in Fig. 12.(a) Concentration field. (b) Dissipation field.

Fig. 14. Multifractal spectra from the averaged D_q curves of the dissipation fields of thirty LES one-dimensional realizations and one hundred one-dimensional recursive refinement fractal/multifractal realizations with lognormal distribution.

Fig. 15. Neutral boundary layer plume realizations of c normalized by the maximum mean concentration at $x/H = 5$. Contours are 0.1, 0.2, 0.5, 1, 2, and 5. Stippled areas are equal to or greater than 1. (a) LES model. (b) Fractal/multifractal model.

Fig. 16. Multifractal spectra from the averaged D_q curves of the dissipation fields of six LES two-dimensional realizations and one hundred two-dimensional recursive refinement fractal/multifractal realizations with lognormal distribution.

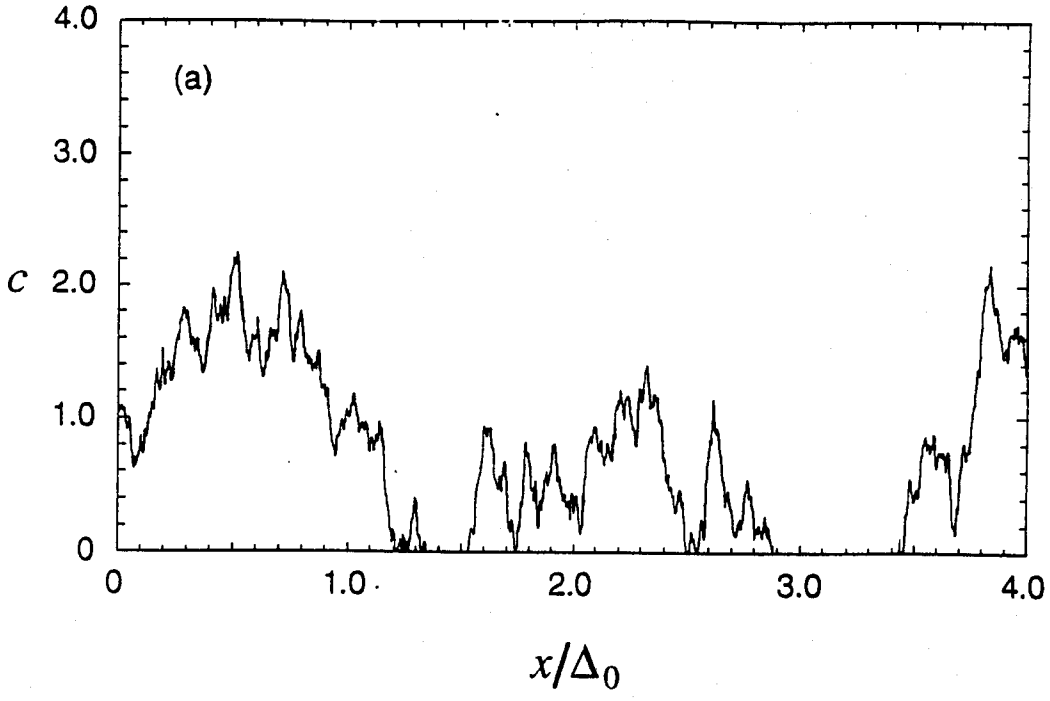
(a)
4.0
3.0
2.0
1.0
0
c
0
1.0
2.0
3.0
4.0
x/Δ_0

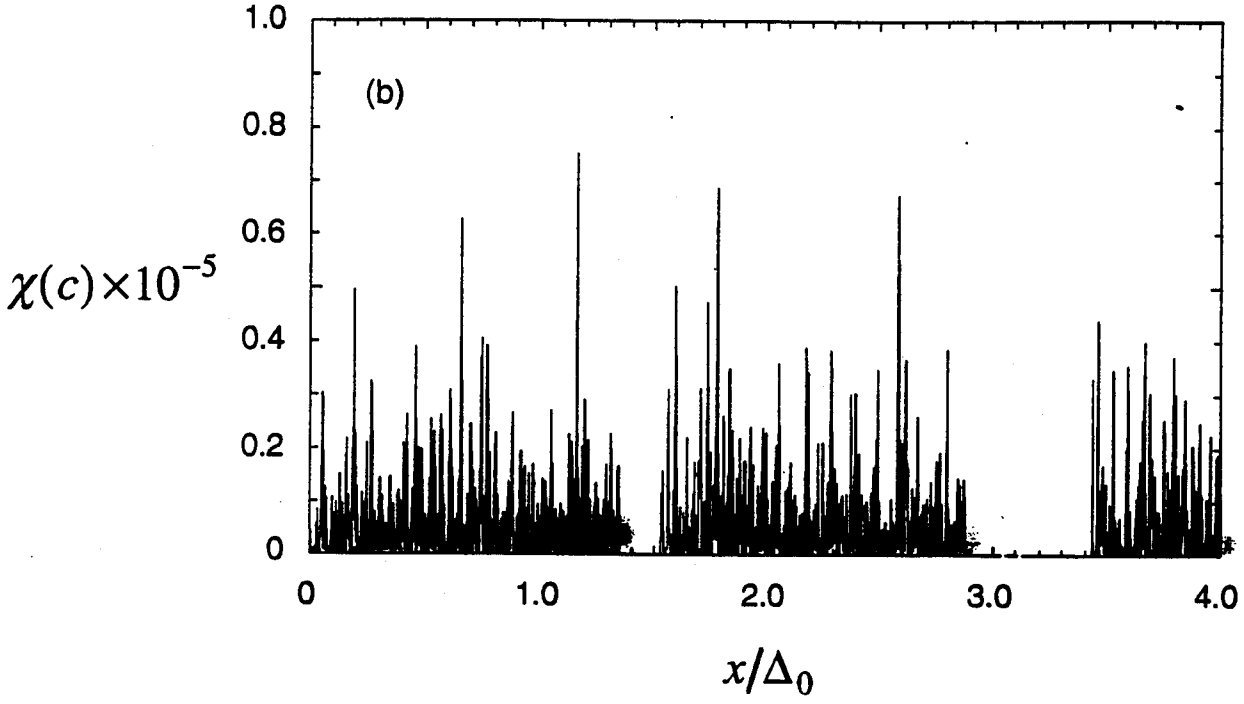
(b)
1.0
0.8
0.6
0.4
0.2
0
$\chi(c)\times10^{-5}$
0
1.0
2.0
3.0
4.0
x/Δ_0

Fig. 1

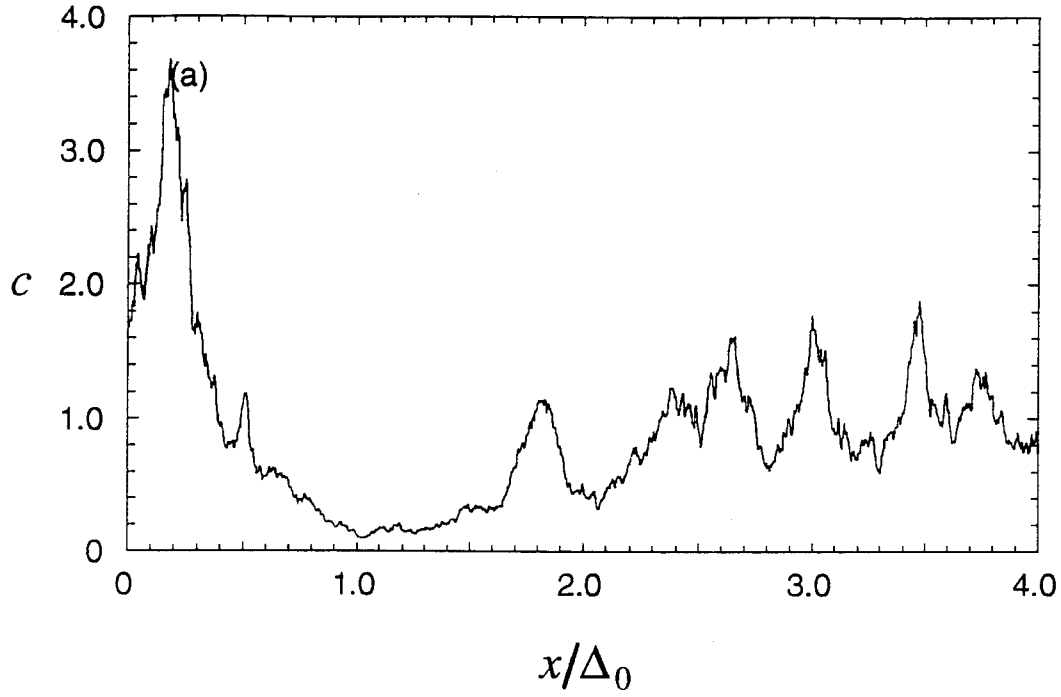
4.0
3.0
2.0
1.0
0
c
(a)
0
1.0
2.0
3.0
4.0
x/Δ_0

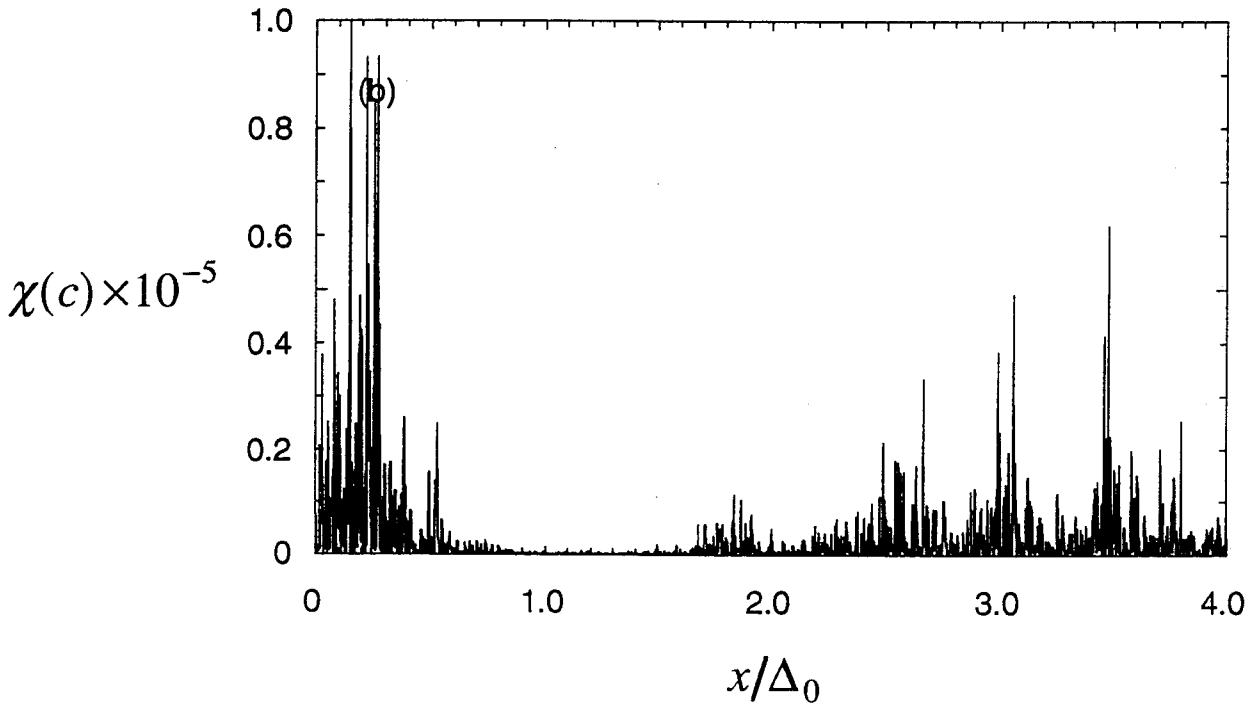
1.0
0.8
0.6
0.4
0.2
0
$\chi(c)\times10^{-5}$
(b)
0
1.0
2.0
3.0
4.0
x/Δ_0

Fig. 2

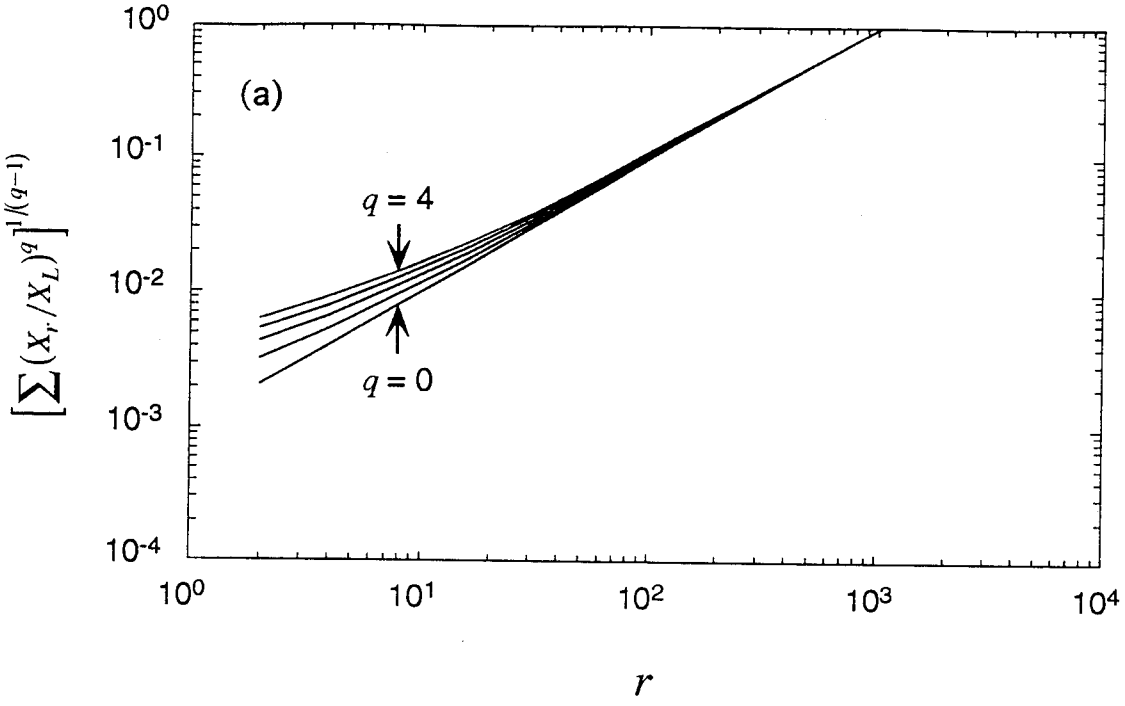
(a)
$q = 4$
$q = 0$
10^0
10^{-1}
10^{-2}
10^{-3}
10^{-4}
10^0
10^1
10^2
10^3
10^4
r
$\left[\sum (X_r / X_L)^q\right]^{1/(q-1)}$

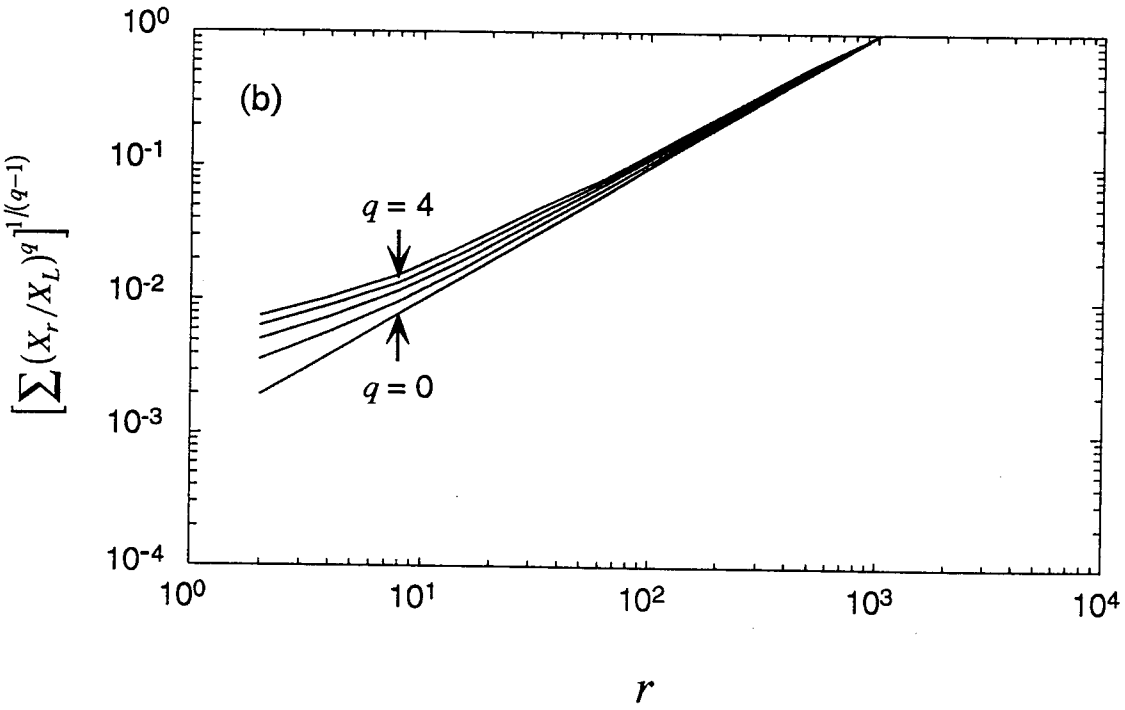
(b)
$q = 4$
$q = 0$
10^0
10^{-1}
10^{-2}
10^{-3}
10^{-4}
10^0
10^1
10^2
10^3
10^4
r
$\left[\sum (X_r / X_L)^q\right]^{1/(q-1)}$

Fig. 3

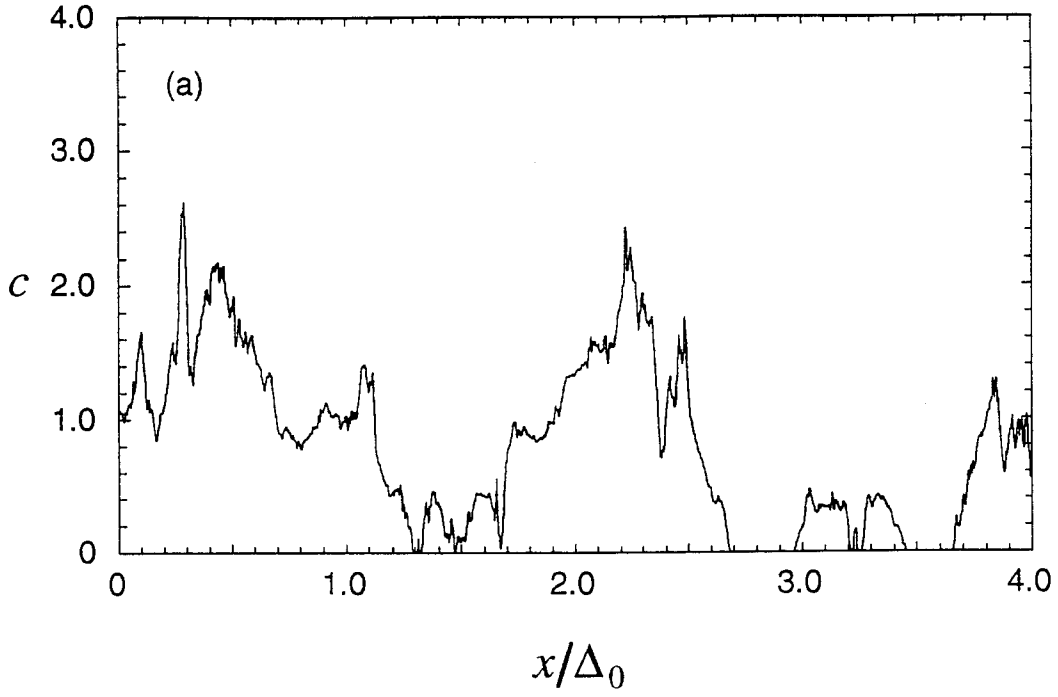
(a)
4.0
3.0
2.0
1.0
0
c
0
1.0
2.0
3.0
4.0
x/Δ_0

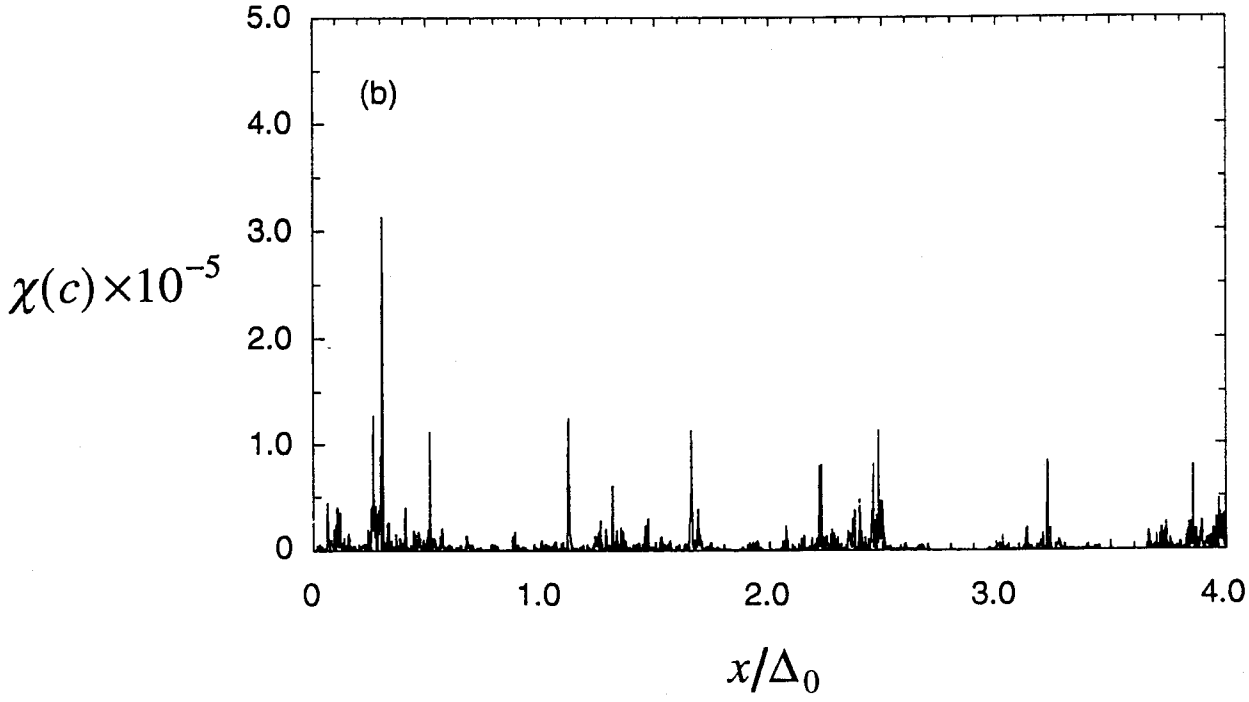
(b)
5.0
4.0
3.0
2.0
1.0
0
$\chi(c)\times10^{-5}$
0
1.0
2.0
3.0
4.0
x/Δ_0

Fig. 4

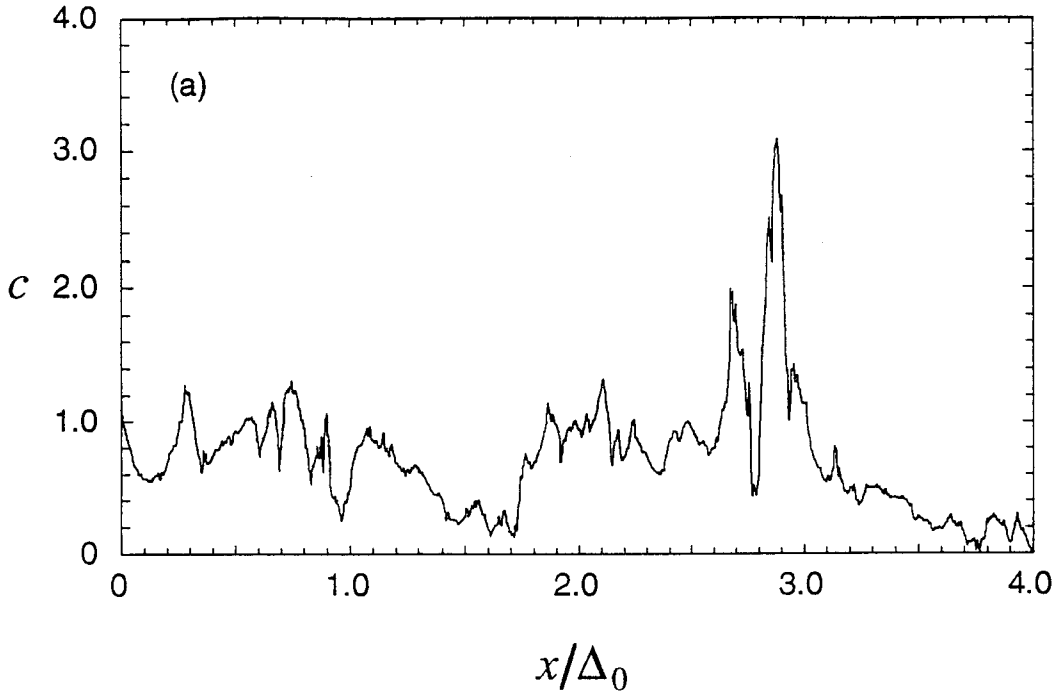
(a)
4.0
3.0
2.0
1.0
0
c
0
1.0
2.0
3.0
4.0
x/Δ_0

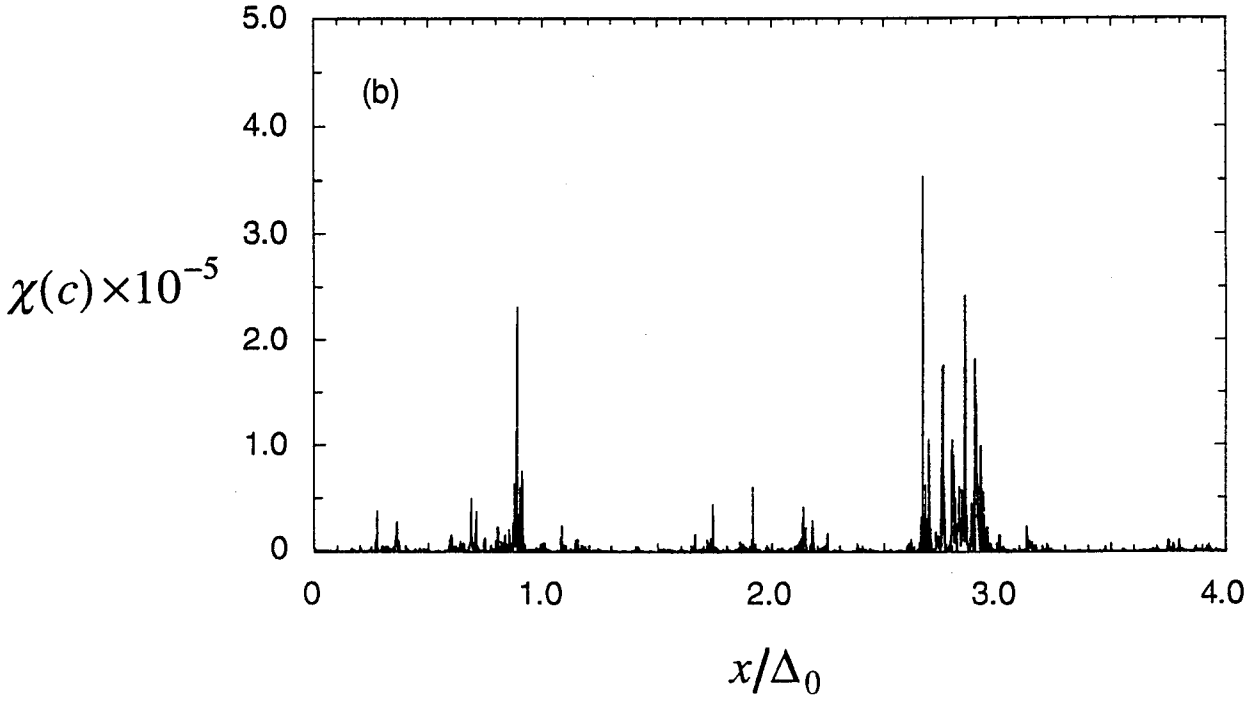
(b)
5.0
4.0
3.0
2.0
1.0
0
$\chi(c)\times10^{-5}$
0
1.0
2.0
3.0
4.0
x/Δ_0

Fig. 5

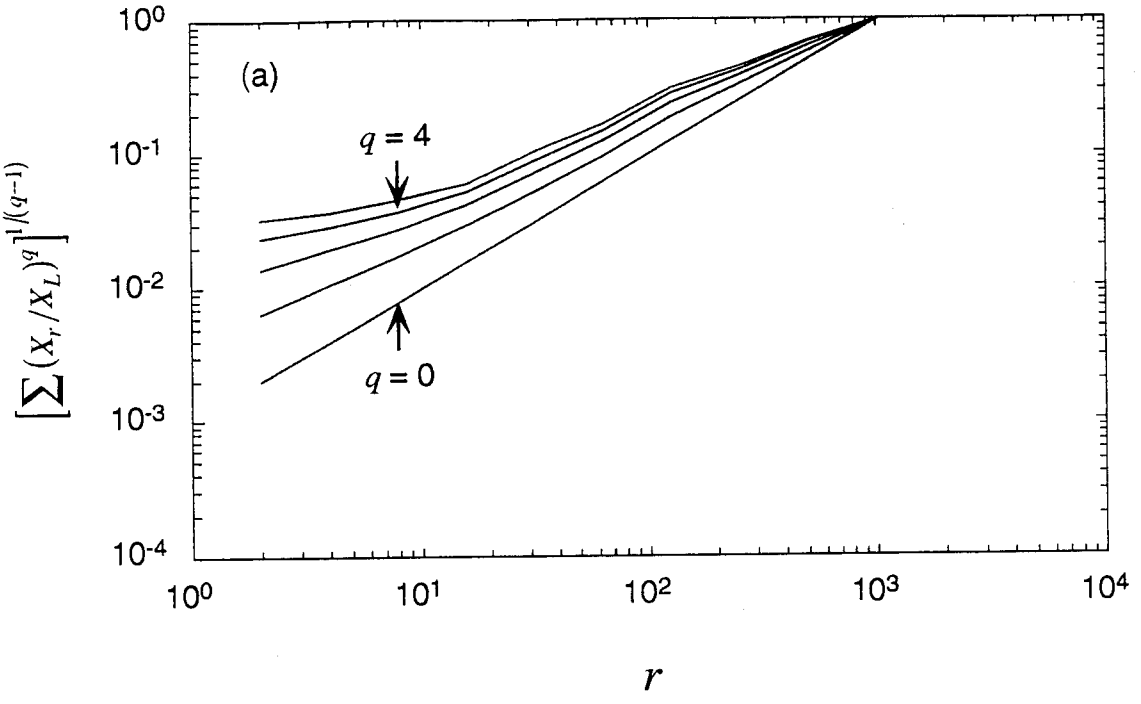
(a)
$q = 4$
$q = 0$
10^0
10^{-1}
10^{-2}
10^{-3}
10^{-4}
10^0
10^1
10^2
10^3
10^4
$\left[\sum (X_r / X_L)^q\right]^{1/(q-1)}$
r

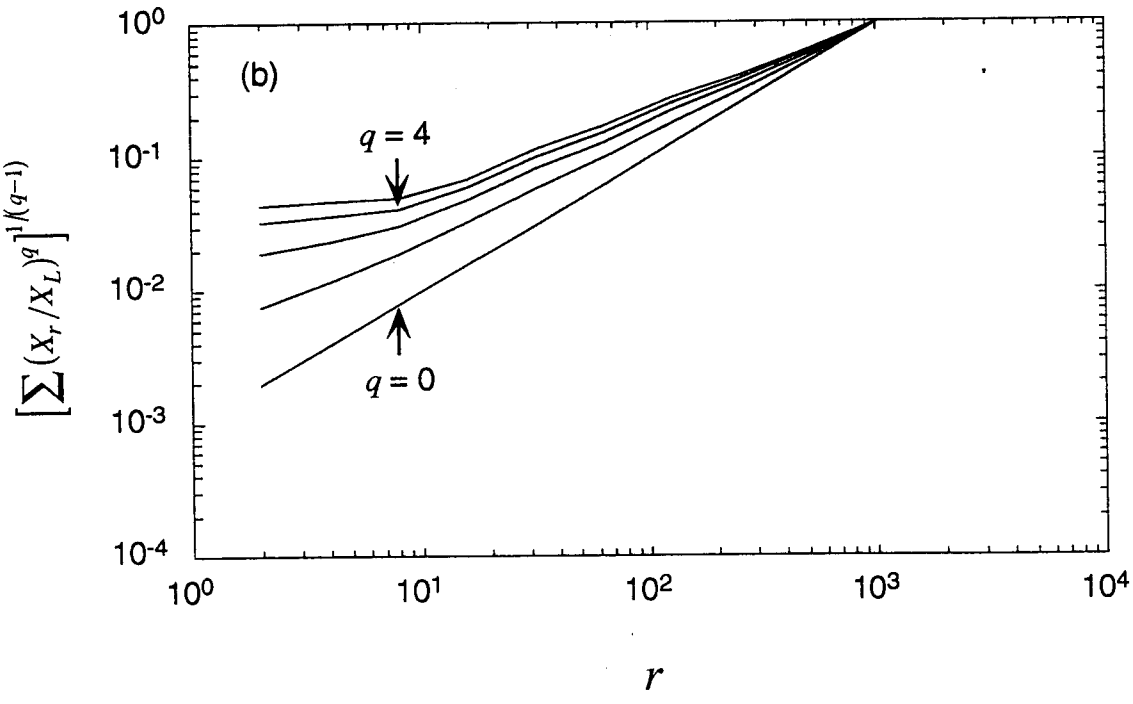
(b)
$q = 4$
$q = 0$
10^0
10^{-1}
10^{-2}
10^{-3}
10^{-4}
10^0
10^1
10^2
10^3
10^4
$\left[\sum (X_r / X_L)^q\right]^{1/(q-1)}$
r

Fig. 6

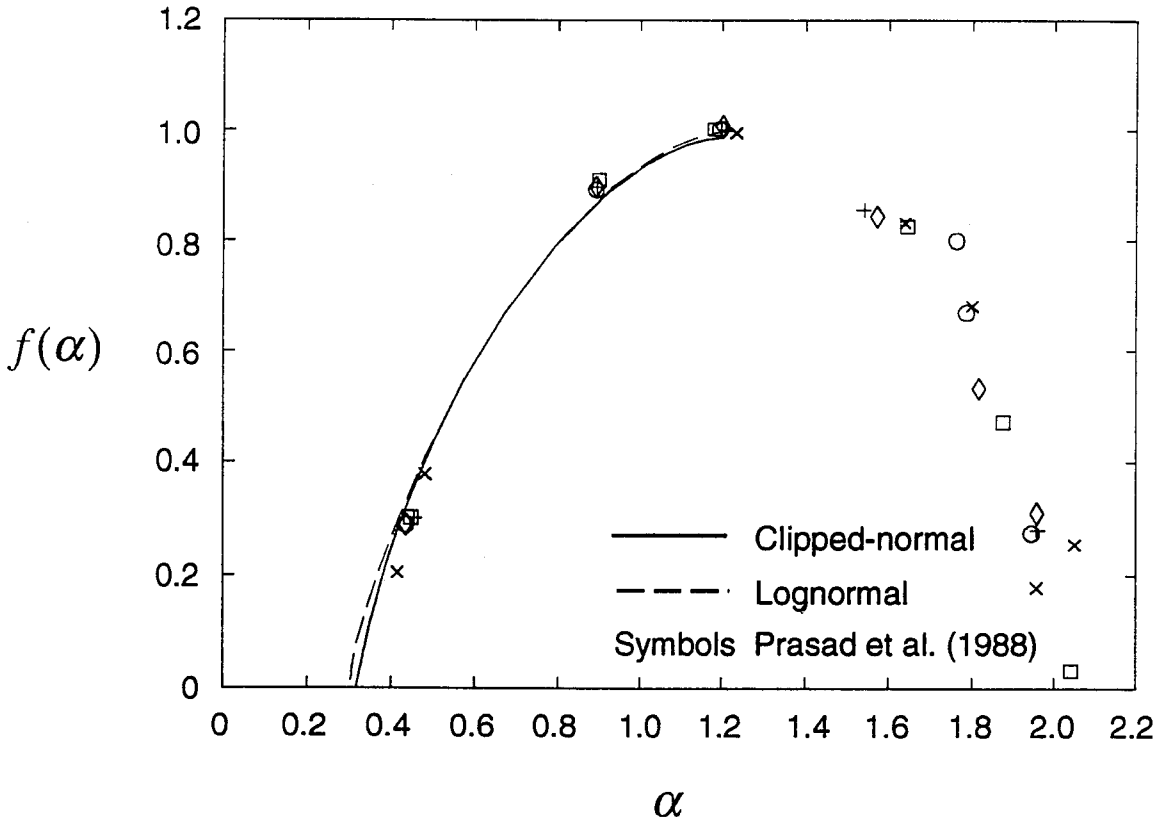
1.2
1.0
0.8
0.6
0.4
0.2
0
$f(\alpha)$
0
0.2
0.4
0.6
0.8
1.0
1.2
1.4
1.6
1.8
2.0
2.2
α
Clipped-normal
Lognormal
Symbols Prasad et al. (1988)

Fig. 7

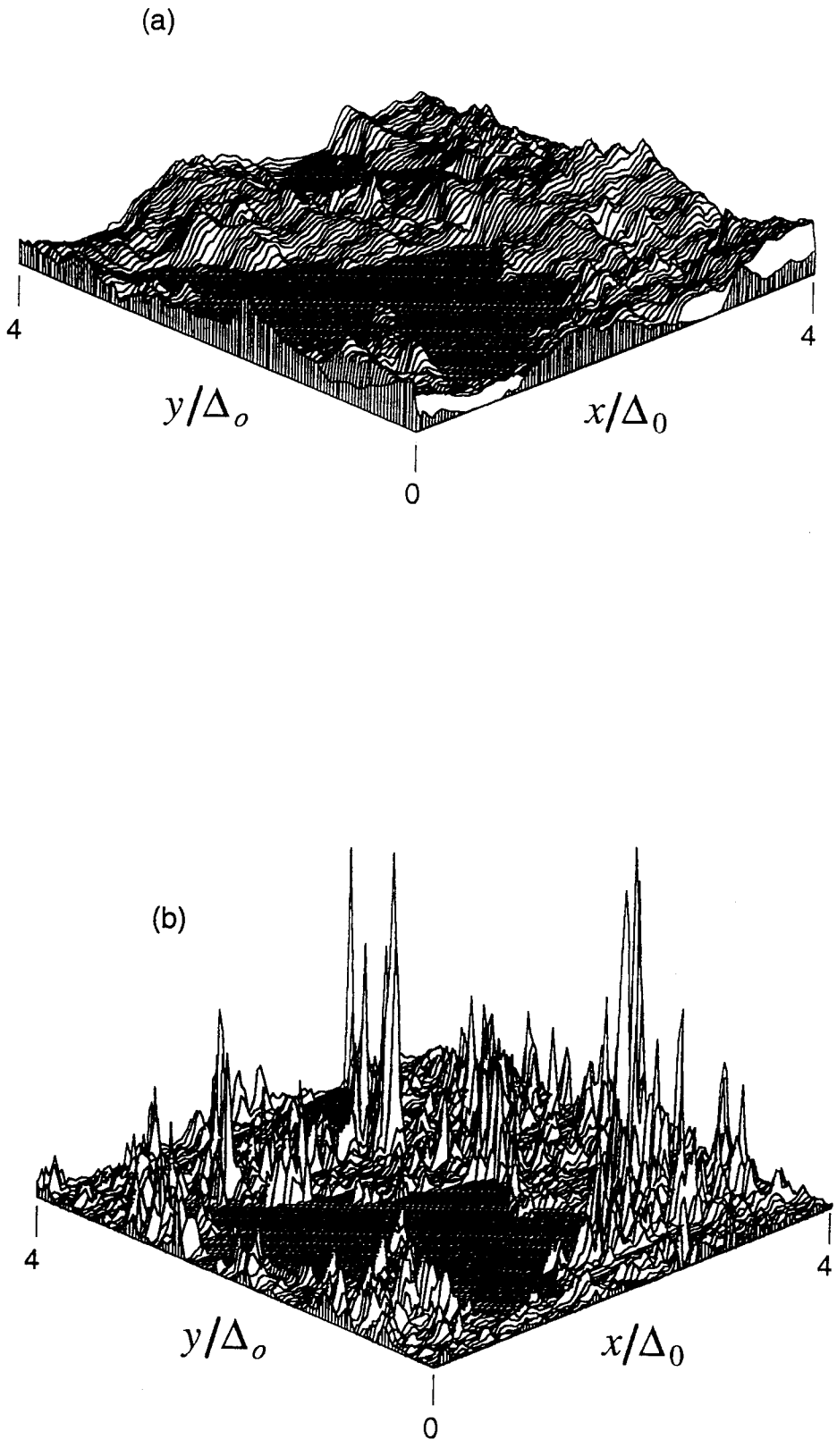

Fig. 8

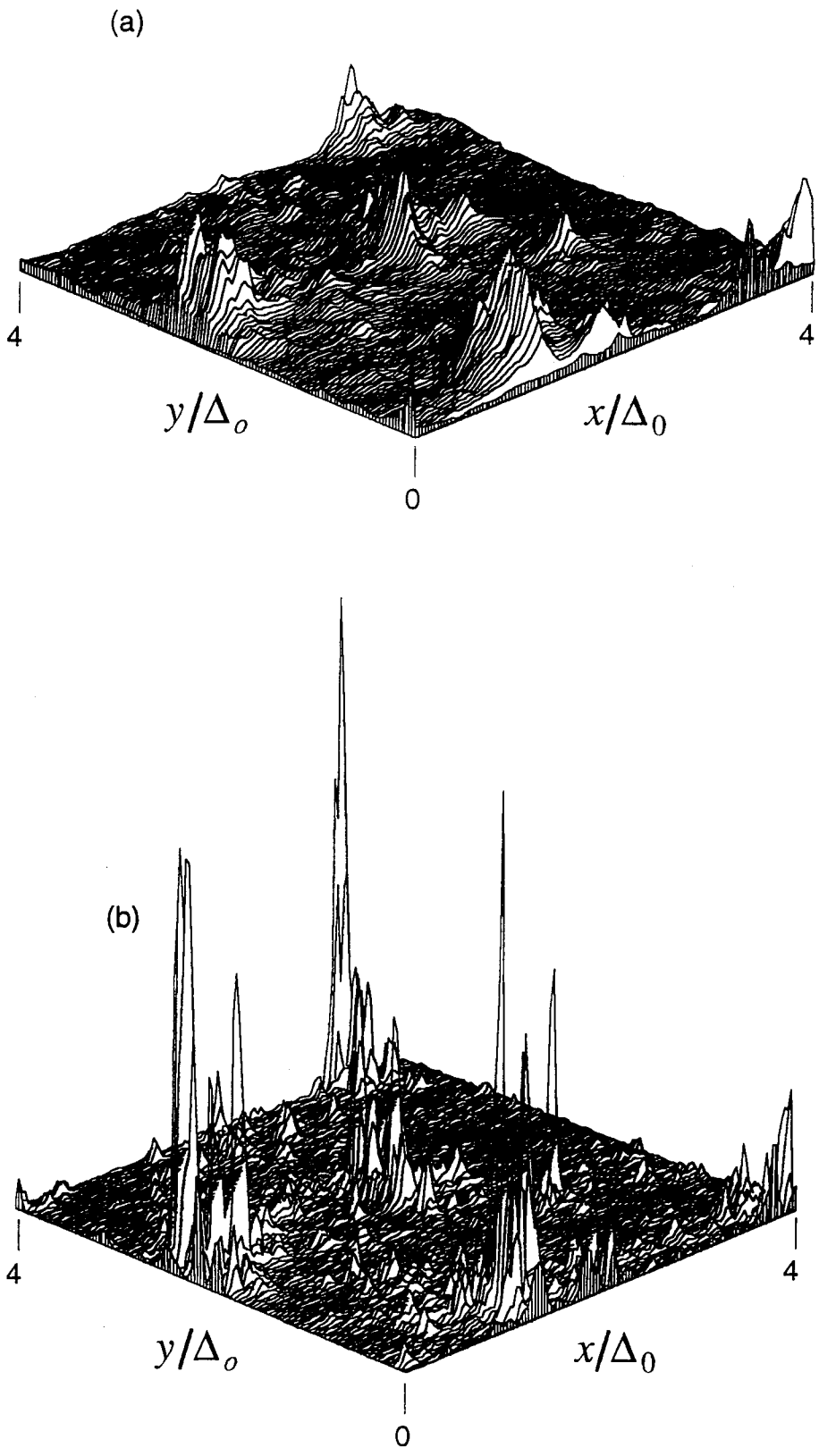

Fig. 9

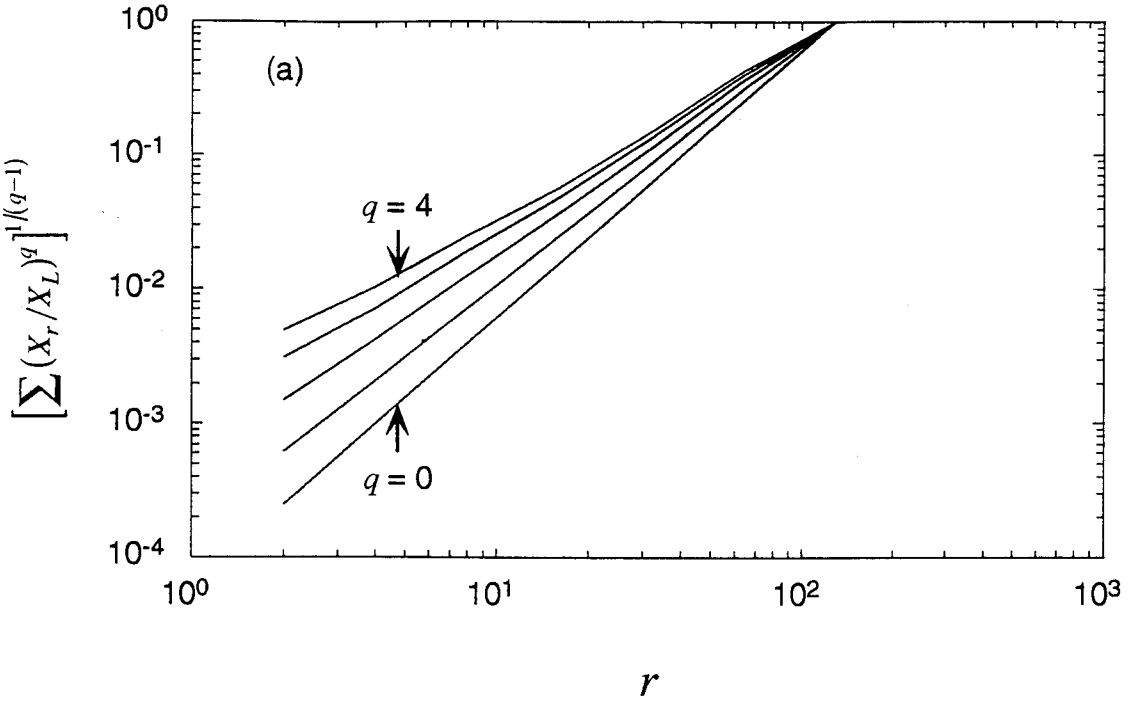
(a)
$q = 4$
$q = 0$
10^0
10^{-1}
10^{-2}
10^{-3}
10^{-4}
10^0
10^1
10^2
10^3
$\left[\sum (X_r/X_L)^q\right]^{1/(q-1)}$
r

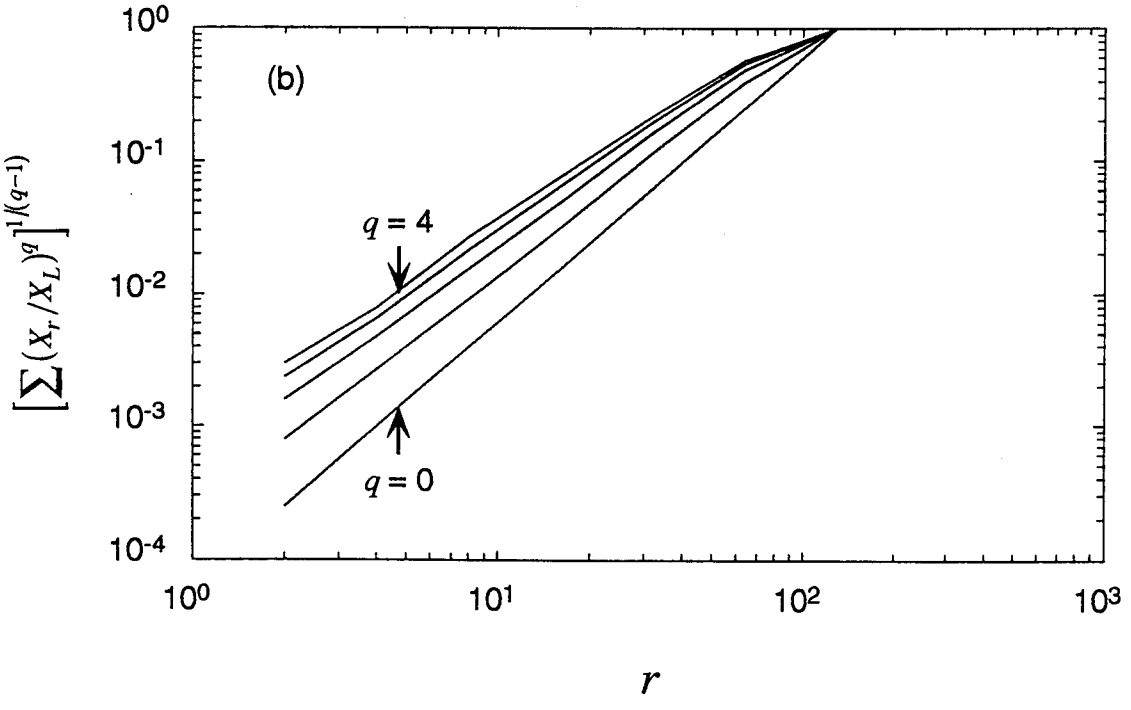
(b)
$q = 4$
$q = 0$
10^0
10^{-1}
10^{-2}
10^{-3}
10^{-4}
10^0
10^1
10^2
10^3
$\left[\sum (X_r/X_L)^q\right]^{1/(q-1)}$
r

Fig. 10

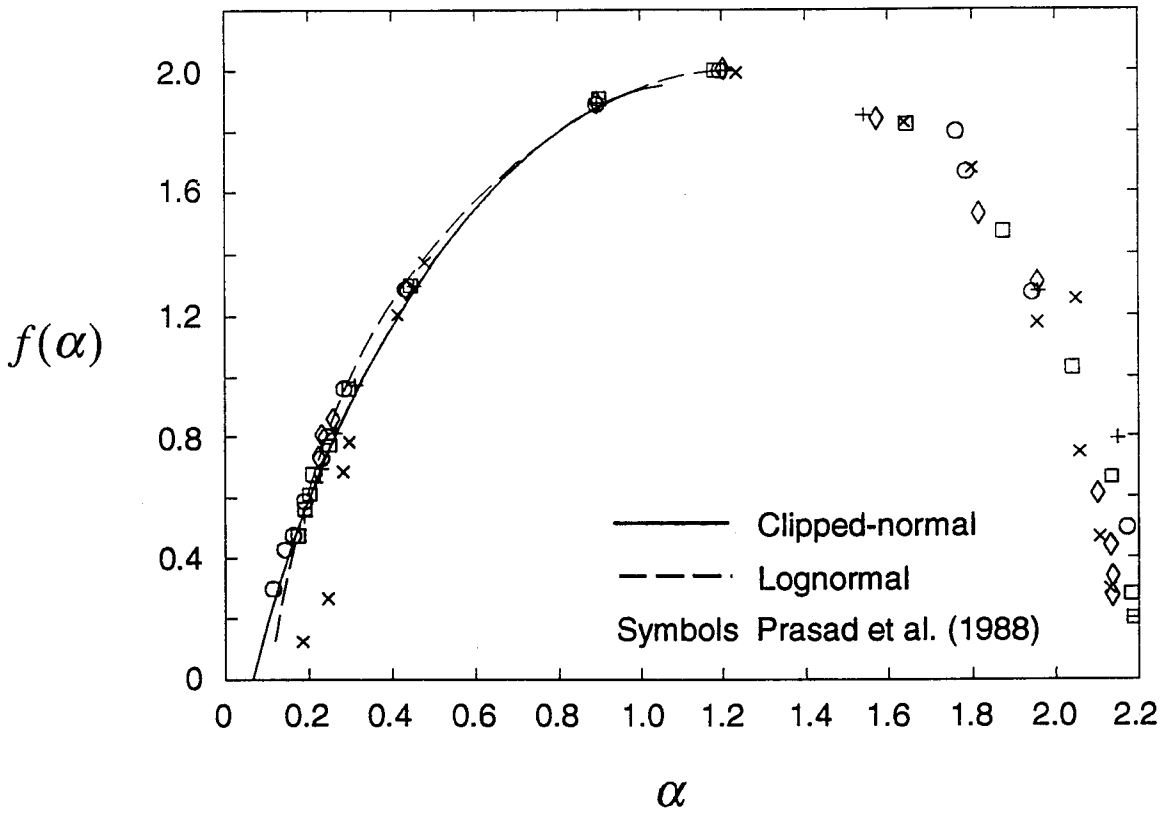
$f(\alpha)$
2.0
1.6
1.2
0.8
0.4
0
0
0.2
0.4
0.6
0.8
1.0
1.2
1.4
1.6
1.8
2.0
2.2
α
Clipped-normal
Lognormal
Symbols Prasad et al. (1988)

Fig. 11

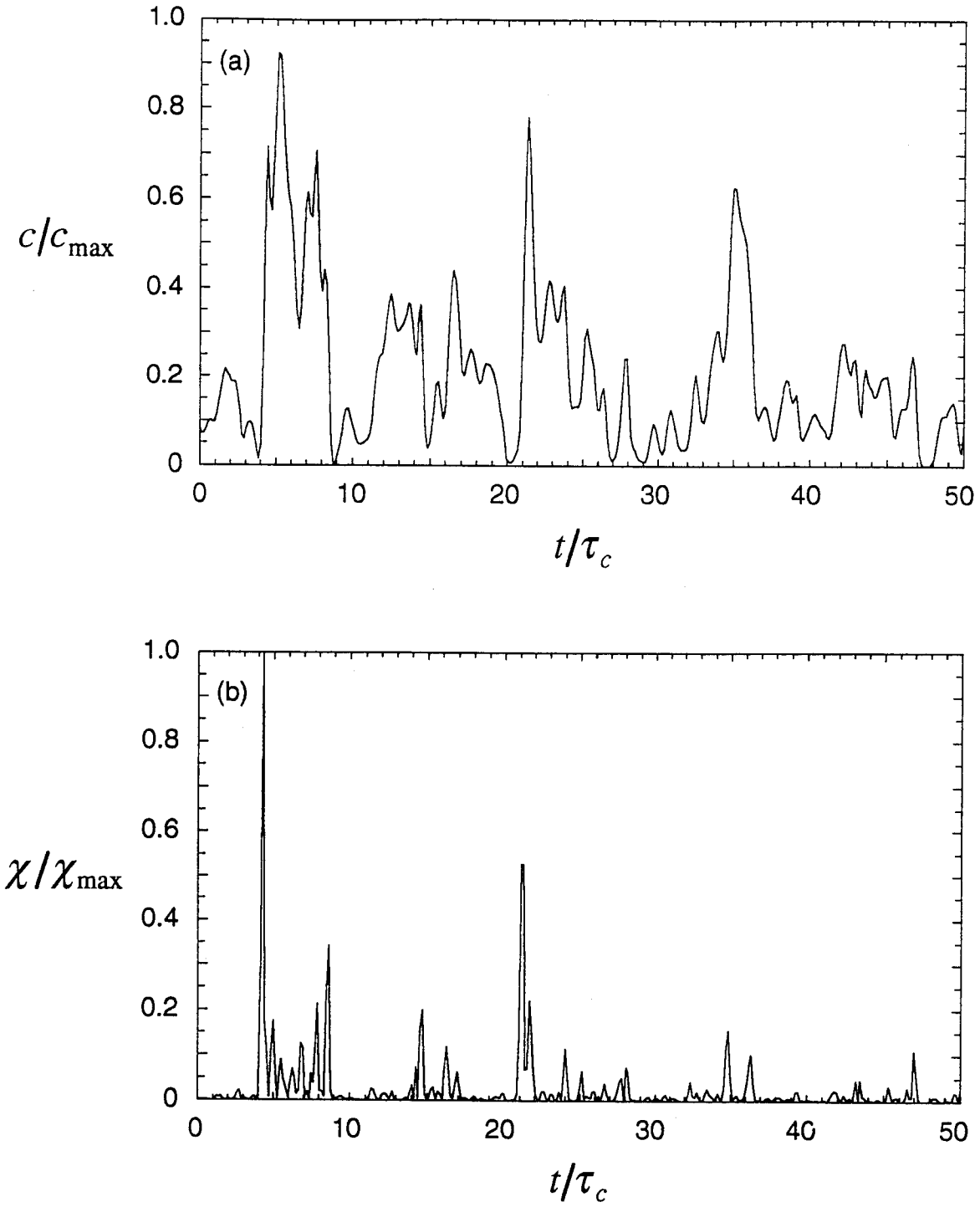
(a)
1.0
0.8
0.6
0.4
0.2
0
c/c_{max}
0
10
20
30
40
50
t/τ_c
(b)
1.0
0.8
0.6
0.4
0.2
0
χ/χ_{max}
0
10
20
30
40
50
t/τ_c

Fig. 12

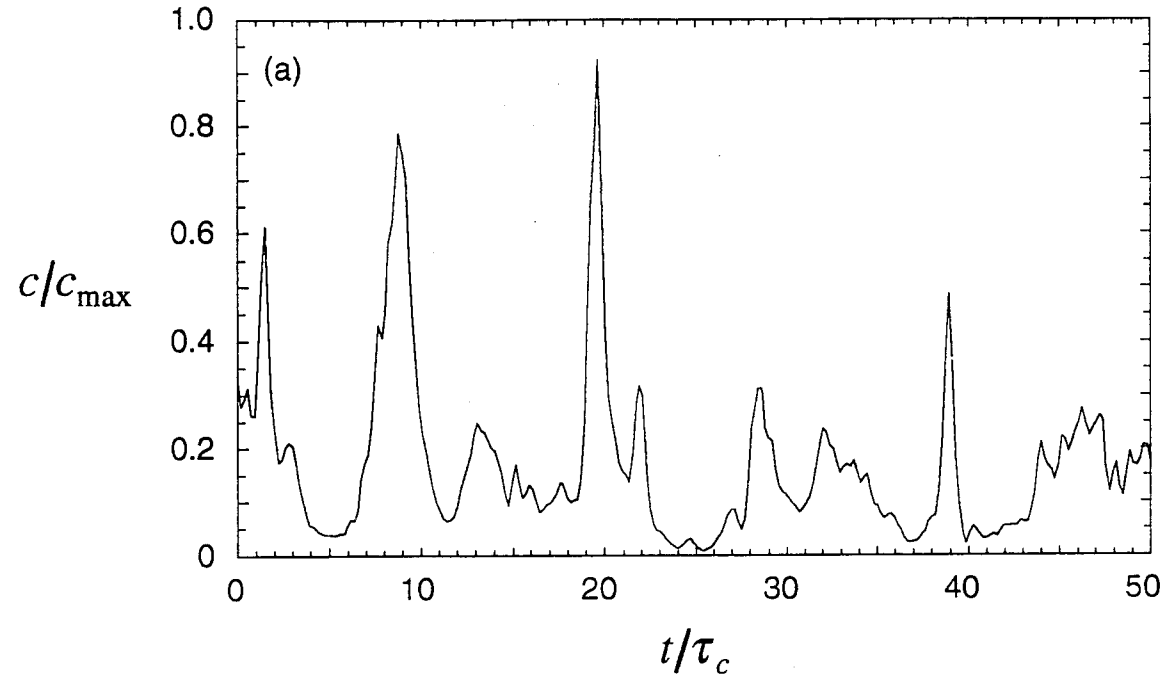
(a)
1.0
0.8
0.6
0.4
0.2
0
0
10
20
30
40
50
$c/c_{\max}$
t/τ_c

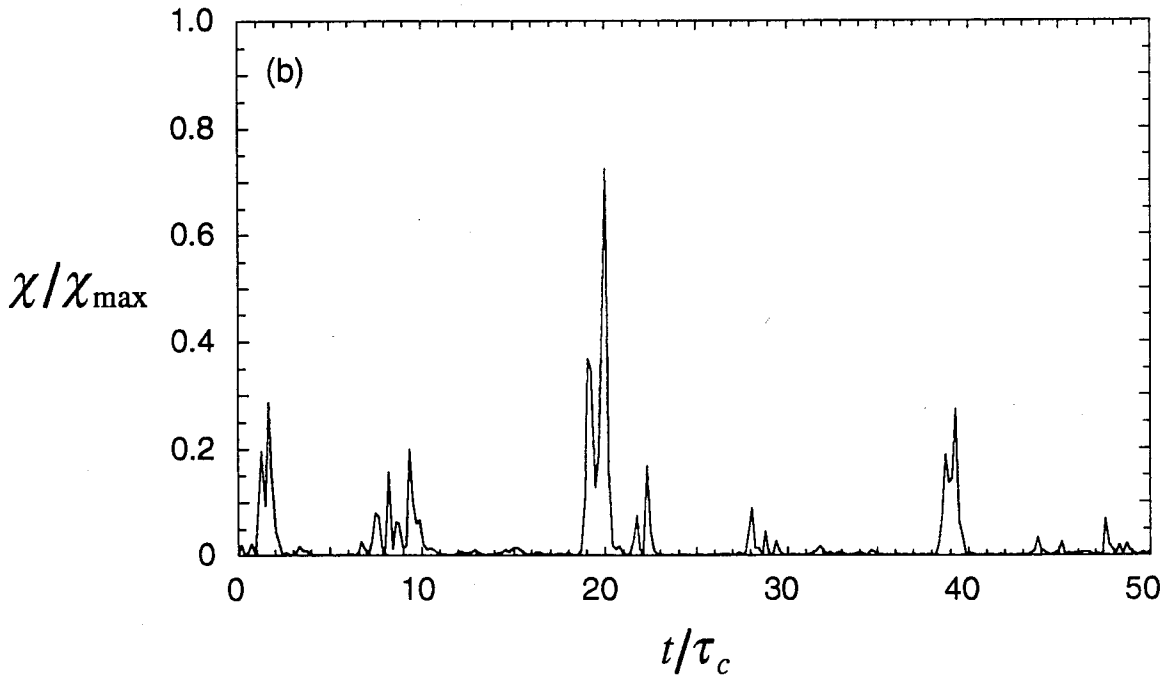
(b)
1.0
0.8
0.6
0.4
0.2
0
0
10
20
30
40
50
$\chi/\chi_{\max}$
t/τ_c

Fig. 13

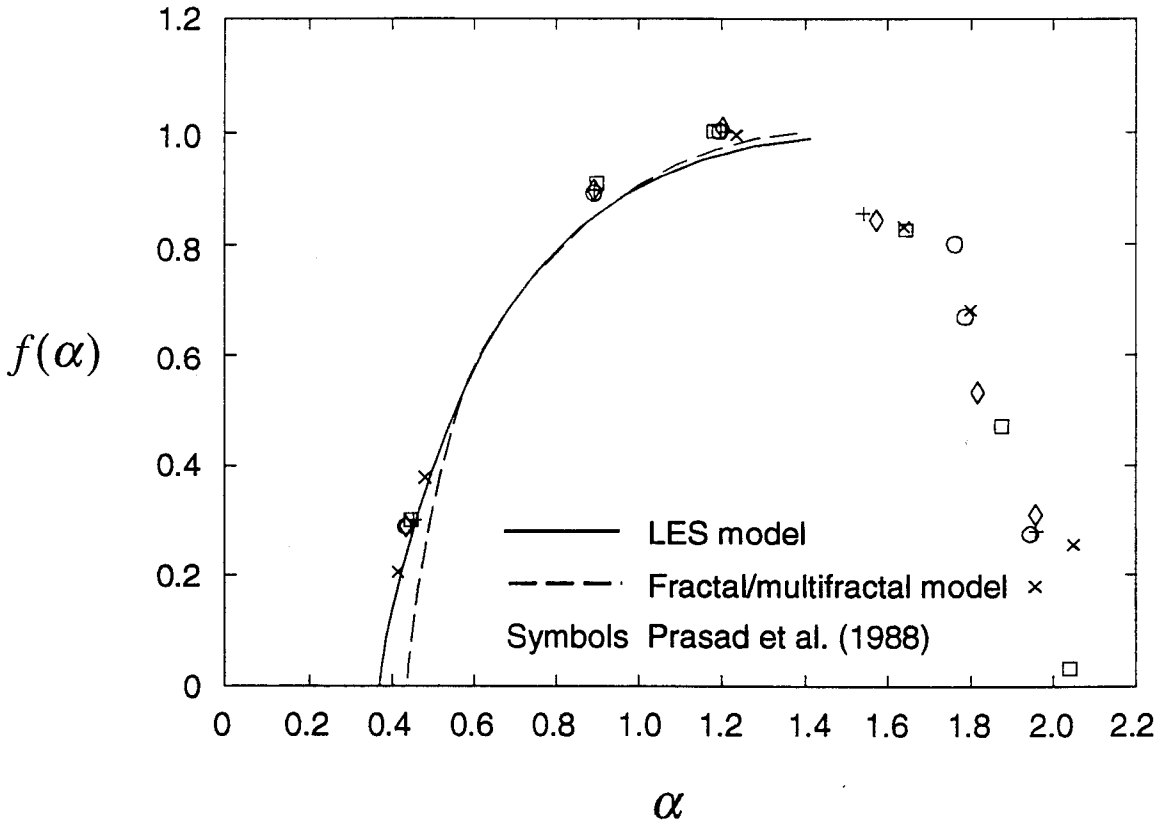
1.2
1.0
0.8
0.6
0.4
0.2
0
$f(\alpha)$
0
0.2
0.4
0.6
0.8
1.0
1.2
1.4
1.6
1.8
2.0
2.2
α
LES model
Fractal/multifractal model
Symbols Prasad et al. (1988)

Fig. 14

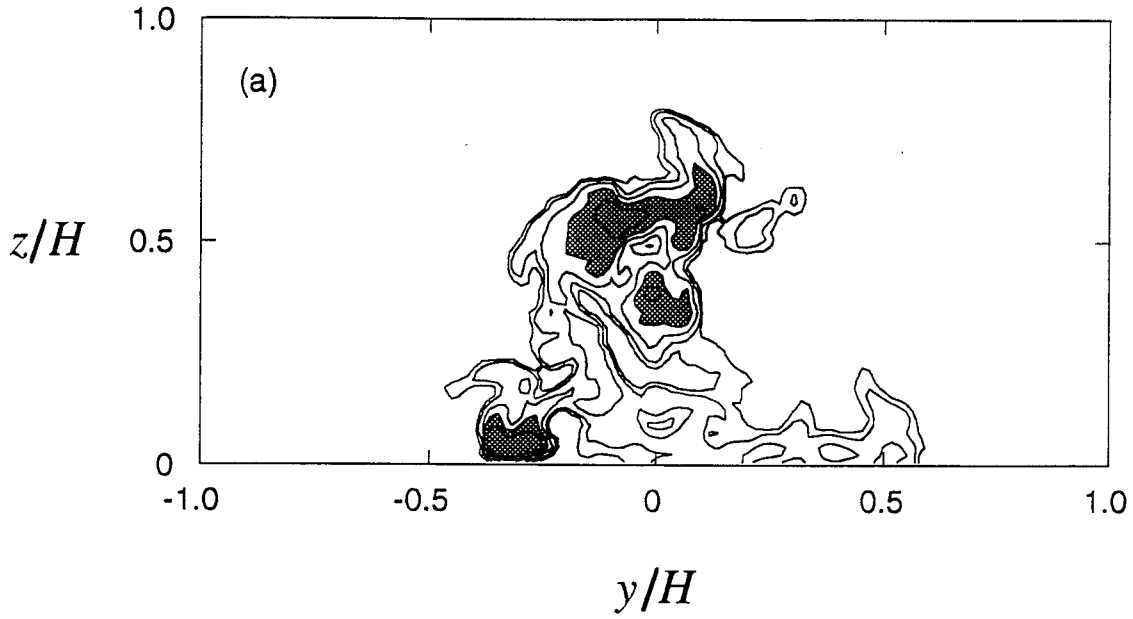

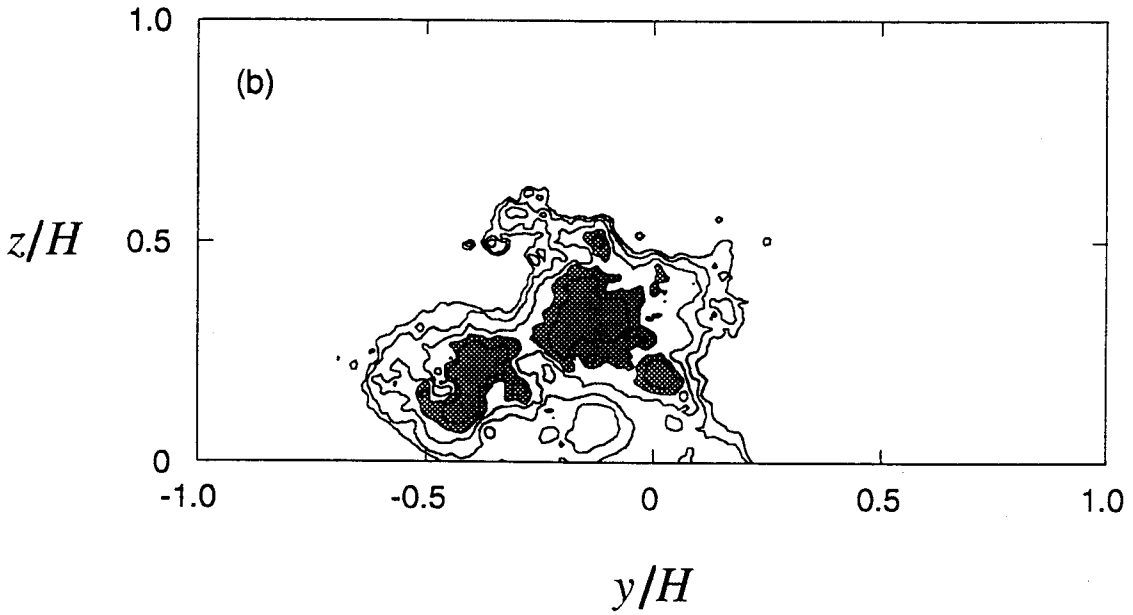

Fig. 15

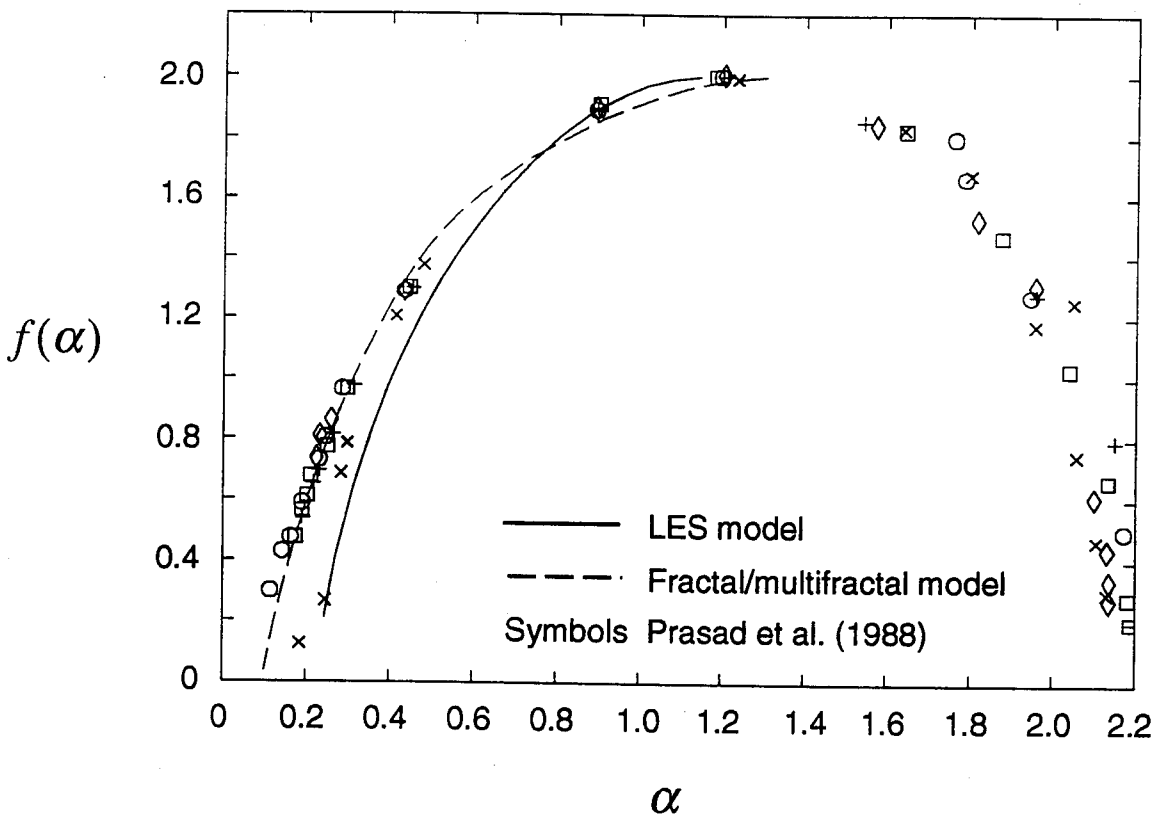
$f(\alpha)$
2.0
1.6
1.2
0.8
0.4
0
0
0.2
0.4
0.6
0.8
1.0
1.2
1.4
1.6
1.8
2.0
2.2
α
LES model
Fractal/multifractal model
Symbols Prasad et al. (1988)

Fig. 16